**This document is downloaded from DR-NTU (https://dr.ntu.edu.sg)
Nanyang Technological University, Singapore.**

Small signal modulation characteristics of quantum dot lasers and the effect of annealing and doping

Zhao, Hanxue

2012

Zhao, H. (2012). Small signal modulation characteristics of quantum dot lasers and the effect of annealing and doping. Doctoral thesis, Nanyang Technological University, Singapore.

https://hdl.handle.net/10356/49514

https://doi.org/10.32657/10356/49514

Downloaded on 18 Apr 2025 14:45:51 SGT

SMALL SIGNAL MODULATION CHARACTERISTICS OF QUANTUM DOT LASERS AND THE EFFECT OF ANNEALING AND DOPING

ZHAO HANXUE

ZHAO HANXUE

School of Electrical and Electronic Engineering

Nanyang Technological University

Singapore

A thesis submitted to the Nanyang Technological University

in partial fulfilment of the requirement for the degree of

Doctor of Philosophy

2012

Acknowledgements

Research is a long and winding journey. People need a compass to navigate through it and an interesting book to read on the road. I am lucky because I had both of these since the day my trip began. My sincere gratitude and appreciation goes to my supervisor Dr. Yoon Soon Fatt. He is the one who told me to be strong and never to lose faith when I was depressed and lost. He made me understand that research is a scrupulous job but that good research is a spiritual style. His guidance, aspiration, and enthusiasm all deeply inspire me in my everyday research life. From him, I know what it takes to be a real scientist.

I would like to thank Dr. Tong Cunzhu for teaching me about theoretical studies on the physical properties of compound semiconductor nanophotonic materials. His continuous valuable support enabled this project to progress smoothly.

I am grateful to Dr. Liu Chongyang and Dr. Loke Wan Khai who were always ready to clarify my doubts and who helped me overcome the obstacles that I encountered during the experimental investigations.

I extend special gratitude to Dr. Ngo Chun Yong for helping me with the annealing process and the discussion section with the most updated information about my research area.

I wish to thank my teammates, Mr. Wang Rui and Ms. Cao Qi, for the critical help they gave during my research trip.

I would also like to thank all of my other group mates: Mr. Xu Dawei, Mr. Xu Zhe, Ms. Liang Yu Yan, Dr. Satrio Wicaksono, Dr. Pham Huynh Tram, Dr. Wang Yang, Mr. Chen Kah Pin, Dr. Tan Kian Hua, Mr. Lim Kim Peng, and Mr. Li Daosheng

for their help and for many useful conversations during the past four years. I also appreciate all of the help given to me by the staff members at the Nanyang Technological University (NTU) Characterization Lab, especially by Mr. Muhd Fauzi Bin Abdullah, Mr. Mohamad Shamsul Bin Mohamad, and Ms. Seet Lye Ping.

Finally, I thank the Singapore Defense Science Organization (DSO) and the Singapore Institute of Manufacturing Technology (SIMTech) for their technical support.

TABLE OF CONTENTS

Acknowledgements 1
Summary….. 11
List of Figures 5
List of Tables 9
List of Abbreviations 10

Chapter 1: Introduction 15
1.1 Background 16
1.2 Motivations and Objectives 18
1.3 Major Contributions 23
1.4 Organization of the Thesis 26

Chapter 2: Literature Review 28
2.1 Quantum Dot Lasers 28
2.2 *P*-type Modulation Doping Technique 31
2.3 Rapid Thermal Annealing Technique 34
2.4 Fundamental Characteristics of QD Lasers 39
2.4.1 Threshold Condition 40
2.4.2 Internal Quantum Efficiency and Internal Optical Loss 41
2.4.3 The Temperature Dependence of Laser Characteristics 42
2.4.4 Small Signal Modulations of the QD Laser 43

Chapter 3: Experimental Background 50
3.1 Quantum Dot Structure 50
3.2 Device Fabrication Process 52
3.3 Rapid Thermal Annealing Process 54
3.4 Characterization Techniques 55
3.4.1 Photoluminescence 55
3.4.2 Transmission Electron Microscopy 57
3.4.3 Electroluminescence Spectroscopy 57
3.4.4 High-Speed Modulation Experimental Set-up 58

Chapter 4: The Bandwidth Limitations of QD Lasers by Small Signal Modulation 64
4.1 Introduction 64
4.2 Small Signal Modulation 66
4.3 Temperature-Dependent Study 70

4.4 Summary 76

Chapter 5: Effects of *P*-doping and Rapid Thermal Annealing on the Two-State Lasing Behaviours of QD Lasers 77
5.1 Introduction 77
5.2 Temperature-Dependent Study 79
5.3 Cavity-Dependent Study 83
5.4 QDs Gain Characteristics 87
5.5 Structural Investigation by TEM Study 99
5.6 Summary 101

Chapter 6: Effects of Rapid Thermal Annealing on the High-Speed Characteristics of Intrinsic QD Lasers 103
6.1 Introduction 103
6.2 QD Laser Static Characteristics 104
6.3 Small Signal Modulation 110
6.4 Summary 118

Chapter 7: Improved Ground-State High-Speed Characteristics of *P*-doped QD Lasers by Optimum Annealing 120
7.1 Introduction 120
7.2 QD Laser Small Signal Modulation 121
7.3 Temperature-Dependent Characterization 129
7.4 Spontaneous Emission Measurement 130
7.5 Summary 132

Chapter 8: Conclusions and Recommendations for Future Research 134
8.1 Conclusions 134
8.2 Recommendations for Future Research 137
8.2.1 Further Investigations on the Intermixing Effects in QDs 137
8.2.2 The Modulation of Short Cavity QD Lasers with a Coplanar Contact Structure 139
8.2.3 Investigation of the Effect of Device Structure on the High-speed Modulation of QD Lasers 140

Author's Publications 141
Bibliography 143

List of Figures

Figure 2.1 The active region presented and the DOS functions of the semiconductor bandgap for bulk, QW, QWr, and QD lasers [36]....30

Figure 2.2 A schematic illustration of the QD energy levels with different built-in carrier distributions for the undoped and *p*-doped structures....33

Figure 2.3 The modulation *p*-doping of the QD barrier in order to increase the gain through the increase of the hole ground state occupancy [19]....33

Figure 2.4 Interdiffusion smears the alloy distribution, resulting in band gap disordering in 3-dimensions. Band gap profiles for the noninterdiffused (left) and the interdiffused (right) QD along the x direction are shown [55]....34

Figure 2.5 The temperature dependence of the PL rise times for QW, as-grown QD, and intermixed QD at an average excitation intensity of 2.5 mW [30]....36

Figure 2.6 The PL spectra at 5 K after annealing at different temperatures for 30 s from (a) an undoped InAs QD structure and (b) a *p*-doped InAs QD structure [61]....38

Figure 2.7 The schematic drawing of an InAs/InGaAs FP ridge waveguide laser....39

Figure 2.8 (a) Small signal modulation and (b) optical output power versus the injection current characteristics of the semiconductor laser diode....44

Figure 2.9 An energy diagram of the QD laser active region and the relaxation process of carriers into the QD ground state [18]....46

Figure 3.1 A schematic illustration of the undoped ten-layer InAs/InGaAs QD laser structure used in this research study....51

Figure 3.2 The TEM image of the InAs/InGaAs QD active region....52

Figure 3.3 The edge emitting RWG QD laser fabrication process....53

Figure 3.4 Cross-sectional SEM image of the RWG InAs/InGaAs QD laser....54

Figure 3.5 Diagram of the rapid thermal processor used for the annealing process....55

Figure 3.6 The mounted laser device, bonded wire and the G-S-G coplanar contacts....59

Figure 3.7 A schematic layout of a high frequency measurement equipment set-up, which involves a Vector Network Analyzer (VNA), a DC current source, a bias-T, a high-frequency

probe, a high-speed photoreceiver, and a temperature controller. 59

Figure 3.8 The frequency response of the photoreceiver. 60

Figure 3.9 The frequency response of the high-frequency probe. 61

Figure 3.10 The influence of bond wire inductivity on the transmission of the parasitic low-pass. The bandwidth is 9.5 GHz for 0 nH and 8.2 GHz for 0.5 nH, corresponding to a bond wire of a 25 μm diameter and a 600 μm length. 63

Figure 4.1 The temperature-dependent CW Power-current-voltage curve of the QD laser measured from 5 °C to 100 °C. 66

Figure 4.2 The lasing spectrum from the InAs/InGaAs QD laser (4×1100 μm^2) with an injection current of 100 mA at room temperature. 67

Figure 4.3 The small signal modulation response of the undoped QD laser measured at RT under different injection current levels. 68

Figure 4.4 The frequency response of the same undoped QD laser measured at 5 °C. 71

Figure 4.5 The frequency response of the same undoped QD laser measured at 50 °C. 71

Figure 4.6 The plot of the calculated thermal-limited (squares) bandwidth (BW), the damping-limited (circles) bandwidth, and the measured (triangles) bandwidth at different temperatures. 72

Figure 4.7 The plot of the dependence of the *D*-factor (solid circle) and the nonlinear gain compression (hollow circle) on the temperature. 73

Figure 4.8 The plot of the dependence of the *K*-factor on the temperature. 73

Figure 4.9 The plot of the differential gain at different temperatures. 74

Figure 5.1 The plot of ln(J_{th}) versus the temperature of the undoped as-grown (open square), 600 °C annealed (open circle), and 650 °C annealed (open triangle) QD lasers. 81

Figure 5.2 The plot of ln(J_{th}) versus the temperature of the *p*-doped as-grown (square), 600 °C annealed (circle), and 650 °C annealed (triangle) QD lasers. 83

Figure 5.3 The plot of η_d^{-1} against L for the undoped as-grown, 600 °C annealed and 650 °C annealed QD lasers at RT. 84

Figure 5.4 The plot of η_d^{-1} against L for the *p*-doped as-grown, 600 °C annealed and 650 °C annealed QD lasers at RT. 84

Figure 5.5 The net modal gain spectra as a function of the wavelength for the undoped as-grown QD laser with injection currents at (a) I=11×$I_{th,\mathrm{GS}}$, (b) I=11.9×$I_{th,\mathrm{GS}}$, (c) I=12.3×$I_{th,\mathrm{GS}}$, and (d) I=14×$I_{th,\mathrm{GS}}$. 88

Figure 5.6 The net modal gain spectra as a function of the wavelength for the undoped 600 °C annealed QD laser with injection currents at (a) I=15×$I_{th,\mathrm{GS}}$, (b) I=17.2×$I_{th,\mathrm{GS}}$, (c) I=17.8×$I_{th,\mathrm{GS}}$, and (d) I=18.9×$I_{th,\mathrm{GS}}$. 89

Figure 5.7 The net modal gain spectra as a function of the wavelength for the undoped 650 °C annealed QD laser with injection currents at (a) I=5×$I_{th,\mathrm{GS}}$, (b) I=5.4×$I_{th,\mathrm{GS}}$, (c) I=6×$I_{th,\mathrm{GS}}$, and (d) I=6.9×$I_{th,\mathrm{GS}}$. 90

Figure 5.8 The maximum net modal gain of the GS (solid square) and the ES (open square) emissions versus a normalized injection current for the undoped as-grown QD laser at RT. 91

Figure 5.9 The maximum net modal gain of the GS (solid circle) and the ES (open circle) emissions versus a normalized injection current for the undoped 600 °C annealed QD laser at RT. 92

Figure 5.10 The maximum net modal gain of the GS (solid triangle) and the ES (open triangle) emissions versus a normalized injection current for the undoped 650 °C annealed QD laser at RT. 93

Figure 5.11 The maximum net modal gain of the GS (solid square) and the ES (open square) emissions versus a normalized injection current for the *p*-doped as-grown QD laser at RT. 94

Figure 5.12 The maximum net modal gain of the GS (solid circle) and the ES (open circle) emissions versus a normalized injection current for the *p*-doped 600 °C annealed QD laser at RT. 95

Figure 5.13 The maximum net modal gain of the GS (solid triangle) and the ES (open triangle) emissions versus a normalized injection current for the *p*-doped 650 °C annealed QD laser at RT. 96

Figure 5.14 The EL spectra of the undoped QD lasers under an injection current level around the GS threshold. 97

Figure 5.15 The EL spectra of the *p*-doped QD lasers under an injection current level around the GS threshold. 97

Figure 5.16 The TEM images of the (a) as-grown, (b) 600 °C annealed and (c) 650 °C annealed QDs. 100

Figure 6.1 The plot of ln(I_{th}) versus temperature for the as-grown and annealed lasers with a 1 mm cavity length. 105

Figure 6.2 The plot of the PL spectra of the as-grown QD sample and the sample annealed at 600 °C for 15 s measured at 5 K. 106

Figure 6.3 The temperature-dependent emission wavelength of the two devices. 107

Figure 6.4 The plot of the reciprocal of external quantum efficiency η_d^{-1} as a function of the cavity length L for the as-grown QD lasers. 108

Figure 6.5 The plot of the reciprocal of external quantum efficiency η_d^{-1} as a function of the cavity length L for the annealed QD lasers. 109

Figure 6.6 The frequency response curves for the as-grown QD lasers measured at (a) 10 °C and (b) 70 °C. 111

Figure 6.7 The frequency response curves for the annealed QD lasers measured at (a) 10 °C and (b) 70 °C. 112

Figure 6.8 The emission wavelengths of the (a) as-grown and (b) annealed QD lasers at the corresponding injection currents at 70 °C. 114

Figure 6.9 The temperature dependence of the differential gain for the as-grown and annealed QD lasers. 116

Figure 6.10 The temperature dependency of the nonlinear gain compression (ε) for the as-grown and annealed QD lasers. 118

Figure 7.1 The frequency response of an as-grown QD laser with a cavity length of 1 mm, measured at 10 °C. 123

Figure 7.2 The lasing spectra of the same as-grown QD laser measured at (a) 280 mA and (b) 290 mA. 124

Figure 7.3 The frequency response of the 600 °C annealed QD laser with a 1-mm cavity length measured at 10 °C. 126

Figure 7.4 The lasing spectrum of the same annealed QD laser measured at 320 mA. 127

Figure 7.5 The measured bandwidth as a function of the normalized bias current $(I\text{-}I_{th})^{1/2}$ for the as-grown (circles) and annealed (squares) lasers at 10 °C. The hollow circle shows the bandwidth with ES lasing for the same as-grown QD laser. 128

Figure 7.6 The plot of $\ln(J_{th})$ versus temperature from 70 °C to 120 °C for the as-grown (square) and 600 °C annealed (circle) QD lasers. 130

Figure 7.7 The plot of the logarithmic values of the injection current ($\ln(I)$) versus the logarithmic values of the total spontaneous emission intensity ($\ln(L_{sp}^{1/2})$) for the as-grown and 600 °C annealed QD devices with cavity length of 2 mm at room temperature. The I_{th} of the as-grown and 600 °C annealed QD laser is 93.6 mA and 81.8 mA, respectively. 132

List of Tables

Table 2.1 The physics meanings of the symbols in Fig. 2.9 and in the rate equations below [18]. 45

Table 5.1 The internal quantum efficiency (η_i) and the internal optical loss (α_i) of the six QD laser samples. 85

Table 6.1 The internal quantum efficiency (η_i) and the internal optical loss (α_i) of the as-grown and annealed QD lasers at different temperatures. 109

List of Abbreviations

0-D	Zero Dimensional
2-D	Two-Dimensional
3-D	Three-Dimensional
A	
ASE	Amplified Spontaneous Emission
C	
CB	Conduction Band
CW	Continuous-Wave
D	
DFB-LD	Distributed Feedback Laser Diode
DI	De-Ionized
DOS	Density of State
E	
EL	Electroluminescence
ES	Excited State
F	
FP	Fabry-Perot
FWHM	Full-Width Half-Maximum
G	
GS	Ground State
H	
HR	High-reflectivity
I	
IPA	Isopropanol
I-V	Current-Voltage
M	
MBE	Molecular Beam Epitaxy
ML	Monolayer
MOCVD	Metal-Organic Chemical Vapor Deposition
P	
PAO	Pulsed Anodic Oxidation
PECVD	Plasma Enhanced Chemical Vapor Deposition

P-I	Light Output Power-Current
P-I-V	Light Output Power-Current-Voltage
PL	Photoluminescence
Q	
QD	Quantum Dot
QW	Quantum Well
QWr	Quantum Wire
R	
RT	Room Temperature
RTA	Rapid Thermal Annealing
RTP	Rapid Thermal Processor
RT-PL	Room Temperature Photoluminescence
RWG	Ridge Waveguide
S	
SA	Self-Assembled
SCH	Separate-Confinement-Heterostructure
SK	Stranski-Krastanow
SRL	Strain-Reducing Layer
T	
TEM	Transmission Electron Microscopy
U	
UV	Ultraviolet
V	
VB	Valence Band
W	
WL	Wetting Layer

Summary

The demand for bandwidth capacity is increasing exponentially due to the spread of high-speed internet services. A significant increase in capacity is achieved in fibre optical access networks. Semiconductor lasers operating at wavelengths around 1.3 μm, where the standard single mode fibre has minimum dispersion, are key components in such networks. Thus, they have attracted much research interest in recent years.

The discovery of self-organized epitaxial quantum dots (QDs) resulted in multiple breakthroughs in the field of the physics of zero-dimensional (0-D) heterostructures and allowed the advancement of optoelectronic devices. The most remarkable advancement involved lasers. The most advanced results obtained for lasers are based on the InGaAs/GaAs QDs by the Stranski-Krastanow growth. InAs is currently the most optimized candidate material for constructing low-cost and high-performance QD lasers on GaAs substrates because of its low threshold current density and its temperature insensitivity compared to lasers made from the conventional InGaAs/InP material system. Superior static performances have been demonstrated for 1.3 μm InAs/GaAs QD lasers. However, InAs/GaAs QD lasers have not fulfilled the initial expectation of demonstrating superior dynamic characteristics over Quantum Well (QW) lasers.

The aim of this research study is to characterize the performances of InAs/InGaAs QD lasers and to suggest a method to improve these performances through *p*-doping and post-growth rapid thermal annealing. A systematic study has been performed on undoped and *p*-doped ten-layer InAs/InGaAs QD lasers to

investigate the characteristic parameters related to lasing behaviour. The high-speed performance of these lasers will be targeted.

During this study, high-speed characterizations were carried out on undoped ten-layer InAs/InGaAs QD lasers. Their temperature-dependent frequency modulation was investigated from 5 °C to 50 °C. The modulation bandwidth of the intrinsic QD laser was found to be highly temperature sensitive. Although the intrinsic damping-limited modulation bandwidth of the InAs/InGaAs QD laser is as high as 23 GHz, the actual modulation bandwidth is limited by carrier thermalization under continuous-wave operations. A saturation of the resonance frequency was found to be the result of thermal reduction in the differential gain, which may originate from carrier thermalization in intrinsic QDs.

In order to improve the performance of the QDs, a series of experiments investigated the effects of *p*-doping and post-growth rapid thermal annealing (RTA) on the lasing behaviours of the QD lasers. *P*-doping improved the temperature dependent characteristics of the ten-layer InAs/InGaAs QD lasers. Meanwhile, an improved internal loss and a higher internal differential efficiency were demonstrated in both the undoped and *p*-doped InAs/InGaAs QD lasers under optimum annealing conditions. By analyzing the modal gain competition of the fabricated QD lasers from the below-ground-state (GS) to the above-excited-state (ES) thresholds, we found that: (i) the onset of ES lasing can be significantly delayed to a higher injection current with optimum annealing conditions, and, (ii) under the same annealing condition, *p*-doped QD lasers can sustain GS lasing to a higher operating temperature compared to the intrinsic ones. A faster carrier relaxation mechanism was produced in QDs under optimum annealing conditions and this is expected to improve the high-speed

modulation characteristics of the QD lasers.

QD intermixing has been expected to improve the carrier capture and relaxation and, hence, the high-speed performance of QD lasers. Followed by the successful enhancement of GS lasing in the undoped QD laser with optimum annealing, investigations were carried out to study the effects of intermixing on the high-speed characteristics of the undoped ten-layer InAs/InGaAs QD lasers. Improvements in the temperature stability of the modulation bandwidth were demonstrated in the undoped QD lasers under optimum annealing conditions. The increase in bandwidth at a high temperature from the annealed QD lasers could be due to the reduction in the temperature dependency of the differential gain and the improvement in the internal quantum efficiency. These improvements are attributed to the defects removal, the reduction of the carrier relaxation time in the order of 10^{-1} ps and the better dots uniformity after optimum RTA. These findings are beneficial for the development of uncooled high-speed QD lasers in fibre optical access networks.

Finally, further investigations studied the effects of post-growth RTA on the high-speed characteristics of the *p*-doped ten-layer InAs/InGaAs QDs where Auger-related recombination processes are more severe. In the *p*-doped QD lasers, an almost 18% improvement in the modulation bandwidth and an approximately 45% improvement in the modulation efficiency were obtained from the annealed QD lasers compared to the as-grown ones. Through measurements of the total spontaneous emission intensity, the observed improvements in the *p*-doped QDs are believed to be due to the reduction in the Auger-related recombination processes and the reduction in the defects density in the *p*-doped QDs upon annealing.

Chapter 1: Introduction

In the past decade, the increasing use of broadband internet services has pushed the copper-wire based access network to its limits [1]. This thirst for speed has exceeded even recent predictions and it has been driven partly by the increased downloading or streaming of video content over the Web, the unanticipated success of high-definition television, and the growing popularity of exchanging photographic, video, and audio content. A significant increase in capacity is achieved in fibre optical access networks, known as fibre-to-the-home (FTTH) or fibre-to-the-premise (FTTP) [1]. Higher performance photonic components are required to assist the transition technology from the point-to-point optical communications systems to these networks.

Semiconductor double heterostructure lasers, the critical components in the fibre communication systems, have the advantages of low power requirements, small size, and cost-effectiveness. Semiconductor lasers emitting at 1.3 μm, where the standard single-mode fibre has minimum dispersion, are key components in fibre optical access networks. Thus, they have attracted much research interest in recent years. The discovery of self-organized epitaxial quantum dots (QDs) resulted in multiple breakthroughs in the field of the physics of zero-dimensional (0-D) heterostructures and allowed the advancement of optoelectronic devices (most remarkably, lasers). The most advanced results obtained for lasers based on the InGaAs/GaAs three-dimensional (3-D) QDs by the Stranski-Krastanow (SK) growth [2].

1.1 Background

Semiconductor heterostructures with self-organized QDs have been studied intensively due to their unique physical properties for high-speed telecommunication applications. Carrier confinements in quasi-zero dimensional QD structures, which behave electronically like artificial atoms, have the potential to achieve a high material gain and a high differential gain (and, thus, a high modulation speed), owing to the fact that the carrier relaxation in the self-organized QDs could be very fast. This expected high modulation speed from QDs has attracted increasing research interest. Through decades of research, the static performances of QD lasers have largely surpassed those of Quantum Well (QW) lasers (at least in the most optimized material system, InAs/GaAs) in several device parameters: threshold current density, temperature-insensitivity, and the linewidth-enhancement factor. The promising optical properties of QD lasers, such as a large differential gain, large cutoff frequencies, and a small chirp, were reported for emission wavelengths less than 1.2 μm [3]. Recently, pioneering results of 22 GHz modulation from QD lasers emitting at 1 μm have been reported [4]. The researchers implemented a tunnel junction for the current injection in the structures of these lasers in order to avoid 'hot' carrier effects. However, achieving a uniform current injection to a multistack of QDs and the precise control of the tunnel junction layers remains difficulties.

However, the dynamic properties of QD lasers emitting at 1.3 μm and above (i.e. at a long wavelength) have not fulfilled the initial expectations for high-speed operation. The highest reported intrinsic modulation bandwidth for 1.3 μm QD lasers is 12 GHz for an undoped InGaAs/GaAs QD laser [5]. The reported modulation speed of the conventional separate-confinement-heterostructures (SCH) 1.3 μm QD laser is limited to 6 to 8 GHz [6, 7], which is still far below the reported value of the QW

lasers [8]. Compared to their QW counterparts, the frequency responses of QD lasers are likely to be limited by their higher gain compression [9] and their slower carrier capture and relaxation mechanisms, etc. [10, 11]. The carrier dynamics behind the high-speed modulation of the QD lasers are much more complicated than the carrier dynamics of the QW lasers.

Through intensive studies of these carrier dynamics, several physical mechanisms have been proposed to be the origin of the bandwidth limitations in QD lasers. The first mechanism is that inhomogeneous broadening caused by the QDs' stochastic size distribution reduces both the optical gain and the differential gain. Currently, the most promising method of fabricating QDs is based on the effect of spontaneous nanoislanding during heteroepitaxial growth by either molecular beam epitaxy (MBE) or by metal-organic chemical vapor deposition (MOCVD). Although the above-mentioned self-organization methods for the production of nanostructures have been used successfully in the fabrication of small, defect-free QDs, their potential in optoelectronics and nanoelectronics are severely hampered by their large spread in size distribution through thermal fluctuations and by the complexity of the growth-process involved. Recently, Deppe *et al.* [12] proposed that inhomogeneous broadened QDs may limit the high-speed modulation response due to the slow electron transportation in the wetting layers (WL) between the lasing QDs and the non-lasing QDs.

This second mechanism proposed to be the origin of the bandwidth limitations in QD lasers results from the closely spaced energy levels of the confined holes and, thereby, the thermally activated escape of carriers from the QDs to the surrounding GaAs matrix. The bandwidth drops dramatically with increasing operation temperature. These researchers focused on the thermalization of holes in the density

of states (DOS) due to their closely spaced discrete energy levels. Dennis *et al.* [13] investigated the role of the DOS in limiting the modulation response of QDs with deep confinement potentials such as 1.3 μm InAs/GaAs QD lasers.

This third mechanism proposed to be the origin of the bandwidth limitations in QD lasers results from the hot-carrier effect and the associated gain compression due to the large DOS of the WL and the barrier states compared with those in the QWs [13, 14]. The carrier heating forces the injected carriers out of the lasing states of SCH and causes leakage to the adjoining layers. As a result, the conventional QD devices cannot be modulated at bandwidths above 8-10 GHz.

In addition, the fourth mechanism proposed to be the origin of the bandwidth limitations in QD lasers, is their slow carrier relaxation. Fiore *et al.* [15] studied the effects of intradot relaxation on the *K*-factor and the differential gain factor. The effects of maximum model gain and effective carrier capture time on the *K*-factor were studied by Ishida *et al.* [16]. In QDs, electrons are injected into the WL by forwarding bias currents, are captured by the excited state (ES), and then they quickly relax to the ground state (GS) where they reside for recombination [17]. Discrete sublevels in QDs may hinder carrier relaxation towards the ground level (i.e. the GS). In addition, a carrier may recombine to emit at higher levels (i.e. the ES) or go to the nonradiative channel during a carrier cascade toward the ground level.

1.2 Motivations and Objectives

The previous section shows that four unique problems limit the optical performances of the conventional QD lasers. Their performances fall far short of what is expected from an 'ideal' QD laser with a discrete DOS. The problems can be summarized as:

1. The inhomogenous linewidth broadening, associated with the stochastic size distribution of the dots, imposes a limit on the performance of QD lasers.
2. The hole distribution is thermally broadened into many available states with small energy spacing in QDs. Therefore, a large injected hole density is required for a large gain in the ground state.
3. QD lasers suffer from significant hot-carrier effects and the associated gain compression due to the large DOS of the WL and the barrier states compared with those in the QWs.
4. The carrier capture and relaxation into the QD discrete levels are significantly slowed due to a lack of phonons available to satisfy the energy conservation rule [18]. This thus limits the high-speed performance of QDs.

Researchers have proposed several methods to solve these problems. For example, *p*-type modulation doping has been proposed to compensate for the thermally escaped holes [8]. However, large modulation bandwidths and ultralow threshold currents were not observed in QD lasers with *p*-doping, probably due to a modest increase in the differential gain in the *p*-doped QDs [3, 13]. In order to solve the hot-carrier problem, Bhattacharya *et al.* [19] proposed the tunnel injection method incorporated with *p*-doping where electrons are introduced directly into the lasing states by tunnelling. However, even with this approach, the modulation bandwidth at 1.3 μm only extends from 8 GHz to 11 GHz [14]. Furthermore, the realization of a proper tunnel injection by growth could be difficult.

In order to overcome these growth difficulties and improve the material qualities of QDs, post-growth thermal annealing has been proposed to modify the

potential profile and, thus, the optical properties of the quantum-confined heterostructures [20]. In recent years, the approach of post-growth intermixing (interdiffusion) has offered simple, more practical schemes for photonic integrated circuits (PICs) through the modification of the potential profile and, thus, the optical properties of the quantum-confined heterostructures. QW intermixing (QWI), a post-growth bandgap tuning technique, has been employed successfully to tune the wavelength of QW devices. Over the last decade, visible improvements have been reported on the annealed QW devices in aspects such as threshold current, power efficiency, lateral electrical and optical confinement [21-23].

Compared to the QW heterostructures, the intermixing effect is expected to play a more important role in the QD heterostructures due to their large surface area and the strain effect that encloses the QD materials [24]. In addition, the typically small dimension of the QDs renders the intermixing effects more significant in changing the band structure and the optical properties of the material. Therefore, the interdiffusion behaviour in QDs is much more complicated. Research has shown that post-growth annealing affects both the height and the shape of the QD confining potential without killing its zero-dimensional (0-D) DOS, hence changing the transition energies and the intersublevel spacing [25-27]. Several reports show that it is possible to retain the 3-D confinement in QDs after high temperature annealing [28-30], a finding that is crucial for the research on QD intermixing. This suggests the post-growth control of the bandgap and, hence, tuning of the emission wavelength could be achieved if this technique is utilized in the QD laser devices. The decrease of the ground state (GS) photoluminescence (PL) linewidth, with the increase of the intermixing, indicates that the QD size and strain inhomogeneities, which are considered the main drawback of current self-assembled (SA) QDs, can be effectively

reduced by intermixing. Researchers have found that the inhomogenous linewidth broadening, associated with the stochastic size distribution of the dots, imposes a limit on the high-speed performance of QD lasers. The reduction in QD size distribution, suggesting an improved QD material quality resulting from the thermal annealing, is of prime importance for the development of practical QD devices [28-31]. In addition, it has been shown by Marcinkevicius *et al.* [30] that intermixing will improve the carrier lifetime and will reduce the carrier capture and relaxation time, producing a potentially improved modulation speed after intermixing.

Following the success of thermal annealing performed on the QW lasers and the advancement in the QD material systems, strong advantages and necessities prompt the investigation of the annealing effects on the QD laser devices. Although numerous studies of the intermixing effects on the properties of GaAs-based QD materials have been conducted, most of these studies were performed with nonpractical p-i-n QD structures [24, 25]. Few studies (apart from Djie *et al.*'s works about InAs/InAlGaAs quantum dash lasers on an InP substrate [32, 33]) have investigated the intermixing effects on the actual QD laser devices. This lack of research regarding annealed QD laser devices, especially the high-speed modulation characteristics, opens the research gap for us to answer the question about how post-growth annealing affects the performances of QD lasers. Improvements of the characteristic parameters related to the lasing operation are expected to be achieved after the optimization of the post-growth annealing conditions.

This study also aims to find out how *p*-doping affects the optical properties of the QD lasers and the post-growth rapid thermal annealing (RTA) of the QDs. All of these research gaps strongly motivate us to fill in the unanswered blanks and to seek innovative solutions for the performance limitations of the QDs. The successful

development of this technique will open up new research windows for QD lasers by modifying the device performance with an attractive means of simple and cost-effective post-growth control.

In view of the promising potential of the multiple-layer InAs/InGaAs QD laser structure operating at 1.3 μm fibre optical communication system, the objectives of this project are to:

1. Investigate the high-speed modulation limitations and the temperature-dependent behaviours of the ten-layer InAs/InGaAs QD lasers.
2. Understand how *p*-doping affects the gain behaviours and the temperature-dependent characteristics of QD lasers.
3. Investigate the effects of the rapid thermal annealing process on the undoped and *p*-doped InAs/InGaAs QD materials and devices. The role of *p*-doping on the annealing effects is analyzed. The two-state lasing competitions of the annealed QD laser devices with different annealing conditions are studied for both undoped and *p*-doped QD lasers.
4. Study the effects of intermixing on the high-speed characteristics of the undoped and *p*-doped QD devices based on the optimum annealing conditions. The characteristic parameters of the annealed QD lasers under optimum annealing condition are compared with those of the as-grown QD lasers.
5. Suggest and develop a method to improve further the optical performances of the QD lasers.

1.3 Major Contributions

In this thesis, ten-layer InAs/InGaAs QD structures are investigated for the development of future uncooled high-speed fibre optical networks. This study investigates the QD lasers with a narrow ridge waveguide (RWG) structure to reach the design requirements for practical device applications. The bandwidth limitations of the intrinsic QD lasers are investigated. The role of *p*-doping on the temperature-dependent characteristics of QD lasers is studied. Based on the understanding of the roles that *p*-doping and intermixing play in the QD materials, the post-growth rapid thermal annealing technique is introduced to both the undoped and *p*-doped QD laser structures. The results demonstrate that the laser characteristic parameters could be improved by utilizing the thermal annealing process under the optimized conditions. Most importantly, the high-speed characteristics can be improved through optimized annealing. The ability to control the device performance without a re-growth of the QD material structure suggests that rapid thermal annealing may improve the performance of the QD-based systems and thus help to realize their potential application in optoelectronics and nanoelectronics. A list of the significant contributions of this research study is provided below:

A high modulation bandwidth is the primary requirement for fibre optical access networks. We investigated the bandwidth limitations of the intrinsic ten-layer InAs/InGaAs QD lasers. Specifically, the influence of thermal effects on the high-speed performance of 1.3 μm undoped QD lasers with a narrow RWG was explored in a wide temperature range. The role of the temperature-dependent differential gain and the nonlinear gain compression factor in determining the modulation bandwidth was analyzed. While the intrinsic damping-limited modulation bandwidth reaches as high as 23 GHz, the actual modulation bandwidth is limited by

carrier thermalization under continuous-wave operation. The calculation of the temperature-dependent bandwidth of the undoped QD laser showed a close agreement between the thermal-limited bandwidth and the measured results. A saturation of the resonance frequency was found to be the result of thermal reduction in the differential gain, which may originate from carrier thermalization. Therefore, the bandwidth of the undoped InAs/GaAs QD lasers is limited mainly by thermal effects, which may result from carrier thermalization in the undoped QD laser structure.

Post-growth RTA was used to investigate the structural and performance changes in the undoped and *p*-doped QD lasers in this research study. We studied the effects of annealing and *p*-doping on the two-state lasing competition of 1.3 μm InAs/InGaAs QD lasers by analyzing the modal gain competition from the below-ground-state (GS) to the above-excited-state (ES) thresholds. In comparison with the as-grown QD lasers, both undoped and *p*-doped QD lasers exhibited enhancement (suppression) in GS (ES) lasing with annealing at 600 °C for 15 s and they exhibited suppression (enhancement) in GS (ES) lasing with annealing at 650 °C for 15 s. The enhancement of GS lasing is believed to be due to the removal of nonradiative recombination centres, together with the reduction in carrier relaxation time and the increase in the relaxation efficiency. The suppression of GS lasing for QD lasers annealed at the higher temperature (650 °C for 15 s) is believed to be due to carriers leaking out from the shallower interdiffused QD potentials. This implies that the onset of ES lasing could be delayed significantly to a higher injection current under optimum annealing conditions. Therefore, in order to improve the GS lasing of the QD lasers, the optimum annealing condition was determined to be 600 °C for 15 s.

In addition, the effects of *p*-doping on the optical characteristics of QDs and on the annealing effects were investigated. The temperature-dependent threshold

current density and the modal gain behaviours were studied. For QDs annealed under the same conditions, *p*-doped lasers were found to: (i) sustain GS lasing to higher operating temperature and exhibit infinite characteristic temperature T_o but to (ii) have a poorer differential efficiency and a poorer internal loss compared to the intrinsic ones. Moreover, *p*-doped QDs have been found to be more resistant to annealing. Therefore, a tradeoff exists in the laser performances and the choice of intrinsic or *p*-doped QDs will depend on the applications. This insight could provide guidance to a future study on the *p*-doping effect in QD lasers.

Following the successful enhancement of GS lasing by optimum thermal annealing performed on the ten-layer InAs/InGaAs QD structures, a high-speed modulation study was performed on the undoped QD lasers. The characteristic temperature was enhanced by a factor of 2.3 upon optimum annealing. The temperature-dependent modulation results demonstrated improvements in the temperature stability of the bandwidth. The differential gain was increased and the nonlinear gain compression was reduced in the annealed QD laser. The increase in the bandwidth at a high temperature from the annealed QDs could be due to an increase in the internal quantum efficiency and a reduction in the temperature dependency of the differential gain. The carrier capture and relaxation to the GS may have been enhanced after RTA. More importantly, the temperature stability of the high-speed modulation parameters was improved after the optimum RTA. We attributed these improvements to the following factors: (i) a better dots uniformity and (ii) a reduction in the carrier relaxation time in the order of 10^{-1} ps.

Eventually, the high-speed modulation was carried out for the as-grown and annealed *p*-doped ten-layer InAs/InGaAs QD lasers where Auger-related recombination processes are more severe. For the *p*-doped QD lasers, with reference to

the as-grown QD laser devices, significant improvements in the modulation bandwidth and in the modulation efficiency were obtained from the annealed QD lasers. The observed improvements were due to: (i) the removal of defects, which act as nonradiative recombination centres in the QD structure, and (ii) the reduction in the Auger-related recombination processes in the *p*-doped QDs upon annealing. These encouraging results suggest that the RTA is an attractive approach to modify the dynamic characteristics of InAs/InGaAs QD lasers if its condition is carefully designed. This finding is significant for the development of uncooled high-speed QD lasers.

1.4 Organization of the Thesis

This thesis is organized into eight chapters. In this chapter, Chapter 1, the background, the motivations, the objectives of this research, and a brief account of the major contributions were documented followed by a description of the organization of the thesis and a list of the author's publications.

Chapter 2 provides the development of GaAs-based QD material, the background of QD physics, the introduction of the *p*-type modulation doping technique, the review of post-growth thermal annealing techniques, and the fundamental characteristics of the QD ridge waveguide lasers investigated in this work.

Chapter 3 describes the QD material structure used in this work, the device fabrication process, the details of the experimental set-up, and the characterisation techniques.

Chapter 4 examines the bandwidth limitations of the intrinsic QD lasers. The temperature-dependent modulation is analyzed. The roles of carrier thermalization

and intrinsic damping in affecting the high-speed modulation characteristics of QD lasers are summarized.

Chapter 5 demonstrates the lasing characteristics in QD lasers based on the *p*-doping and thermal annealing techniques. The lasers' parameters are improved by *p*-doping. The device performances under different annealing conditions are investigated. The competition between the ground state and the excited state in short cavity length lasers is studied. Finally, the effect of *p*-doping on the intermixing introduced by thermal annealing is investigated.

Chapter 6 reports the high-speed modulation characteristics of the undoped QD lasers under the optimum annealing condition. High-speed modulations under different temperatures are analyzed. Comparisons of the differential gain and the gain compression are carried out between the undoped as-grown and annealed QD lasers. The effect of annealing on the temperature-dependent carrier dynamics in the intrinsic QD lasers is also studied.

Chapter 7 demonstrates further studies on the annealing effects where the high-speed modulation characteristics of the *p*-doped QD lasers under optimum annealing condition are studied. The dominated carrier recombination mechanisms before and after annealing are analyzed.

Chapter 8 provides the conclusions of the thesis and suggests some recommendations for future research. In particular, recommendations are given in order to achieve a higher modulation speed from short cavity length QD lasers. Further investigations of the intermixing effects on QDs at higher annealing temperatures should be carried out. The dependence of the device performance on the device geometry is also highlighted.

Chapter 2: Literature Review

Since the last decade, self-organized QD lasers have been studied intensively. In this chapter, basic QD physics will be reviewed followed by the discussion of the several techniques used so far to improve the characteristics of QD lasers, especially their dynamic properties. In addition, the fundamental characteristics of QD lasers will be summarized.

2.1 Quantum Dot Lasers

In heterostructure lasers, the idea of 'exploiting quantum effects in heterostructure semiconductor lasers to produce wavelength tunability' and of achieving 'lower lasing thresholds' via 'the change in the density of states which results from reducing the number of translational degrees of freedom of the carriers' was introduced by Dingle and Henry in 1976 [34]. The main advantage of using size-quantized heterostructures in lasers was expected to originate from the increased density of states (DOS) for charge carriers near the band edges. When used as an active medium of a laser, this results in a concentration of most of the injected non-equilibrium carriers in an increasingly narrow energy range near the bottom of the conduction band (CB) and the top of the valence band (VB), which enhances the maximum material gain and reduces the influence of temperature on the device performances. Electron confinement within a sufficiently narrow region of semiconductor material can significantly change the energy spectrum. Since all of the dimensions are comparable to the de Broglie wavelength, the carriers within the QDs are confined in all three dimensions.

The performances of QD lasers are superior to those of other semiconductor quantum nanostructures (the bulk semiconductor, the QW laser, and the Quantum Wire (QWr) laser) due to the 3-D carrier confinement from the isolated QD island of 0-D freedom for electrons. Figure 2.1 compares the DOS functions of the various dimensional systems and shows that the carrier confinement increases from 0-D to 3-D as the system moves from bulk to QD.

For bulk materials at a low temperature, the injected electrons fill all of the available states from the band edge. However, as the temperature increases, the carriers begin to spread to higher energy states according to the Fermi-Dirac distribution. Therefore, high threshold currents and high temperature-sensitivity characterize bulk semiconductor lasers. For a QW laser with a step-like DOS at each sub-band edge and a high concentration of injected carriers having the same energy, population inversion can be achieved at an earlier stage with lower threshold currents. However, because of the nature of two-dimensional (2-D) quantization in QWs, QW lasers remain somewhat temperature sensitive. In some applications, this temperature sensitivity requires complicated and expensive circuitry to be installed in order to overcome these effects and maintain a constant output power.

QD is the ultimate example of size quantization. It represents a semiconductor crystal with the size of several nanometres coherently inserted into a larger bandgap semiconductor matrix. In the ideal QD, the DOS consists of a series of δ functions (as shown in Fig. 2.1) and, therefore, population inversion can be achieved in principle with the injection of only one electron-hole pair per dot. This achievement is the origin of the low threshold advantage that is claimed for the QD lasers. The prediction of a temperature-insensitive threshold current for a QD laser was made in 1982 [35].

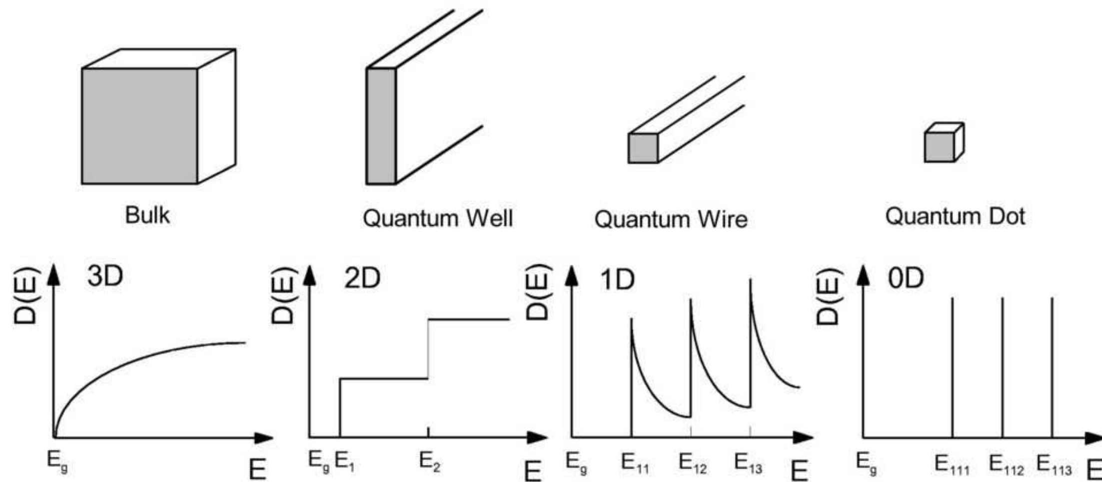

Figure 2.1 The active region presented and the DOS functions of the semiconductor bandgap for bulk, QW, QWr, and QD lasers [36].

The first self-organized InGaAs QD laser was realized by Kirstaedter *et al.* in 1994 with a threshold current density of 120 A/cm^2 at 77 K [37]. In 1996, room temperature operation was demonstrated for similar InGaAs/GaAs QD structures [38]. However, at room temperature and above, the threshold current density remained relatively high and the devices tended to lase via QDs excited states (ES) for both short and moderate cavity lengths. The device parameters remained worse than those of the best QW devices did for some time due to the thermally activated escape of carriers from the QDs to the surrounding GaAs matrix, which was then realized as the main obstacle for high performance QDs.

In order to improve the material properties and the device performances, the approach of establishing a multiple-layer-stacked QDs structure as the active region of the laser device was represented by Ledentsov *et al.* in 1996 [39]. This multiple-layer-stacked QDs structure increased the density of the QDs, where a stable ground state (GS) lasing with a reduced threshold current density of 90 A/cm^2 at room temperature was demonstrated. A further reduction of the threshold current density to 13 A/cm^2 was achieved in lasers with triple stacks of QDs [40]. The characteristic

feature of the lasers based on vertically coupled QDs is the gradual decrease in the threshold current density with the increase in the number of QD planes, which is explained in terms of the prevention of gain saturation on the QD ground state [41].

It is well-known that the surface density (N_{QD}) of a QD layer is one of the key factors affecting the performance of a QD laser diode [41]. In a single-layer QD, the achievable modal gain, which is limited by saturated gain (G^{sat}), is proportional to the surface density (i.e. $G^{sat} \propto N_{QD}$). The finite N_{QD} in a SA single-layer QD structure directly limits the available optical gain in the GS, which leads to undesirable ES lasing at a high current and/or a high temperature [42]. Due to the low optical confinement factor, the GS modal gain for a single QD sheet is typically 4 cm^{-1}. Salhi *et al.* [43] reported a GS modal gain exceeding 41 cm^{-1} from a QD laser with seven QD layers. In general, the higher the number of QD layers, the less pronounced the effect of gain saturation. However, a further increase in the number of QD layers will bring growth difficulties, resulting in threading dislocations due to the accumulated strain in the layers. To date, the optimum value of the stack number is ~ten for high performance QD lasers, which demonstrate a high output power and a reasonably low threshold current density [44].

2.2 *P*-type Modulation Doping Technique

In the early days, InAs and InGaAs QD lasers did not achieve better performances over planar QW lasers, both statically and dynamically, due to their closely-spaced hole energy levels [45]. This closely-spaced hole energy level resulted in the thermal broadening of the hole states at a high temperature. The thermal broadening of the hole states will decrease the attainable GS gain and the differential gain in conventional QDs and make the maximum gain highly temperature sensitive

[45]. However, a large injected hole density is required for a large gain in the GS. Recently, the acceptor (*p*) doping of the dots was proposed to solve this problem, thereby improving the temperature characteristics and the gain of QD lasers [8, 46, 47]. By applying *p*-doping to the QDs, excess holes are introduced (refer to Fig. 2.2 for the carrier distribution for the undoped and *p*-doped QDs) so that the GS of the QDs is always filled by holes [45].

These extra holes ensure a population inversion with less injected holes from the contacts. Consequently, the electron population in the dots and their leakage into barrier layers and waveguide layers are reduced as well (refer to Fig. 2.3 [19]). Therefore, the temperature dependence of the gain is established predominantly by the electron energy levels, which are widely spaced in energy. Therefore, the effect of the closely-spaced hole energy levels can be suppressed at higher temperatures. In this manner, the characteristic temperature (T_o), the gain and the differential gain of QD GS lasing can be enhanced and the deleterious effects are reduced (such as gain saturation due to hot carriers and carrier leakage associated with the thermal broadening of holes). *P*-doped QDs demonstrated a faster carrier relaxation and capture and allowed GS lasing in shorter cavities and at higher temperatures [48-50]. Wei *et al.* [51] concluded that the photon density saturates at high currents because of a rapid increase of the threshold current. This rapid increase is caused by a thermally activated leakage of holes as the temperature increases with the increasing injection current, which has a significant effect on the resonance frequency [13, 16, 52, 53]. Improvements of bandwidth have been predicted theoretically due to the enablement of a shorter cavity length from the increased maximum gain through *p*-doping [13]. Furthermore, the excess holes provided by *p*-doping can occupy the wetting layer (WL) states, which may severely limit the potential benefits of this technique [3, 54].

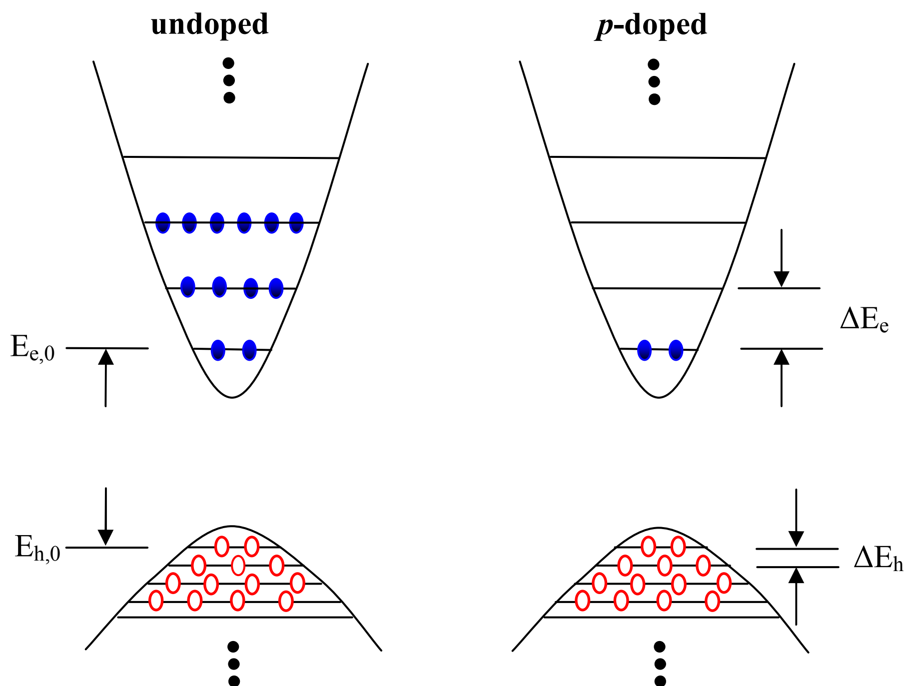

Figure 2.2 A schematic illustration of the QD energy levels with different built-in carrier distributions for the undoped and *p*-doped structures.

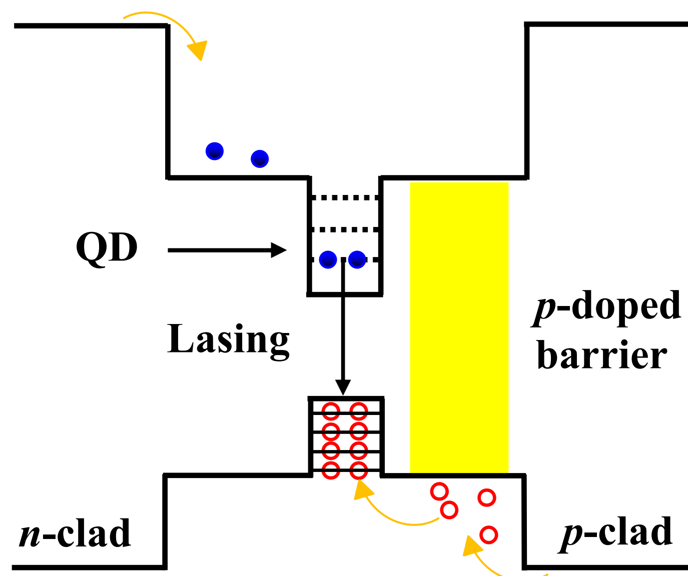

Figure 2.3 The modulation *p*-doping of the QD barrier in order to increase the gain through the increase of the hole ground state occupancy [19].

2.3 Rapid Thermal Annealing Technique

The post-growth annealing technique is a simple and effective method that modifies the structural and optical properties of the semiconductor structure to avoid the re-growth process. Normally, atomic interdiffusion or intermixing will occur during high temperature annealing treatments. The interdiffusion effect is expected to play an important role in QDs because of their large surface-area-to-volume ratio compared to bulk or QW structures [55, 56]. In the current InGaAs/GaAs QD systems, since the dimension of the QDs is typically in the order of a few nanometers, a small interdiffusion between the dots and the surrounding materials is expected to produce a significant change in the band structure and in the optical properties of the materials (see Fig. 2.4) [55].

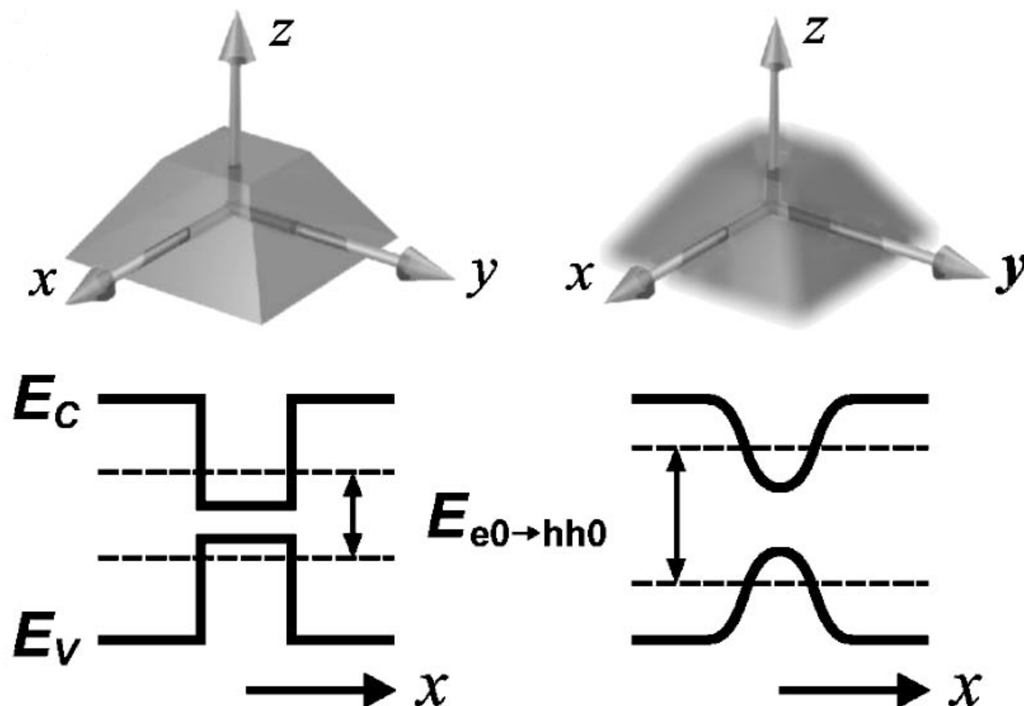

Figure 2.4 Interdiffusion smears the alloy distribution, resulting in band gap disordering in 3-dimensions. Band gap profiles for the noninterdiffused (left) and the interdiffused (right) QD along the x direction are shown [55].

The QD intermixing (QDI) technique is believed to be capable of both improving the performance of the active QD media and integrating the active QD sections with a passive waveguide [57]. Therefore, intense research studies on the effect of QDI have been conducted in the last few years [27, 58]. Rapid thermal annealing (RTA) has been found to result in the interdiffusion of the In and Ga atoms between the QDs and their cap layer, hence modifying the QD size, shape and composition. Intermixing has been found to be a powerful tool to adjust the transition energy and the sharpness of the photoluminescence (PL) transitions [59]. In the early stage of QDI, the nondestructive PL measurement was applied with promising results [28, 30]. An observable narrowing and blueshift in the PL spectra, directly caused by the interdiffusion between QDs and their surrounding cap layer, indicated an improved optical property and tunability of the band gap that is necessary for device applications.

In order to investigate the interdiffusion behaviour in the QD structure better, several methods have been performed both experimentally and theoretically [28, 30, 55, 60]. Time-resolved photoluminescence (TRPL) with subpicosecond temporal resolution can provide the information about the various carrier transportation times, such as carrier lifetime, capture time, and relaxation time. A theoretical 3-D QD diffusion model combined with experimental PL measurements and transmission electronic microscopy (TEM) was proposed to determine the effect of annealing-induced interdiffusion on the electronic energy levels and energy variation in the dot ensemble [55]. A significant decrease of the radiative carrier lifetime has been obtained by Malik *et al.* through an experimental study of intermixed QDs [60]. The PL rise time, which accounts for the carrier transport in the barriers, capture, and relaxation in the QDs', has been observed to decrease after annealing (see Fig. 2.5)

[30]. Therefore, an improved high-speed performance is highly expected from QDI.

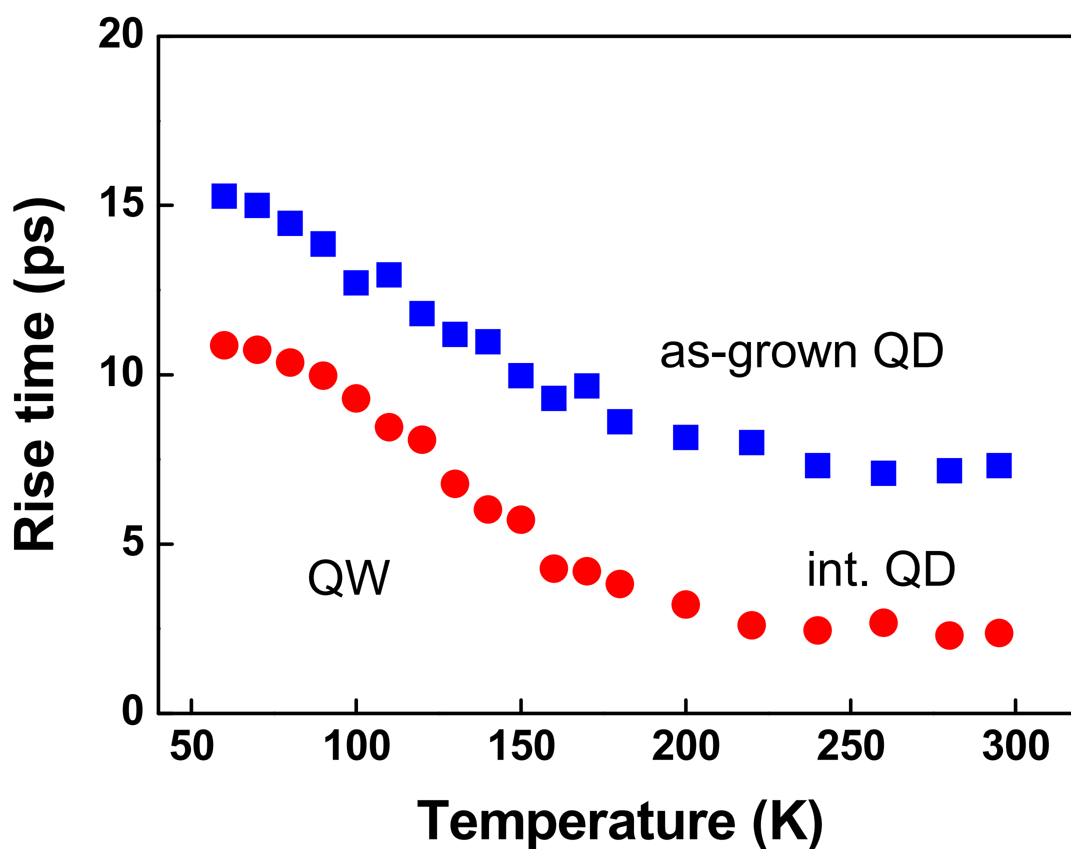

Figure 2.5 The temperature dependence of the PL rise times for QW, as-grown QD, and intermixed QD at an average excitation intensity of 2.5 mW [30].

Preliminary intermixing studies on InAs/InGaAs Dots-in-a-Well (DWELL) structures grown by MBE have been carried out in our research group [61]. Improvements in the PL intensity have been shown for the undoped and *p*-doped samples annealed at 590 °C and 600 °C (refer to Fig. 2.6). Furthermore, the *p*-doped sample exhibited a higher thermal energy onset for the occurrence of significant intermixing, which is due to the presence and diffusion of Be atoms in the *p*-doped structure [61].

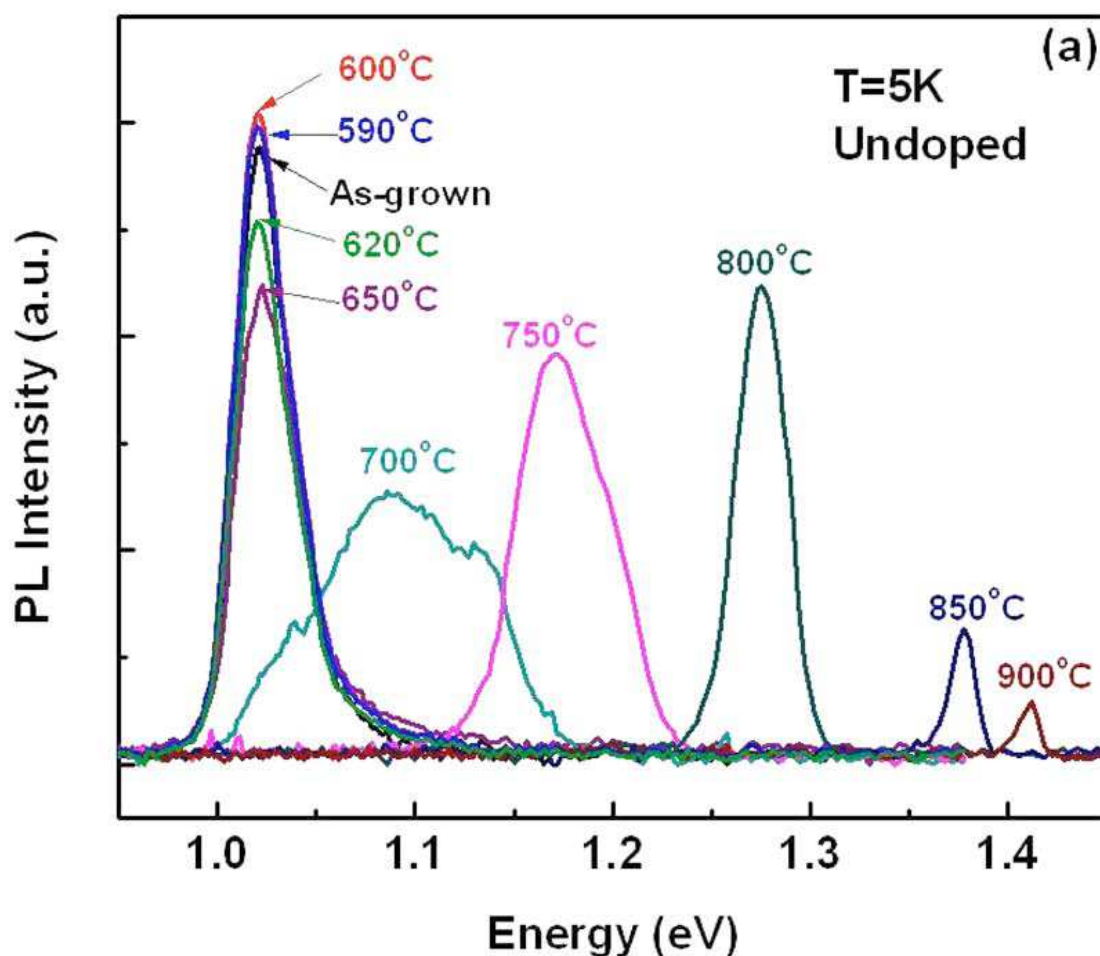

(a)

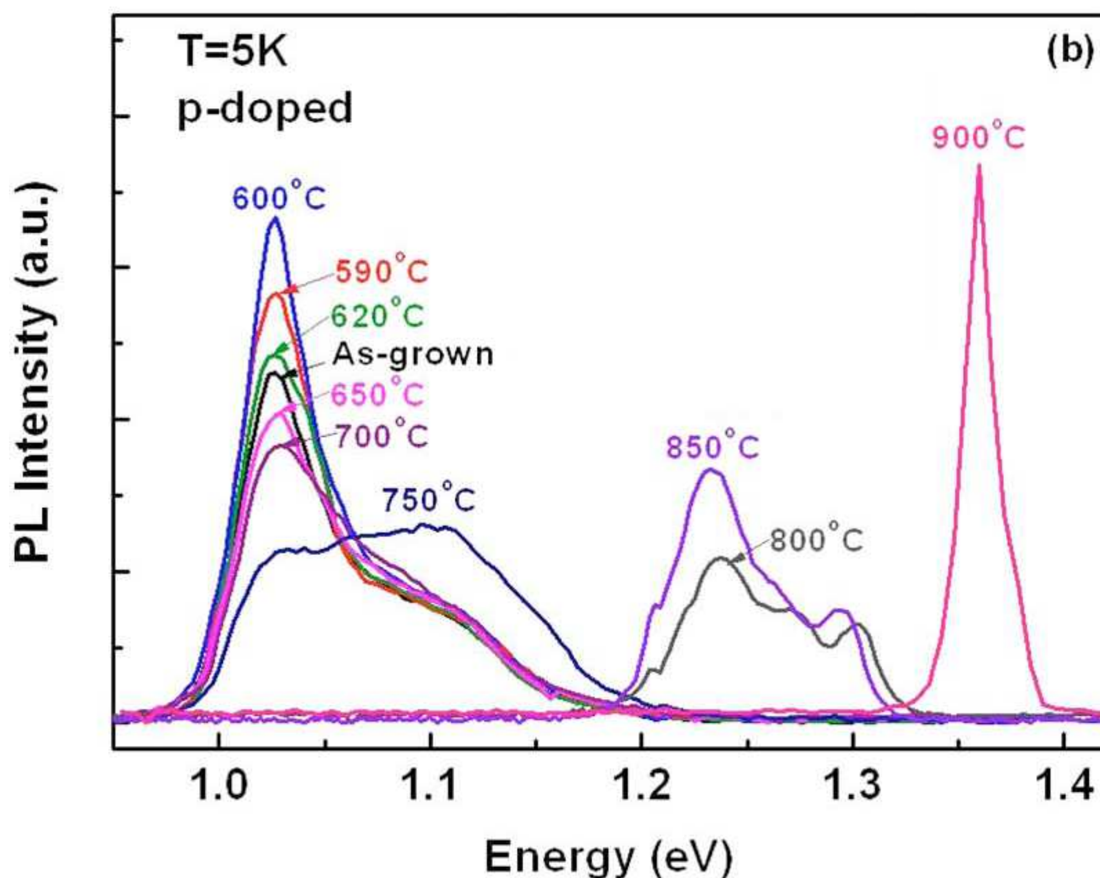

(b)

Figure 2.6 The PL spectra at 5 K after annealing at different temperatures for 30 s from (a) an undoped InAs QD structure and (b) a *p*-doped InAs QD structure [61].

In addition, experimental evidences have shown that intermixing can greatly reduce the inhomogeneous broadening by producing better dot uniformity [28-31]. Researchers have found that the inhomogenous linewidth broadening, associated with the stochastic size distribution of the dots, imposes a limit on the performance of QD lasers. Recently, Deppe *et al.* [12] proposed that inhomogeneous broadened QDs may limit the high-speed modulation response due to the slow electron transportation in the WL between the lasing QDs and the non-lasing QDs.

2.4 Fundamental Characteristics of QD Lasers

The word 'laser' is an acronym for light amplification by stimulated emission of radiation. However, today, laser commonly means 'a light generating device' [62]. Three elements are necessary to build a laser: a gain medium, an optical resonator, and a pump source.

The first realization of lasing in QD materials was observed in 1994 [63]. In order to achieve lasing, proper electrical and optical confinements are required for a laser. In this research study, we focus on GaAs-based QD narrow ridge waveguide (RWG) lasers. The schematic for these lasers is shown in Fig. 2.7.

Multiple QD layers are inserted in the active region as the gain medium for light amplification and are sandwiched between *p*- and *n*-doped wider bandgap $Al_{0.35}Ga_{0.65}As$ cladding layers. The refractive index of the active region is higher than that of the cladding layers. Therefore, vertical carrier (electron and hole) confinements and optical confinements are formed by the band offsets and the refractive index difference. The two facets of the crystal are cleaved in order to form two parallel

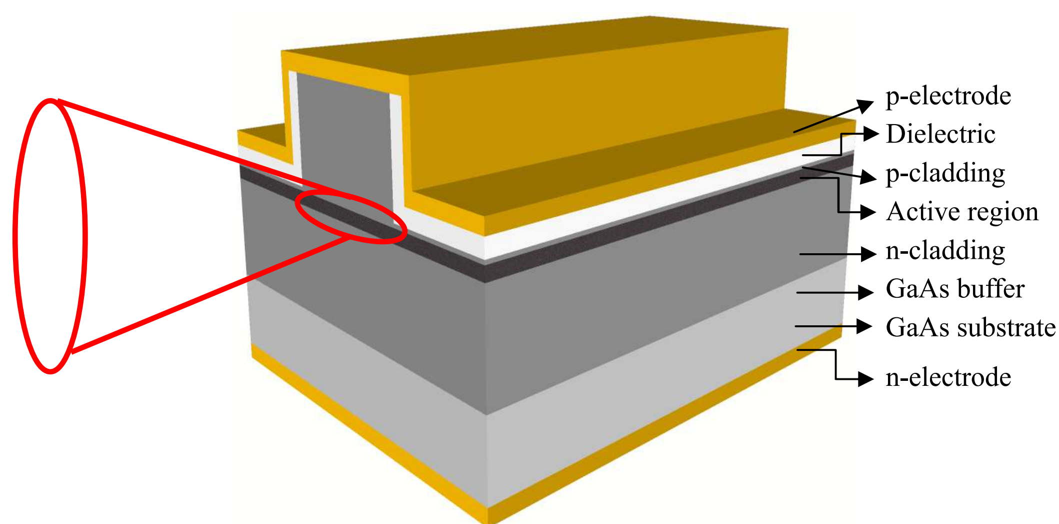

Figure 2.7 The schematic drawing of an InAs/InGaAs FP ridge waveguide laser.

mirror surfaces between which light propagates resonantly, forming a Fabry-Perot (FP) resonator. In order to achieve population inversion for net gain and lasing, carriers are injected into the active region by forward biasing the diode. Within the laser, light is confined to the active region along the growth direction. Light confinement in the lateral direction can be achieved by several methods, among which RWG has been chosen due to its simplicity. The RWG laser uses a ridge formed by wet etching and insulator passivation by Pulsed Anodic Oxidation (PAO) to confine both the optical field and the electrical field in the lateral direction. In the longitudinal direction, an FP laser usually supports multiple longitudinal modes because the gain spectrum is much wider than the spacing between the longitudinal modes.

2.4.1 Threshold Condition

A laser diode is based on stimulated emission. When the current is injected into the laser device, carriers diffuse and drift to the active region through the waveguide. When the injection current is increased, the separation between the quasi-Fermi levels increases. When the separation exceeds the bandgap energy, population inversion is established and stimulated emission is enhanced. To achieve lasing, the injection current should exceed the threshold current when the optical gain is large enough to compensate for the optical loss caused by the absorption in the resonator and the transmission through the facets [64]. The threshold condition can be expressed as [64]:

$$g_{th} = \frac{1}{\Gamma}\left(\alpha_i + \frac{1}{2L}\ln\left(\frac{1}{R_1 R_2}\right)\right) \tag{2.1}$$

where g_{th} is the material gain at the threshold, α_i is internal optical loss, L is cavity length, R_1 and R_2 are the reflectivity at the two facets, and Γ is the optical confinement

factor. The optical confinement factor is a measure of the fraction of the optical field that overlaps with the gain region.

2.4.2 Internal Quantum Efficiency and Internal Optical Loss

The light output power as a function of the injection current (*P-I*) is the most fundamental characteristic of a laser, from which the threshold current and the external differential efficiency can be extracted [64]. The external differential efficiency (η_d) is proportional to the slope of the *P-I* curve above the threshold and can be expressed as [64]:

$$\eta_d = \frac{\Delta P / h\upsilon}{\Delta I / q} \tag{2.2}$$

where h is the Plank constant, v is the frequency of the photon, q is the charge of an electron, and ΔP is the change of total light output power when the injection current is changed by ΔI above the threshold. The external differential efficiency (η_d) is related to internal quantum efficiency (η_i) by [64]:

$$\eta_d^{-1} = \eta_i^{-1} \left(\frac{\alpha_i + \frac{1}{L} \ln \frac{1}{R}}{\frac{1}{L} \ln \frac{1}{R}} \right) \tag{2.3}$$

where R=0.32 is the optical power reflectivity of the two cleaved facets. The external differential efficiency can be improved in short cavity lasers at the cost of a higher facet loss and, thereby, a higher threshold current density.

Both the internal quantum efficiency (η_i) and the internal optical loss (α_i) can be extracted from a plot of the reciprocal of external differential efficiency (η_d^{-1}) as a function of the cavity length (L). The internal quantum efficiency represents the fraction of injected carriers that reach the active region and is an important parameter by which to judge the material quality. The extraction of values for η_i and α_i assumes

that they are independent of the cavity length. However, from Equation 2.1, a higher threshold gain is needed for a shorter cavity laser, resulting in an increased threshold carrier density. This increased threshold carrier density, in turn, affects η_i and α_i. Therefore, calculations show that short cavity lasers (L < 1 mm) should be avoided when using this method to extract the values for η_i and α_i [65].

2.4.3 The Temperature Dependence of Laser Characteristics

The light output power and the emission wavelength of a semiconductor laser are dependent on the ambient temperature. Generally, with increasing temperature, the threshold current increases and the external differential efficiency decreases due to a reduced optical gain, an increasing carrier loss in the active region, and an increased carrier leakage. Carrier losses are caused by recombination at defects, spontaneous recombination, and Auger recombination. Carrier leakage includes all processes that prevent carriers from being trapped in the active region. The relation between threshold current density (J_{th}) and temperature (T) can be expressed as [64]:

$$J_{th}(T) = q \cdot d\left[A(T) \cdot n_{th}(T) + B(T) \cdot n_{th}^2(T) + C(T) \cdot n_{th}^3(T)\right] + J_{leak}(T) \tag{2.4}$$

where d is the thickness of the active region, $A(T)$ is the monomolecular (defects) recombination coefficient, $B(T)$ is the spontaneous emission coefficient, and $C(T)$ is the nonradiative Auger recombination coefficient. The temperature dependence of the optical gain is reflected in the temperature dependence of the threshold carrier density $n_{th}(T)$. The leakage current $J_{leak}(T)$ is caused by the thermally induced leakage of carriers over the barriers, the lateral current spreading in the conductive cladding layer above the active region, and the lateral carrier diffusion in the active region [64].

Generally, with increasing temperature, the coefficient $B(T)$ decreases while $A(T)$ and $C(T)$ increase, resulting in an increased threshold current [66]. The threshold

current as a function of the temperature can be expressed empirically as:

$$I_{th}(T) = I_{th}(T_r)\exp(\frac{T - T_r}{T_0}) \tag{2.5}$$

where T_r is a reference temperature, $I_{th}(T_r)$ is the threshold current at that temperature, and T_o is the characteristic temperature (one of the most important parameters for semiconductor lasers). The T_o value is usually constant in a range of temperatures, and a small T_o indicates a larger variation of the threshold current with temperature.

As previously stated, several methods have been proposed to improve the characteristic temperature of QD lasers. Tunnel injection has been proposed to cool the hot electrons in the QDs [67]. *P*-type modulation doping was introduced to suppress the hole thermal broadening, thus reducing the carrier thermalization and improving the T_o [8] .

2.4.4 Small Signal Modulations of the QD Laser

Small signal modulation is achieved by varying the injection current of the laser diodes, hence resulting in a variation of the optical output power as depicted in Fig. 2.8(a). The optical output power of the laser increases linearly with the injected current above threshold (see Fig. 2.8(b)). Therefore, by injecting a current with a DC component and a small signal AC modulation, the output power will have the corresponding DC and AC components. By direct modulation of the laser diodes, carrier dynamics can be analyzed from the modulation results.

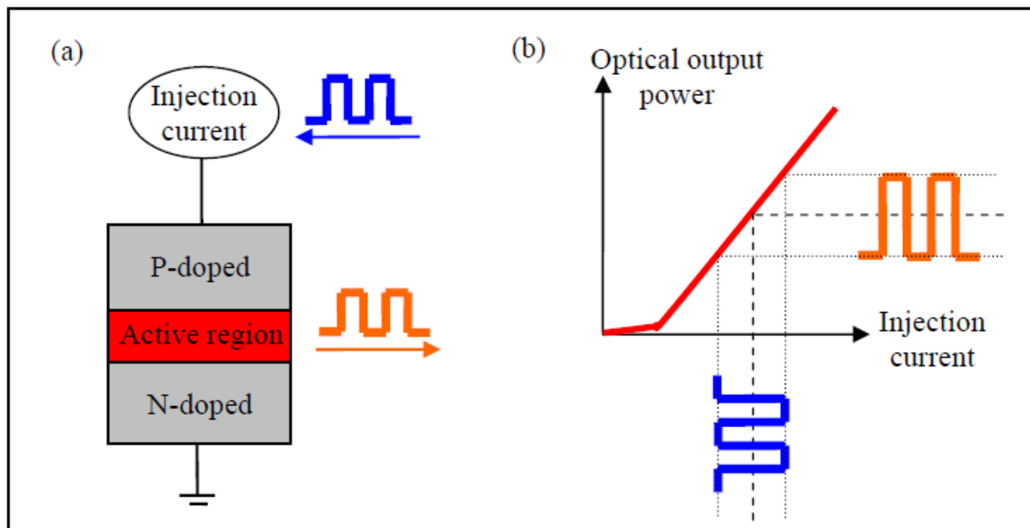

Figure 2.8 (a) Small signal modulation and (b) optical output power versus the injection current characteristics of the semiconductor laser diode.

Figure 2.9 illustrates the energy diagram of the laser active region including self-organized QDs and the relaxation process of carriers into the QD ground state (GS). It is assumed that only a single discrete electron and hole ground state is formed inside a QD and that a charge neutrality always holds in each QD (i.e. electrons and holes are treated like excitons). The injected carriers diffuse through the SCH layer, are captured into the wetting layer (WL), and then relax into the QD. For simplicity, one common time constant is used to describe the capture and relaxation process in the QD. Some carriers recombine radiatively or nonradiatively both outside (in the WL) and inside the QD. Some carriers in the GS emit photons into the lasing mode primarily due to the stimulated emission process. The associated time constants (as illustrated in Table 2.1) are: (i) diffusion in the SCH region (τ_s), (ii) carrier recombination in the SCH region (τ_{sr}), (iii) carrier emission from the WL to the SCH region (τ_{qe}), (iv) carrier emission from the QD to the WL (τ_e), (v) carrier recombination in the WL (τ_{qr}), (vi) carrier relaxation into the QD (τ_d), and (vii) recombination in the QD (τ_r) [18].

Table 2.1 The physics meanings of the symbols in Fig. 2.9 and in the rate equations below [18].

Symbols	Physical meanings
τ	Carrier lifetime
τ_s	Diffusion in the SCH region
τ_{sr}	Carrier recombination in the SCH region
τ_{qe}	Carrier emission from the wetting layer to the SCH region
τ_e	Carrier emission from quantum dot to the wetting layer
τ_{qr}	Carrier recombination in the wetting layer
τ_d	Carrier relaxation into the quantum dot
τ_r	Carrier recombination in the quantum dot
N	Carrier density
S	Photon density
v_g	Group velocity
g'	Differential gain
Γ	Optical confinement factor
ε_m	Gain compression coefficient
τ_p	Photon lifetime
V_a	Active QD layer volume
τ_{cap}	Capture relaxation time in QD
γ	Damping factor

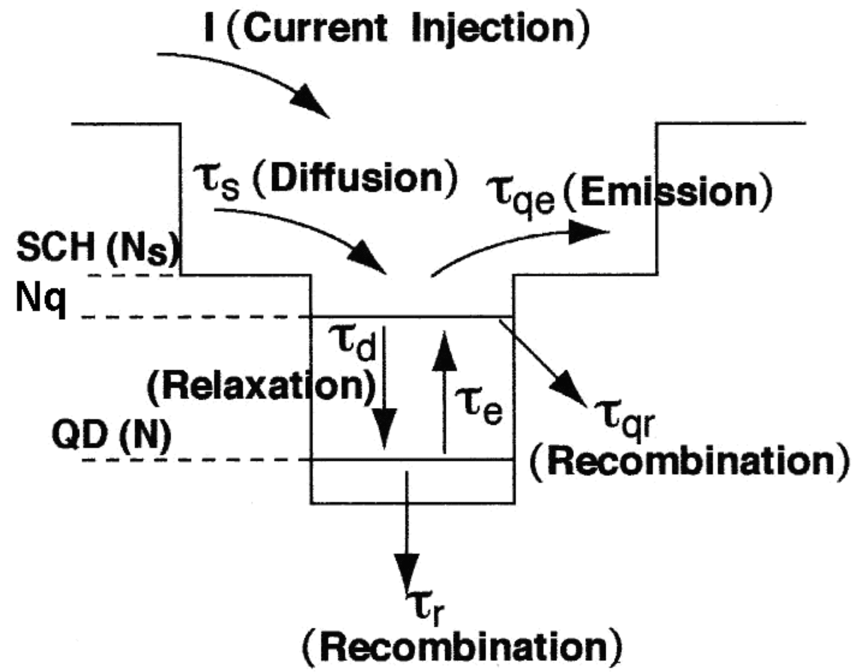

Figure 2.9 An energy diagram of the QD laser active region and the relaxation process of carriers into the QD ground state [18].

The quantitative analysis of the carrier dynamics is an essential tool to help investigate and understand the factors that affect the bandwidth limitations. The dynamics of semiconductor lasers have been conventionally modelled using a set of coupled first order linear differential equations for the carrier density and the photon density in the cavity. The following rate equations are used to analyze the small signal modulation of QD lasers [18]:

$$\frac{d}{dt}N_s = \frac{I}{e} - \frac{N_s}{\tau_s} - \frac{N_s}{\tau_{sr}} - \frac{N_q}{\tau_{qe}} \tag{2.6}$$

$$\frac{d}{dt}N_q = \frac{N_s}{\tau_s} + \frac{N}{\tau_e} - \frac{N_q}{\tau_{qr}} - \frac{N_q}{\tau_{qe}} - \frac{N_q}{\tau_d} \tag{2.7}$$

$$\frac{d}{dt}N = \frac{N_q}{\tau_d} - \frac{N}{\tau_r} - \frac{N}{\tau_e} - \frac{v_g g'\Gamma}{1+\varepsilon_m \Gamma S / V_a} S \tag{2.8}$$

$$\frac{d}{dt}S = \frac{v_g g'\Gamma}{1+\varepsilon_m \Gamma S / V_a} S - \frac{S}{\tau_p} \tag{2.9}$$

where S is the photon density in the active region, N_s is the carrier number in the SCH layer, N_d is that in the WL, N is that in the QDs, τ_p is the photon lifetime, and V_a is the active-layer volume.

For a current injection (I) with a microwave modulation angular frequency (ω):

$$I = I_o + I_\omega e^{i\omega t} \tag{2.10}$$

$$S = S_o + S_\omega e^{i\omega t} \tag{2.11}$$

The solution can be found by substituting Equations (2.10) and (2.11) into Equations (2.6) to (2.9). The resonance frequency $f_r=\omega_r/2\pi$ is found to be proportional to the square root of the photon density or optical output power:

$$f_r \approx \frac{1}{2\pi}\sqrt{v_g \cdot g' \cdot \frac{S_o}{\tau_p}} \tag{2.12}$$

The frequency-dependent modulation response of a semiconductor laser is defined as $M_{(\omega)}=qS_{(\omega)}/I_{(\omega)}$ [68]. The resultant response function can be described by the following three-pole transfer function [69]:

$$H(f) = const \frac{\omega_r}{\left[(\omega_r^2 - \omega^2)^2 + \gamma^2\omega^2\right]^{1/2}} \cdot \frac{1}{\left[1+\omega^2/\omega_p^2\right]^{1/2}} \tag{2.13}$$

where the first part represents the intrinsic carrier-photon interaction (second-order system) with the resonance frequency ω_r and the damping rate γ. The second part represents additional extrinsic limitations due to carrier transport (carrier capture and relaxation from the WL to the GS) and parasitic elements related to the laser structure.

By fitting the measured small signal modulation response to Equation (2.13), the resonance frequency and the damping rate can be extracted for a given QD laser at a given bias current. From the rate equation analysis, it follows that the damping rate is ideally proportional to the square of the resonance frequency [69]:

$$\gamma = K f_r^2 + \frac{1}{\chi \tau_n} \tag{2.14}$$

where τ_n is the differential carrier lifetime, and χ is a factor that accounts for carrier transport effects. From a plot of the damping rate as a function of the square of the resonance frequency, we can determine the K-factor for a given QD laser. The K-factor, as shown in Equation (2.15), can then be used to estimate the maximum intrinsic bandwidth (damping limited) in the absence of other limitations [69]:

$$K = 4\pi^2 \left(\tau_p + \frac{\varepsilon \chi}{v_g g'} \right) \tag{2.15}$$

$$f_{3dB,damping} = \frac{2\sqrt{2}\pi}{K} \tag{2.16}$$

where ε is the gain compression coefficient. At high bias currents, the resonance frequency may saturate and reach a maximum value of $f_{r,max}$ because of thermal effects. In the absence of other limitations, the maximum thermal-limited modulation bandwidth ($f_{r,thermal}$) is then [69]:

$$f_{3dB,thermal} = \sqrt{1+\sqrt{2}}\, f_{r,\max} \tag{2.17}$$

Finally, in the absence of damping and thermal limitations, the maximum modulation bandwidth, limited by the parasitic and transport effects ($f_{r,parasitics}$), would be [69]:

$$f_{3dB,parasitics} = (2+\sqrt{3}) f_p \tag{2.18}$$

A parameter of great significance is the rate at which the resonance frequency increases with the current above threshold, which is called the modulation efficiency or *D*-factor. From a rate equation analysis, we have [69]:

$$f_r = D\sqrt{I - I_{th}} \tag{2.19}$$

$$D = \frac{1}{2\pi}\sqrt{\frac{\eta_i \Gamma v_g \left(dg/dn\right)}{qV_a \chi}} \tag{2.20}$$

where I is the bias current, I_{th} is the threshold current, and dg/dn is the differential gain. The high value of the *D*-factor is a result of the small cavity and gain volumes and the high photon density.

Chapter 3: Experimental Background

The aim of this chapter is to present the experimental details employed in this study. The topics presented will be: (i) the QD structure design and growth, (ii) the device fabrication process, (iii) thermal processing using the rapid thermal processor (RTP), and (iv) the characterization techniques.

3.1 Quantum Dot Structure

The ten-layer self-assembled (SA) InAs/InGaAs QD laser structures investigated in this research study (see Fig. 3.1) were grown on GaAs (100) substrates by molecular beam epitaxy (MBE), which consists of the QD active region sandwiched between two 1.5 μm C- and Si-doped $Al_{0.35}Ga_{0.65}As$ cladding layers for optical confinement. The QD active region consisted of ten-layer InAs QDs (2.32 monolayer (ML)) capped by 5 nm $In_{0.15}Ga_{0.85}As$ with a 33 nm GaAs spacer between every two QD layers. The indium-containing layers were grown at ~485 °C while the (Al)GaAs layers were grown at ~580 °C. The QD area density was about 3×10^{10} cm^{-2}. The Transmission Electron Microscopy (TEM) image of the ten-layer QD active region is shown in Fig. 3.2. In the *p*-doped QD structure, a 10-nm-thick C-doped GaAs layer was located in the middle of each 33-nm-thick GaAs barrier between the QD layers. The doping concentration was 16 acceptors per QD. The growth was terminated by a 200-nm-thick GaAs capping layer. The wafers were processed into 4-μm-wide ridge waveguide (RWG) lasers at room temperature.

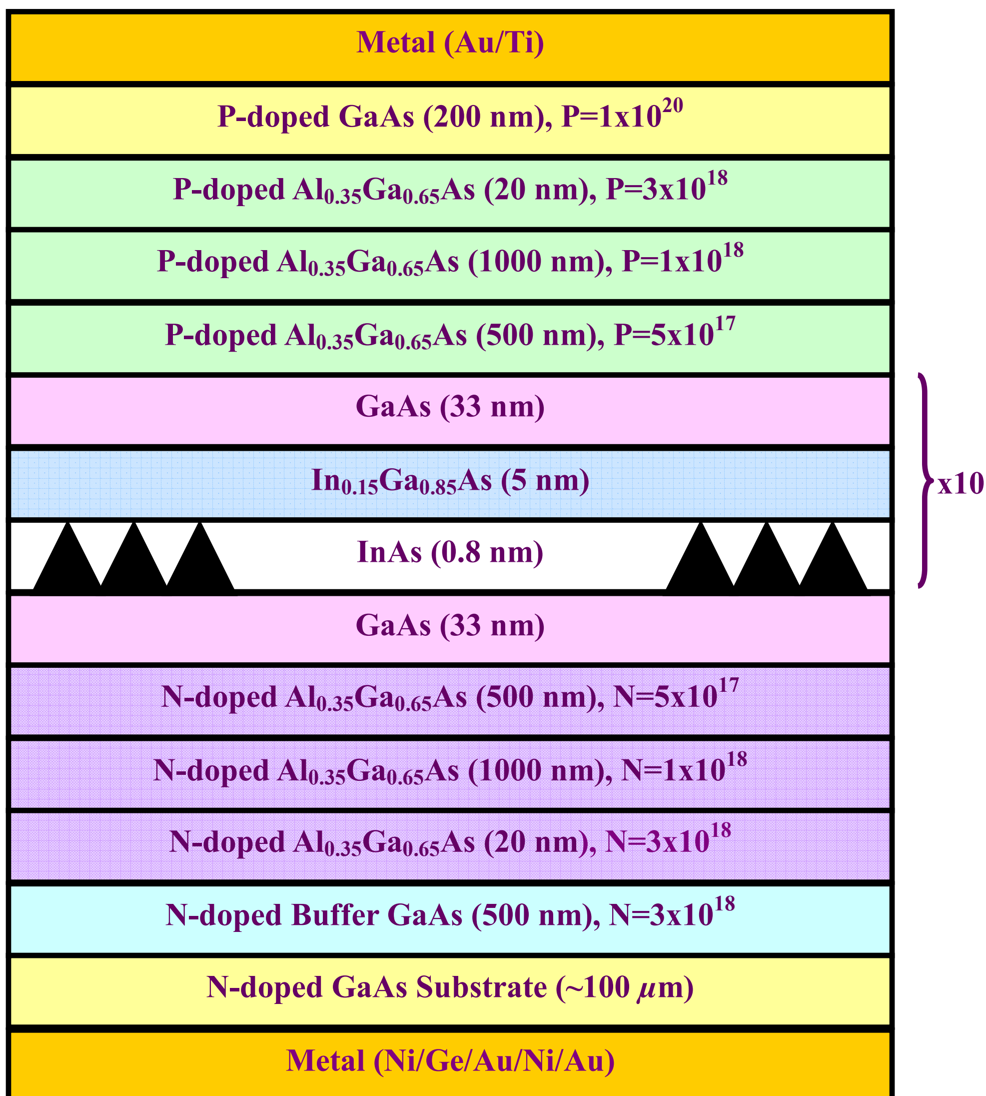

Figure 3.1 A schematic illustration of the undoped ten-layer InAs/InGaAs QD laser structure used in this research study.

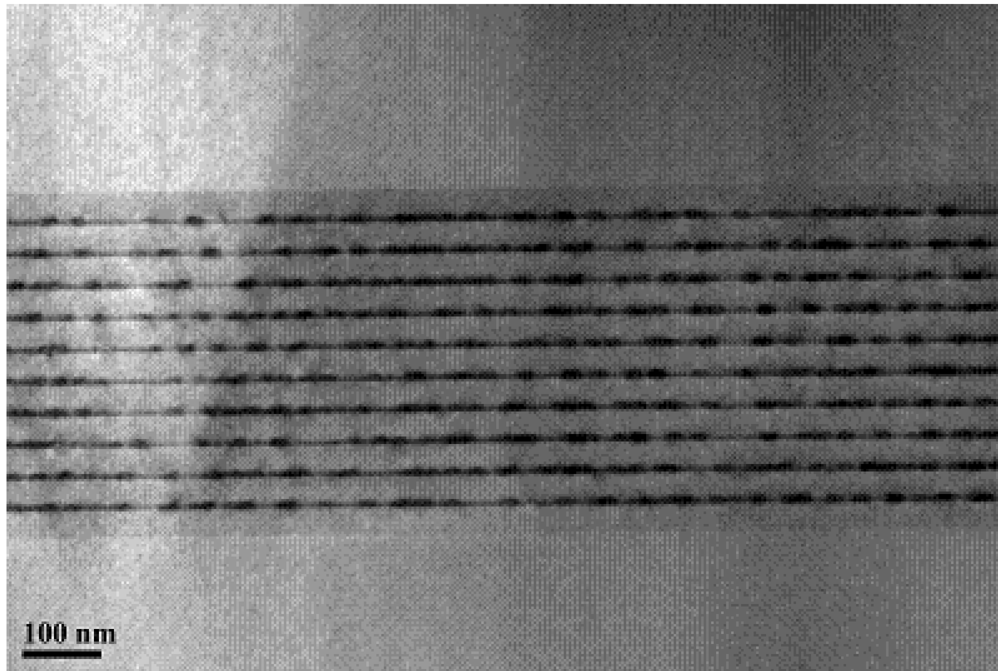

Figure 3.2 The TEM image of the InAs/InGaAs QD active region.

3.2 Device Fabrication Process

The entire fabrication process of the edge emitting RWG QD laser is diagrammed in Fig. 3.3 [70]. The QD laser wafer was first cleaned by acetone, IPA, and DI water solutions. After coating with positive photoresist (AZ 1518), the wafer was exposed under UV light and was developed to form the laser stripe pattern. The wafer was processed into 4-μm-wide RWG lasers by a standard photolithography process and wet chemical etching at room temperature using a solution of $H_3PO_4/H_2O_2/H_2O$ (1:1:5) to form the ridge. A good control of the etch depth was necessary to achieve a narrow RGW structure since the refractive index step between the ridge and the trench region is determined by the etch depth. Through optimization of the ridge height [42, 71], the optimized thickness of the *p*-doped layers above the QD active region outside the ridge was etched. Before the removal of the photoresist, the wafer was subjected to a dielectric oxidation process for better electrical and optical confinement. The novelty of the fabrication process was the utilization of

pulsed anodic oxidation (PAO) [72] to form native oxide at room temperature for both electrical and optical confinement. A 200±5 nm-thick oxide layer was formed by PAO, followed by *p*-type Ohmic contact layers (Ti/Au, 50/300 nm), deposition by electron beam evaporation, and then *n*-type Ohmic contact layers (Ni/Ge/Au/Ni/Au, 5/20/100/25/300 nm) deposition on the backside of the substrate after the substrate was lapped down to ~100 μm. In order to form the alloy, all of the samples were annealed at 410 °C for 3 minutes in N_2 ambient after each period of metallization. Finally, the wafer was cleaved into laser bars of various cavity lengths and the cleaved facets were left uncoated for further testing and characterization. The cross-sectional scanning electron microscopy (SEM) view of the RWG QD laser is shown in Fig. 3.4.

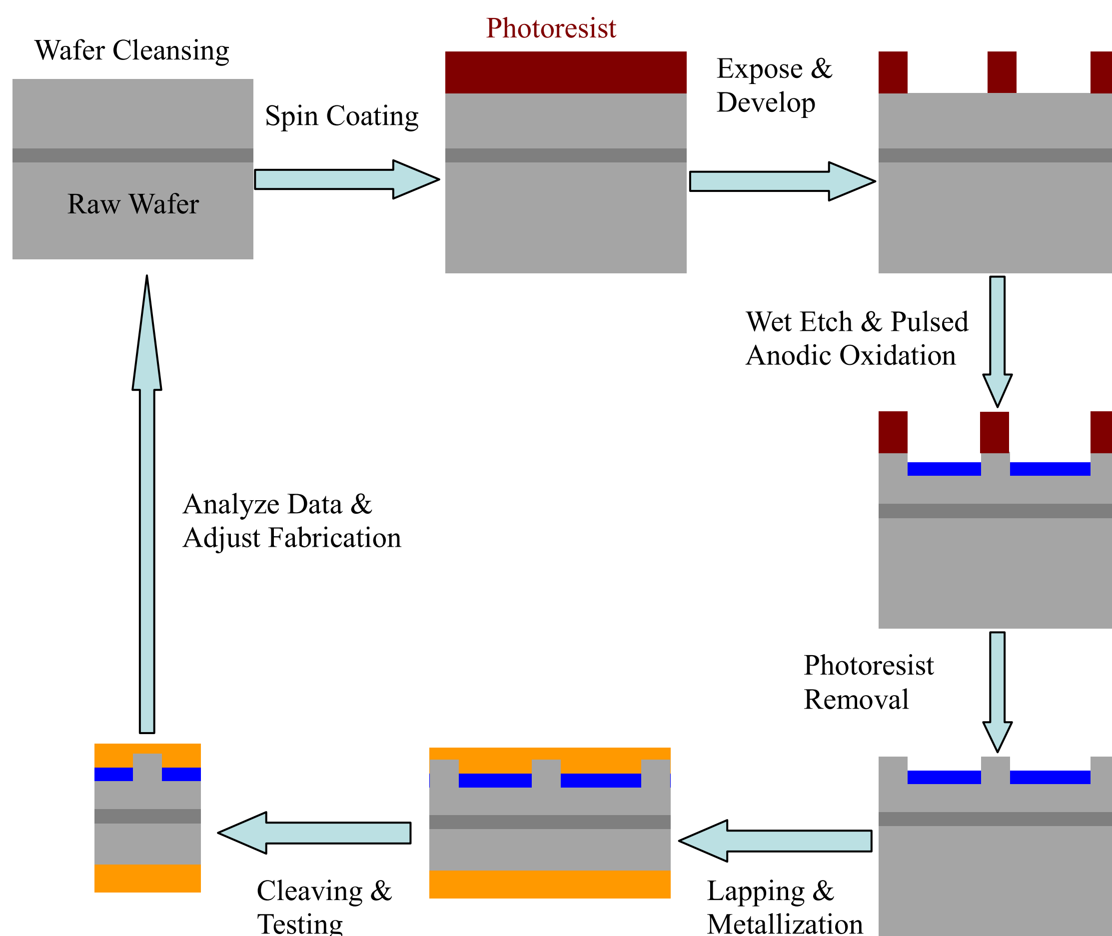

Figure 3.3 The edge emitting RWG QD laser fabrication process.

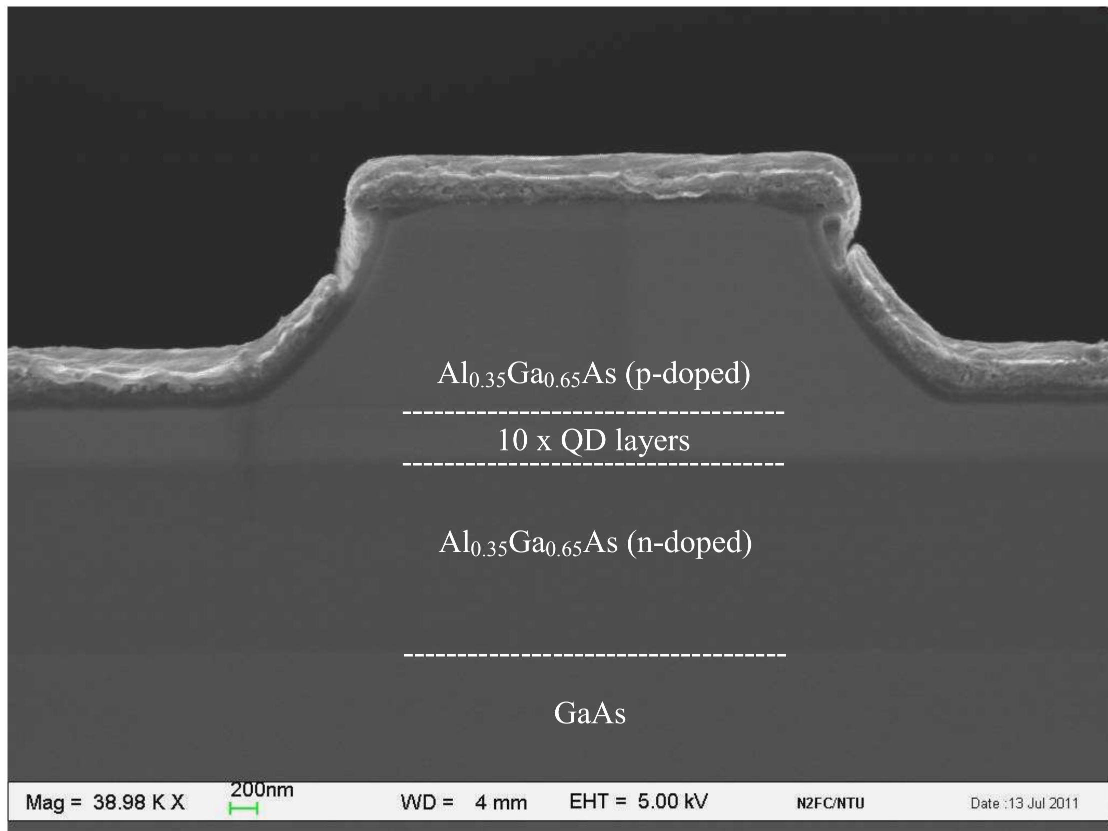

Figure 3.4 Cross-sectional SEM image of the RWG InAs/InGaAs QD laser.

3.3 Rapid Thermal Annealing Process

The rapid thermal processor (RTP) system is a single-wafer reactor in which the thermal process is carried out. The RTP system consists of four major components: (i) energy source, (ii) process chamber, (iii) temperature measurement apparatus, and (iv) temperature controller. A schematic diagram of a typical RTP system using tungsten halogen lamps is shown in Fig. 3.5. The process chamber is usually made of quartz, silicon carbide, or stainless steel and has quartz windows for the optical radiation to illuminate the wafer. A measurement system is placed in a control loop to set the wafer temperature. The wafer temperature in the RTP system can be measured with a non-contact optical pyrometer or a thermocouple.

Before the laser fabrication process, the samples were annealed in a Jipelec/Jetstar RTP in N_2 ambient to prevent contamination. The temperature was controlled by a thermocouple with a high accuracy of ±1 ºC.

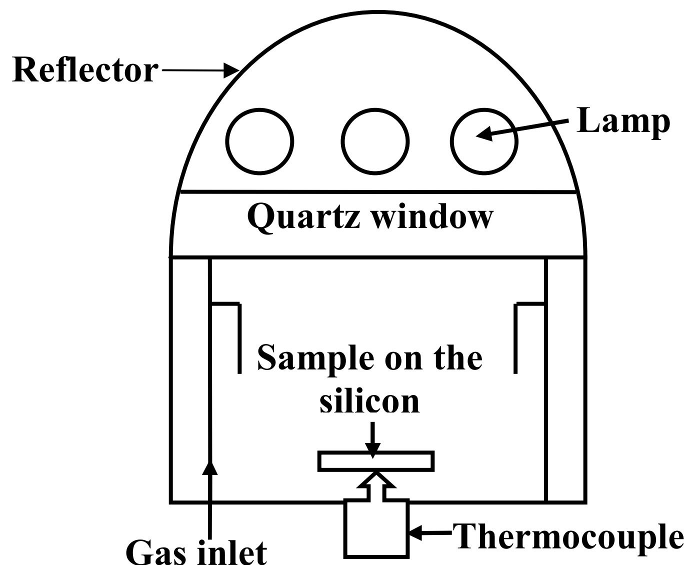

Figure 3.5 Diagram of the rapid thermal processor used for the annealing process.

3.4 Characterization Techniques

In this section, the main characterization techniques employed in this study are discussed. These tools were used to understand the structural and optical characteristics of InAs/InGaAs QDs grown on GaAs substrates.

3.4.1 Photoluminescence

Photoluminescence (PL) is one of the many standard available techniques for the material and optical characterization of semiconductor layers. In the case of QD structures, PL involves the absorption of a photon in the high band gap material to create an electron-hole pair. The electron and the hole then thermalize and diffuse into the low band gap semiconductor where they recombine to produce the photon characteristics of the QD. At high excitation levels (i.e. photopumping), population

inversion can be created and lasing can take place. One of the advantages of photopumping is that the light emission properties can be studied without the complication of a PN junction for carrier injection. PL is the optical radiation emitted by a physical system resulting from excitation to a nonequilibrium state by irradiation with light. When a laser beam is focused on semiconductor materials, three processes can be observed: (i) the creation of electron-hole pairs by absorption of the excitation photon; (ii) the radiative recombination of electron hole pairs; and (iii) the escape of the recombination radiation from the semiconductor materials.

PL measurement is usually performed below room temperature since doing so produces a sharper and smoother profile. At a lower temperature, the linewidth or the full-width half-maximum (FWHM) of the profile is generally smaller. This is due to lesser phonon vibration in the crystal at the lower temperature, less phonon scattering, and, thus, less sideband intensity. At room temperature, the large concentration of phonons and exciton levels merge into a continuum absorption spectrum. Therefore, the absorption spectrum from excitons can hardly be separated from the continuum absorption spectrum and this broadens the linewidth. In addition, at a lower temperature, the charge carrier density decreases and reduces the sideband intensity. This decrease in the charge carrier density is due to the change in the Fermi level to a more abrupt profile at lower temperatures. Besides, the intensity of the PL spectrum is higher at a lower temperature owing to a lower phonon scattering, which leads to a higher recombination efficiency.

In this research study, the PL measurements were performed at room temperature and at a low temperature for the as-grown and thermally annealed samples. The excitation source was the Ar-ion laser source with a peak wavelength of 514.5 nm. The output signal was collected by a liquid nitrogen cooled Ge detector.

The system scan had a resolution of 2 nm due to the limitation of the stage controller.

3.4.2 Transmission Electron Microscopy

Transmission electron microscopy (TEM) is a microscopy technique whereby a high-energy electron beam is transmitted through an ultra-thin sample (typically 5-μm thick), interacting with the sample as it passes through it. A diffraction image is formed from the electrons transmitted through the specimen and a real image of the structure can be obtained from a Fourier-transform of the diffraction image. For heteroepitaxial layers investigation, cross-sectional TEM is especially useful to observe the quality of the various heterointerfaces and dislocations mechanism at these interfaces. TEM can provide a sub-nanometer resolution capable of accurately measuring thin QD structures and different type of defects. The proper preparation of useful TEM samples and the proper alignment of the TEM electron beam optics to produce high-quality images require extensive hands-on experience.

3.4.3 Electroluminescence Spectroscopy

Instead of using an excitation source as in the PL measurement, the electroluminescence (EL) spectra were produced by biasing the samples electrically. The input electrical signal was injected into the laser diode by the current source. The output light was collected using a 100-μm-diameter core multimode silica-based fibre connected to an optical spectrum analyzer (OSA) through an optical fibre. Using this simple experimental set-up, the gain spectra could be extracted from the amplified spontaneous emission (ASE) spectra using the Hakki-Paoli method [73]. By measuring the modulation depth of the Fabry-Perot (FP) resonances in the emission spectra, the output was sent to the computer for data processing. A MATLAB program was constructed to reject all data input except the maxima and minima of the

FP resonances. The maxima and minima were stored sequentially in separate matrix arrays until the whole spectrum was scanned. The program then computed the net modal gain using the equation [73]:

$$G_{net} = \Gamma g - \alpha_i = \frac{1}{L}\ln\frac{\sqrt{S}-1}{\sqrt{S}+1} + \frac{1}{2L}\ln\left(\frac{1}{R_1 R_2}\right) \tag{3.1}$$

where α_i is the internal loss, S is the ratio of intensity maximum and minimum in the FP resonances, L is the cavity length, and R_1 and R_2 are the facet reflectivities.

3.4.4 High-Speed Modulation Experimental Set-up

In order to measure the small signal modulation characteristics, the QD laser devices were mounted on a submount with Ground-Signal-Ground (G-S-G) coplanar contacts. Figure 3.6 shows the mounted laser device, bonded wire and the G-S-G coplanar contacts. Figure 3.7 shows the set-up for the small signal modulation of the QD lasers measured under the continuous-wave (CW) biasing condition using a vector network analyzer (VNA), a DC current source, a Bias-T, a high-frequency probe, and a high-speed photoreceiver. A thermoelectric temperature controller was used to regulate the device temperature during measurements. The VNA provided a modulation signal at frequency sweep from 10 MHz to 20 GHz. The modulation signal, combined with a DC bias current in a bias-T, was injected into the laser diode with a high-frequency probe. The optical output from the laser was coupled to a fibre. The optical signal was converted to an electrical signal using a high-speed photoreceiver and was fed back to the VNA.

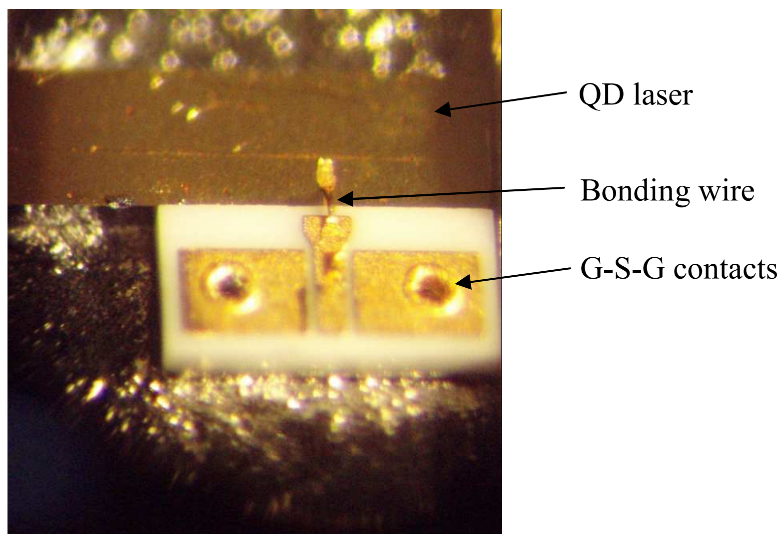

Figure 3.6 The mounted laser device, bonded wire and the G-S-G coplanar contacts.

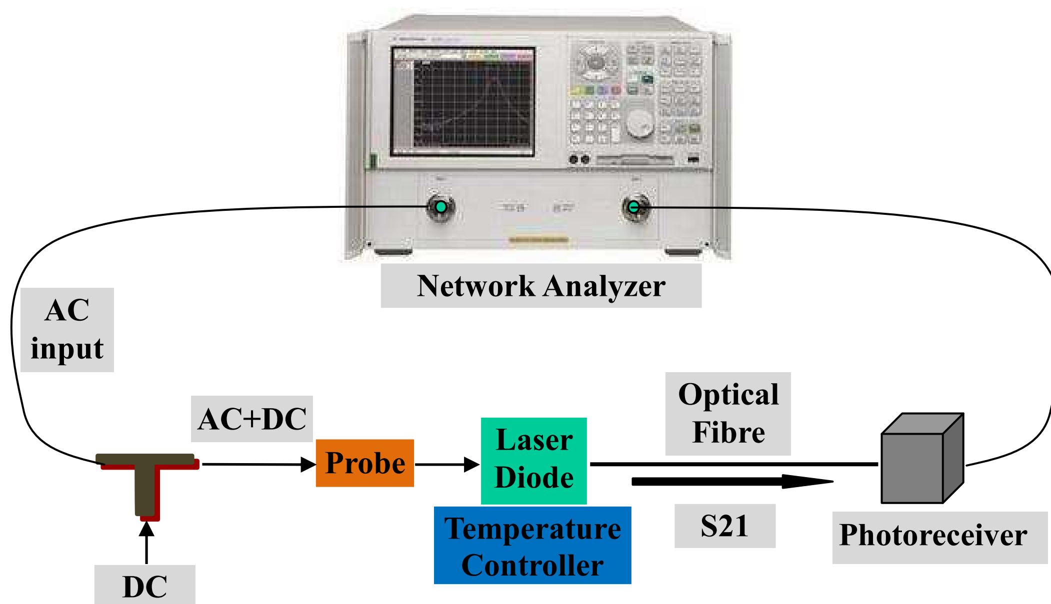

Figure 3.7 A schematic layout of a high frequency measurement equipment set-up, which involves a Vector Network Analyzer (VNA), a DC current source, a bias-T, a high-frequency probe, a high-speed photoreceiver, and a temperature controller.

The data was averaged to reduce noise. The measured modulation response was corrected for the frequency responses of the photoreceiver (refer to Fig. 3.8) and the probe (refer to Fig. 3.9). By plotting the corrected and normalized modulation

response (S21) as a function of the modulation frequency, the -3dB bandwidth of the laser diode could be determined. In addition to observing the change of frequency response with respect to the change of injection current, the effect of temperature on the small signal modulation was studied to investigate the carrier dynamics of QD lasers. The photoreceiver and the high-frequency probe are calibrated and their frequency responses are provided in the data specifications by the equipment suppliers.

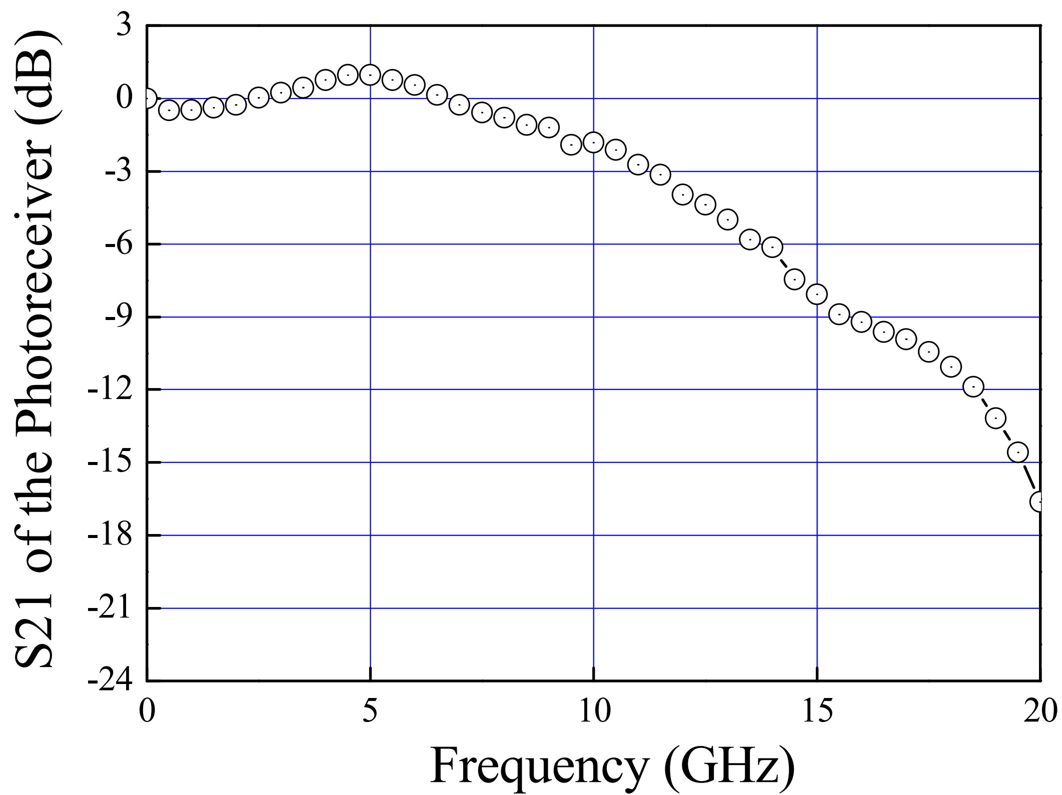

Figure 3.8 The frequency response of the photoreceiver.

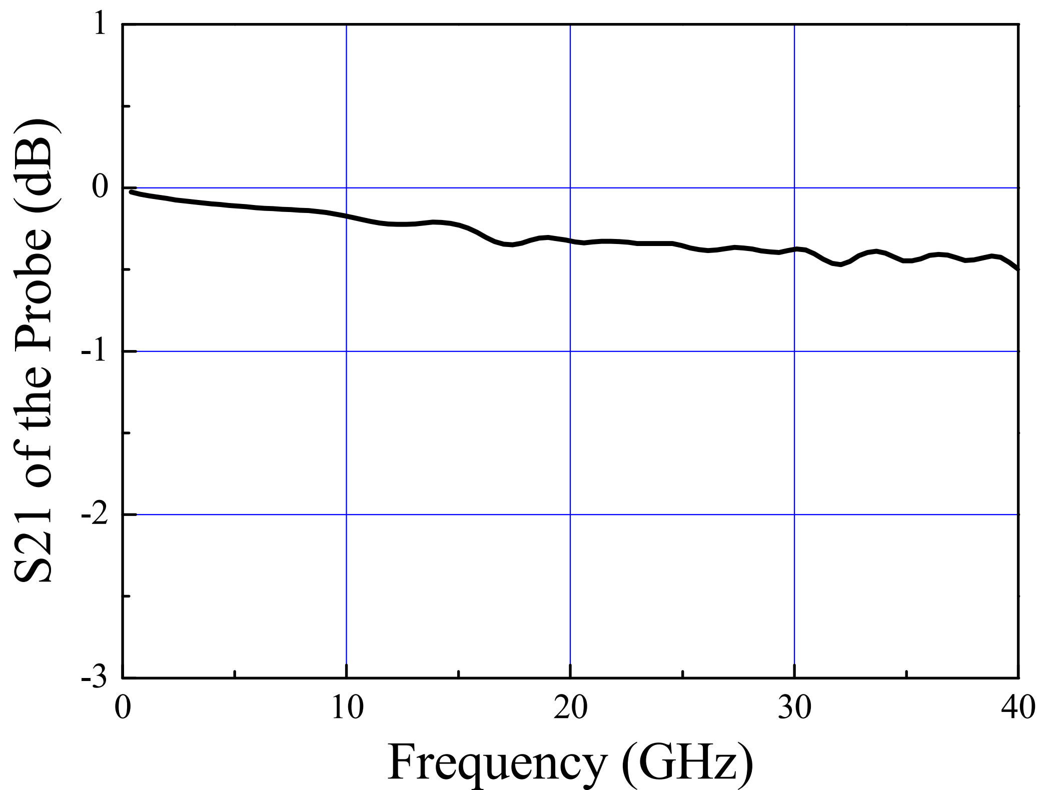

Figure 3.9 The frequency response of the high-frequency probe.

The electrical properties of the complex laser chip structure, including the metallization layers, the cladding layers, the active region, the substrate, and the insulation layer, can be described in terms of an equivalent RC circuit, where R is the series resistance of the device and C is the parasitic capacitance paralleled with R. Therefore, the parasitic acts as a frequency low pass between the input and the intrinsic laser diode with a bandwidth f_p. In this research study, the bonding wire was bonded onto the ridge waveguide of the laser diode to reduce the parasitic effects. Therefore, for the devices investigated in this work, the parasitic cut-off frequency was almost temperature-independent and only restricted the measured bandwidth minimally.

A typical value for the series resistance of 1-mm-long narrow stripe lasers is around 3-7 Ω. In order to accurately calculate the parasitic cut-off frequency, the

estimation of the series resistance of the laser chip is far more demanding since it depends on the particular epitaxial structure and the doping of the device. However, a description of the corresponding model and the subsequent fitting of parameters is beyond the scope of the theoretical part of this thesis. Generally, the etch depth of the ridge waveguide has a major influence on the series resistance. Deeply etched mesas suppress current spreading and lead to an increase of the series resistance. From our previous study [74], the optimum ridge height corresponds to an etching depth where all of the *p*-doped layers above the active region were removed. In theory, when the ridge reaches an undoped layer, the effective device capacitance is much smaller than that of lasers with ridge height stops at high doping layers.

Taking the effect of the bonding wire on the frequency modulation into account, an inductance L was introduced in series with the laser diode. No analytical expression for f_p with L can be given. Therefore, Fig. 3.10 shows a numeric simulation of the influence of L on the transmission of the parasitic low-pass performed with Microwave Office [75]. To make sure that the bonding wire did not limit the measured device performance, the lengths of the bond wires were restricted to below 300 μm in our submount.

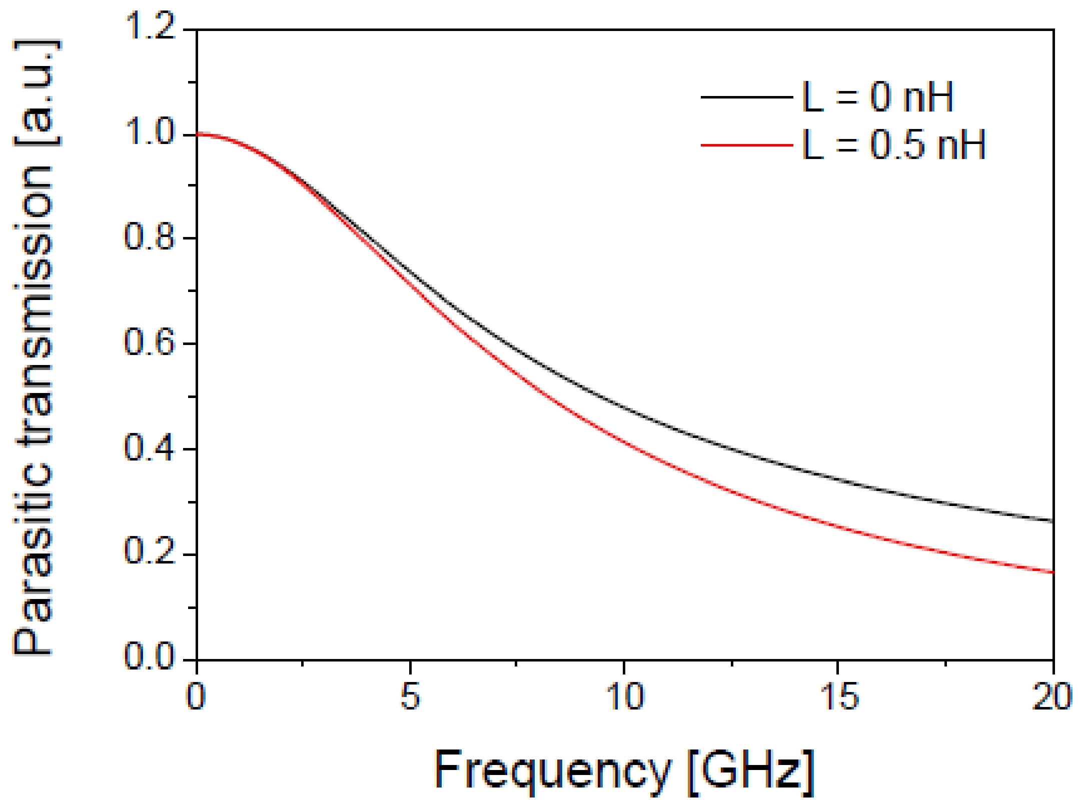

Figure 3.10 The influence of bond wire inductivity on the transmission of the parasitic low-pass. The bandwidth is 9.5 GHz for 0 nH and 8.2 GHz for 0.5 nH, corresponding to a bond wire of a 25 μm diameter and a 600 μm length.

Chapter 4: The Bandwidth Limitations of QD Lasers by Small Signal Modulation

In this chapter, we investigate the bandwidth limitations of 1.3 μm InAs/InGaAs QD lasers. The influence of thermal effects and intrinsic damping on the high-speed modulation characteristics of 1.3 μm InAs/InGaAs QDs are studied through the temperature-dependent small signal modulations. The effects of operation temperature on the K-factor, the differential gain, and the nonlinear gain compression are also discussed.

4.1 Introduction

High temperature stability in laser operation is an essential characteristic for long wavelength semiconductor lasers used in optical communication systems. The realization of the uncooled high-speed operation of 1.3 μm QD lasers has attracted intense research interest due to its application in optical communications. Over the past decade, the promising dynamic properties of QDs such as their large differential gain, their high cut-off frequency, and their small chirp were reported in devices with emission wavelengths less than 1.2 μm [3]. Improved temperature characteristics of QD lasers, such as a temperature-invariant threshold current [3], a high characteristic temperature (T_o) [76] and a linewidth enhancement factor [77], have been realized through the p-doping technique. However, QDs emitting at 1.3 μm and above (i.e. long wavelength QDs) have not fulfilled the initial expectations of improved temperature-insensitive modulation bandwidths, which have largely remained below 12 GHz for the intrinsic QDs [5].

With the increase in QD size and the strain effect of the cap layer, the self-assembled (SA) InAs/GaAs QDs can emit at 1.3 μm. The energy levels are still discrete. However, the number of energy levels increases and the level separation, especially for holes, becomes much narrower (8-11 meV for hole) than that in the short wavelength QDs. This results in a significant hole thermalization [8]. Other problems reported in the 1.3 μm SA QDs include the finite GaAs barrier and the thin wetting layer (WL) [78]. These disadvantages consequently lead to the temperature-sensitive performance observed in 1.3 μm QD lasers, such as the low characteristic-temperature which is at or above room temperature [79], the strong temperature-dependent maximum gain and the modulation bandwidth.

Many theoretical [13, 15] and experimental [16, 77, 80] investigations have been performed to study the bandwidth limitations in long wavelength QD lasers. Fiore *et al.* [15] studied the effects of intradot relaxation on the *K*-factor and the differential gain of QD lasers. Deppe *et al.* [13] reported the role of the density of states (DOS), especially the thermalization of holes due to their closely spaced discrete energy levels. These limit the modulation speed of the QDs with deep confinement potentials, such as the 1.3 μm InAs/GaAs QDs. According to these investigations, the *K*-factor [15, 16] is recognized as one of the key factors for the modulation bandwidth of QD lasers, which accounts for the effects of photon lifetime, the differential gain, and the nonlinear gain compression.

However, despite theoretical and experimental investigations on the effect of the differential gain on the DC performance of the 1.3 μm QD laser and the directly modulated uncooled 1.3 μm QD laser [81], the effect of carrier thermalization on the high-speed performance of the 1.3 μm QD laser has not been analyzed systematically. Obviously, the modulation speed (or bandwidth) of the 1.3 μm QD laser should be

temperature-dependent due to the temperature-sensitive gain profile of the QDs. Since few investigations exist on the effects of temperature on the bandwidth of 1.3 μm QD lasers, a study of this aspect will provide a greater understanding of the carrier dynamics in long wavelength QD lasers.

4.2 Small Signal Modulation

Figure 4.1 shows the measured continuous-wave (CW) Power-current-voltage (P-I-V) performance of a QD laser device with a cavity length of 1.1 mm from 5 °C to 100 °C. At room temperature (RT), the threshold current (I_{th}) and the slope efficiency were 55 mA and 0.27 W/A, respectively. The maximum output power of 96 mW occurred at an injection current of 395 mA.

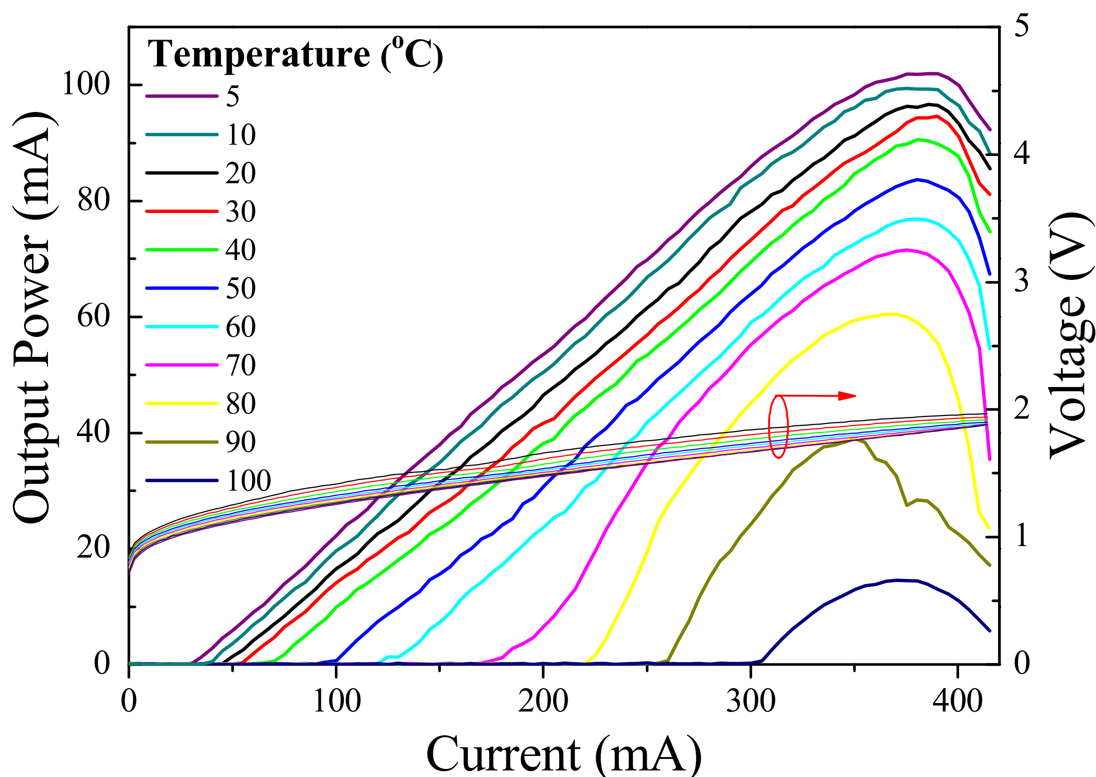

Figure 4.1 The temperature-dependent CW Power-current-voltage curve of the QD laser measured from 5 °C to 100 °C.

Figure 4.2 shows the lasing spectrum of the same laser device under an injection current of 100 mA at room temperature for verification. The lasing wavelength was centered at 1306.5 nm. Furthermore, no lasing at the excited state (ES) was observed. The characteristic temperature T_o was around 41 K from 5 °C to 50 °C.

The small signal modulation responses measured under different injection current levels at RT were normalized to the response of the measurement system (see Fig. 4.3). The largest bandwidth (BW) of 6.1 GHz was obtained at an injection current level of 390 mA. For injection currents of more than 395 mA, the resonance frequency f_r decreased with increasing injection currents since two competing factors affected the resonance frequency: (i) an increase of the resonance frequency with increased injection currents and (ii) a decrease of the resonance frequency due to the thermal effects arising from self-heating. Therefore, f_r will be influenced by the competition between these two factors.

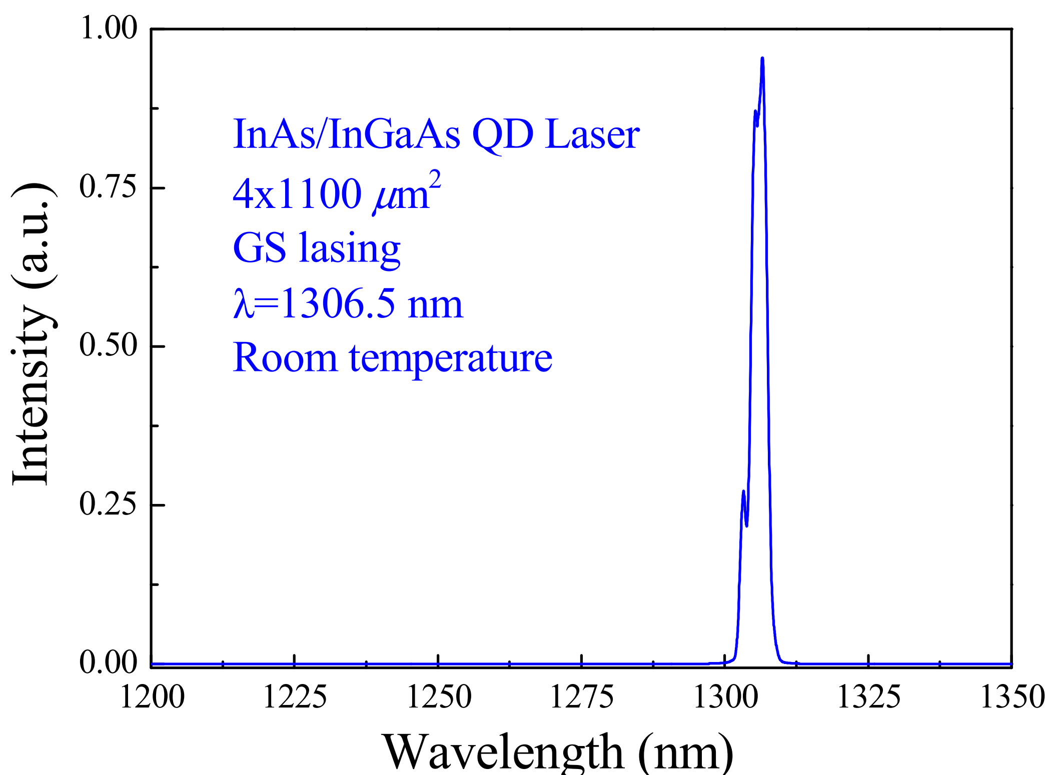

Figure 4.2 The lasing spectrum from the InAs/InGaAs QD laser (4×1100 μm^2) with an injection current of 100 mA at room temperature.

While an initial increase in the injection currents could lead to higher f_r, a further increase might have a detrimental effect due to the onset of self-heating. Therefore, when the injection currents increase to a level higher than 395 mA, the thermal effects arising from the internal heating, which results from the increased currents, become dominant. A further increase in the injection currents thus leads to a degradation in the modulation bandwidth and the issue of this thermal effect on the device performance is the aim of our investigation in this chapter. Increasing the injection current by a few 'milli ampere' may lead to a significant increase in the self-heating inside the devices.

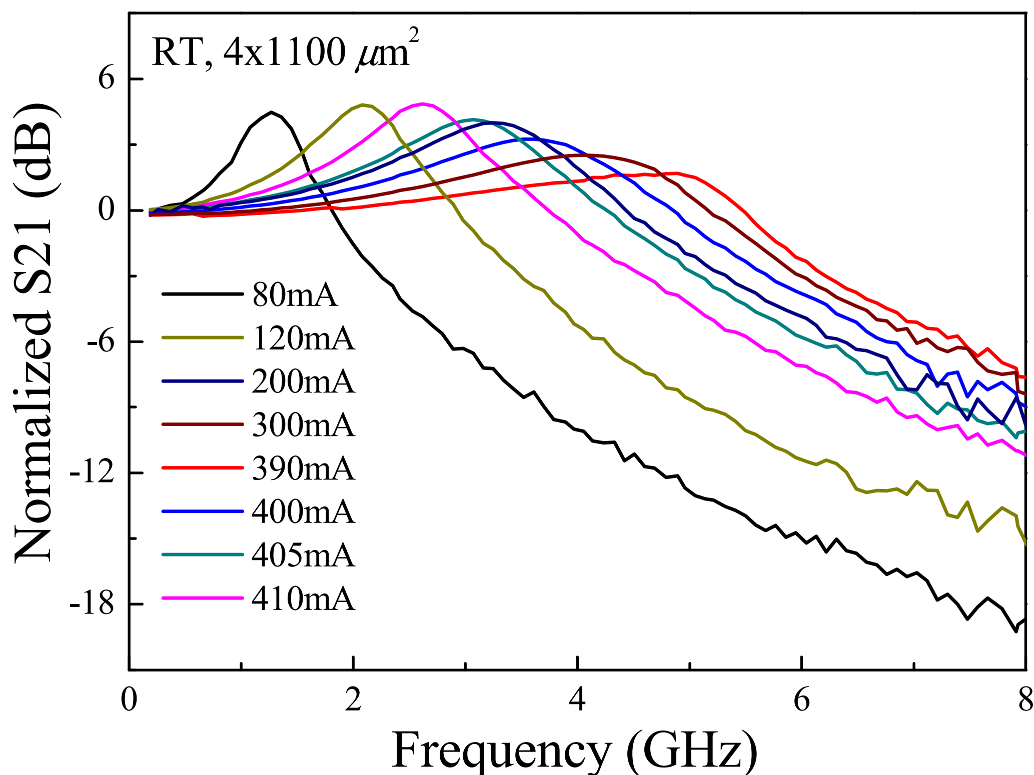

Figure 4.3 The small signal modulation response of the undoped QD laser measured at RT under different injection current levels.

The small signal modulation responses were further fitted into a transfer function that accounted for the intrinsic response of the laser and the extrinsic effects [69]:

$$H(f) = const \cdot \frac{f_r^2}{f_r^2 - f^2 + j\frac{f}{2\pi}\gamma} \cdot \frac{1}{1 + j\frac{f}{f_p}} \tag{4.1}$$

where f_r is the resonance frequency, γ is the damping rate, and f_p is the parasitic cut-off frequency. From the fitting, we obtained the values of the damping rate γ and the resonance frequency f_r at different bias currents. The parasitic cut-off frequency was almost temperature-independent and only restricted the bandwidth minimally. According to the plot of f_r versus the square root of the normalized bias current $(I-I_{th})^{1/2}$, the slope (known as the D-factor or the modulation efficiency) was determined to be 0.28 GHz/mA$^{1/2}$ at RT:

$$D = \frac{1}{2\pi}\sqrt{\frac{\eta_i \Gamma v_g (dg/dn)}{qV_a}} \tag{4.2}$$

From the plot of the damping rate versus f_r^2, the K-factor was determined to be 0.83 ns at RT:

$$K = 4\pi^2\left(\tau_p + \frac{\varepsilon}{v_g (dg/dn)}\right) \tag{4.3}$$

Furthermore, the K-factor is directly related to the damping-limited bandwidth ($f_{3dB,damping}$) by [69]:

$$f_{3dB,damping} = \frac{2\sqrt{2}\pi}{K} \tag{4.4}$$

The internal quantum efficiency (η_i) and the internal optical loss (α_i) of the devices were estimated to be 51% and 4 cm^{-1} by measuring lasers with different cavity lengths (1-3 mm) [82, 83]. The internal quantum efficiency and the internal

optical loss exhibited a weak dependency on the temperature. With the values of η_i and α_i, the differential gain (dg/dn) and the nonlinear gain compression (ε) factors were extracted. The gain derivatives, with respect to the carrier population, define the differential gain while the nonlinear gain compression factor is used to describe the gain dependence on the photon density. From the value of the D-factor, the differential gain is obtained to be 11.1×10^{-15} cm^2 at RT, which is almost ten times higher than the differential gain reported in the literature [84] (a differential gain of 1×10^{-15} cm^2 at 300 K for a device emitting at 1263 nm). The nonlinear gain compression factor is determined to be 12×10^{-16} cm^3 at RT.

4.3 Temperature-Dependent Study

Temperature-dependent direct small signal modulations were then performed on the same QD laser diode from 5 °C to 50 °C. The modulation responses measured at 5 °C and 50 °C were normalized to the response of the measurement system and are shown in Figs. 4.4 and 4.5, respectively.

Similar parameter fittings into Equation (4.1) were done using the obtained frequency response curves at different temperatures from 5 °C to 50 °C. The resonance frequency, bandwidth, and damping rate were extracted from the fittings. Figure 4.6 shows the maximum measured (triangles) bandwidth ($f_{3dB,measured}$) as a function of temperature. The maximum measured bandwidth decreased almost linearly with the temperature as the temperature increased from 5 °C to 50 °C. The highest $f_{3dB,measured}$ of 7.51 GHz was obtained at 5 °C.

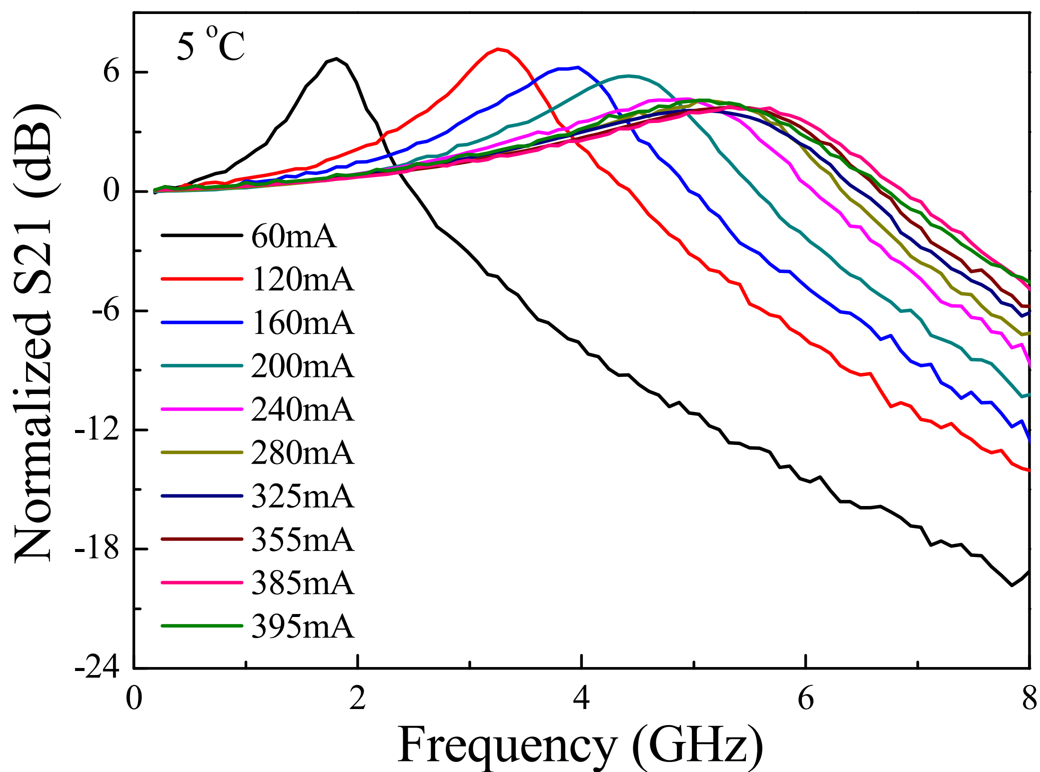

Figure 4.4 The frequency response of the same undoped QD laser measured at 5 °C.

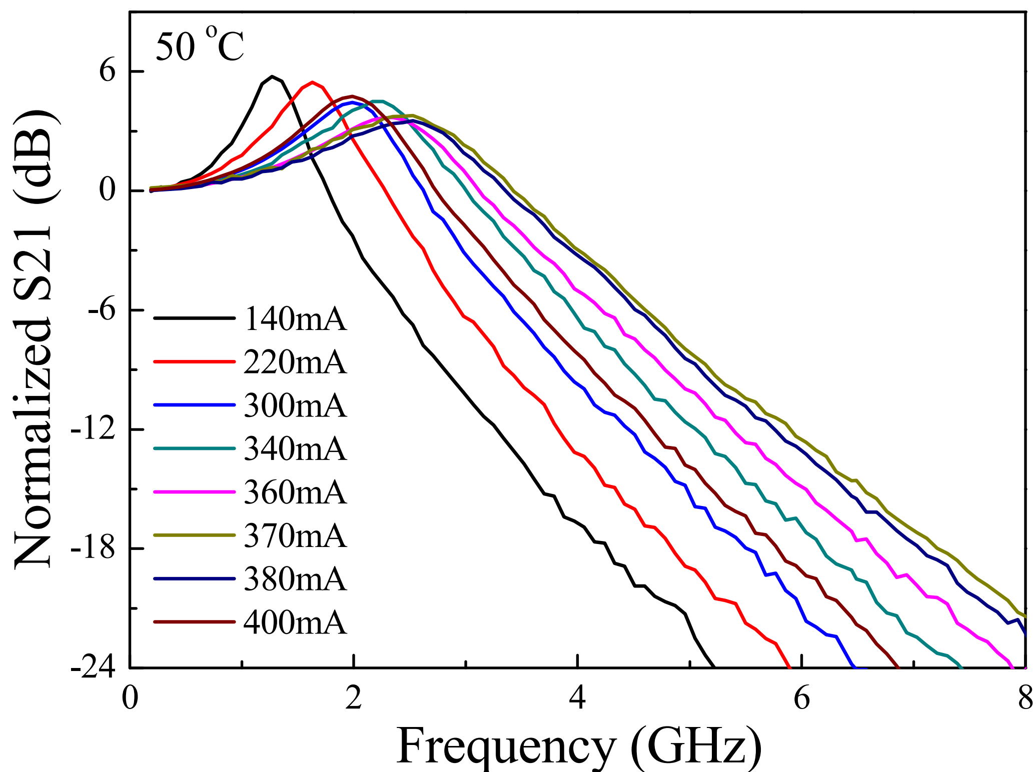

Figure 4.5 The frequency response of the same undoped QD laser measured at 50 °C.

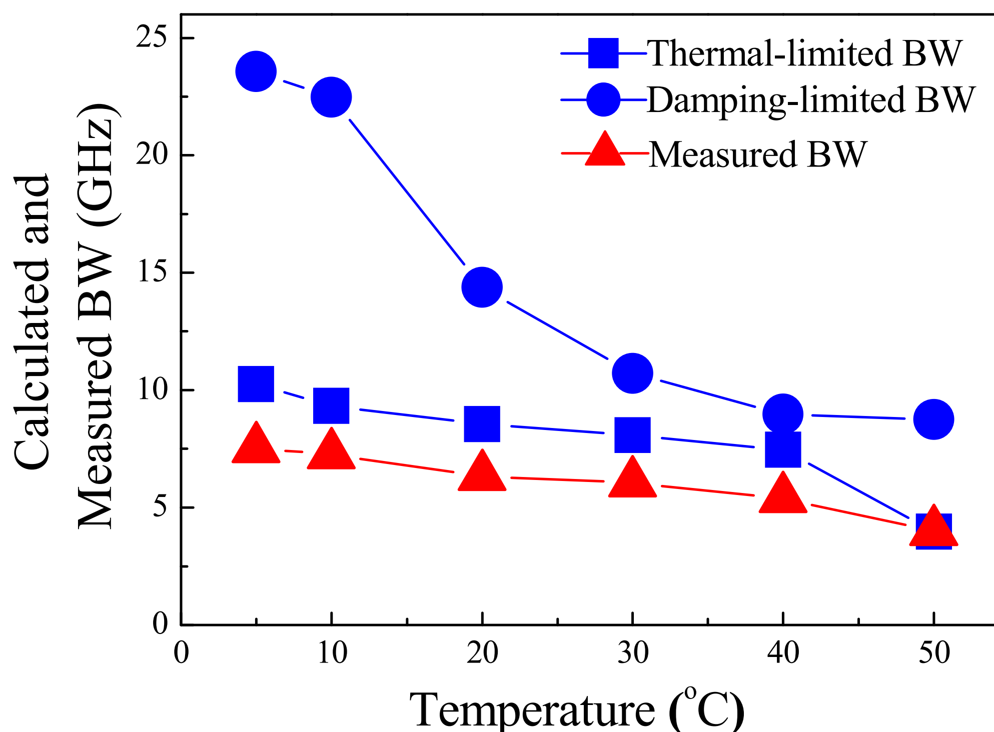

Figure 4.6 The plot of the calculated thermal-limited (squares) bandwidth (BW), the damping-limited (circles) bandwidth, and the measured (triangles) bandwidth at different temperatures.

The *D*-factors were determined to be 0.36 GHz/mA$^{1/2}$ at 5 °C and 0.15 GHz/mA$^{1/2}$ at 50 °C, respectively, as shown in Fig. 4.7 (left axis, solid circles). The extracted nonlinear gain compression factor as a function of temperature is also shown in Fig. 4.7 (right axis, hollow circles). The *K*-factor of the QD laser as a function of temperature is summarized in Fig. 4.8. There was a significant increase in the *K*-factor as the temperature increased. The calculated *K*-factor increased approximately by a factor of three over the temperature range of 5 °C to 50 °C. The differential gain from 5 °C to 50 °C decreased following this increase in temperature (as shown in Fig. 4.9).

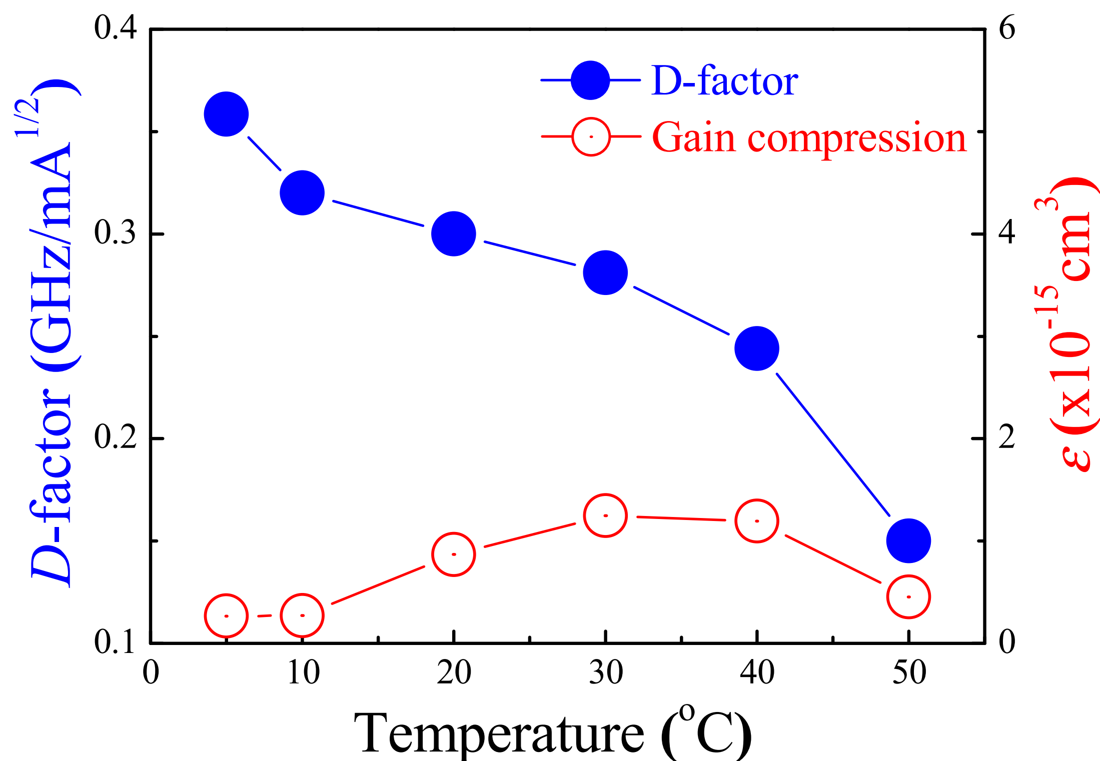

Figure 4.7 The plot of the dependence of the *D*-factor (solid circle) and the nonlinear gain compression (hollow circle) on the temperature.

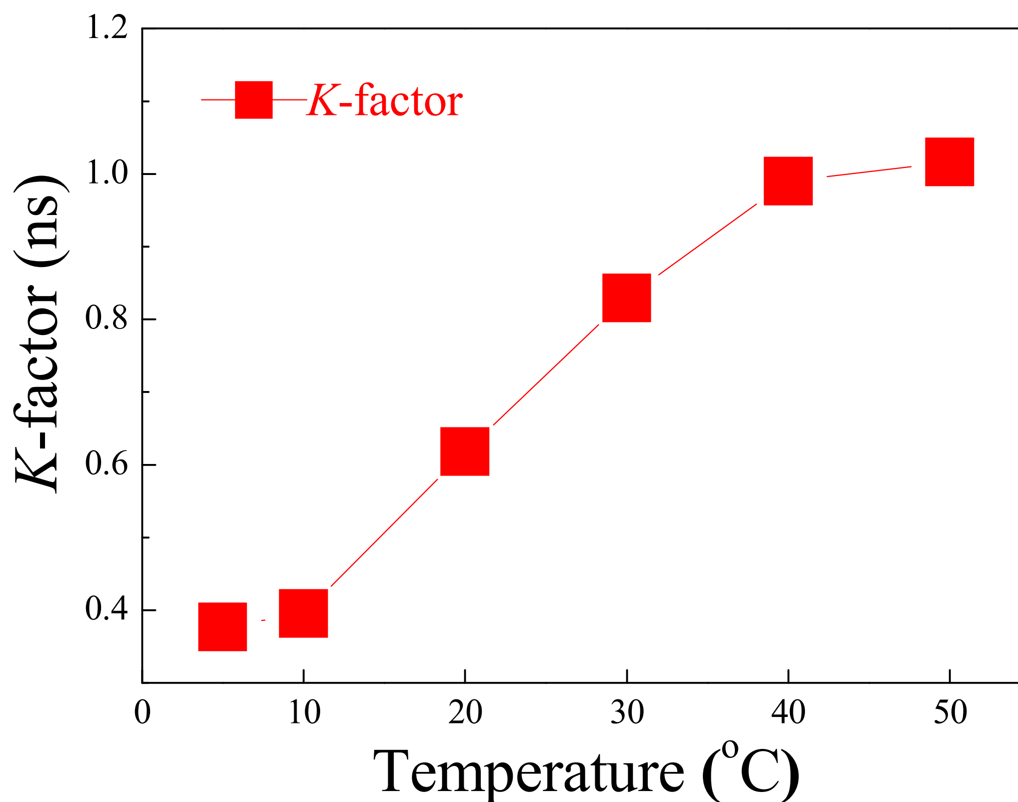

Figure 4.8 The plot of the dependence of the *K*-factor on the temperature.

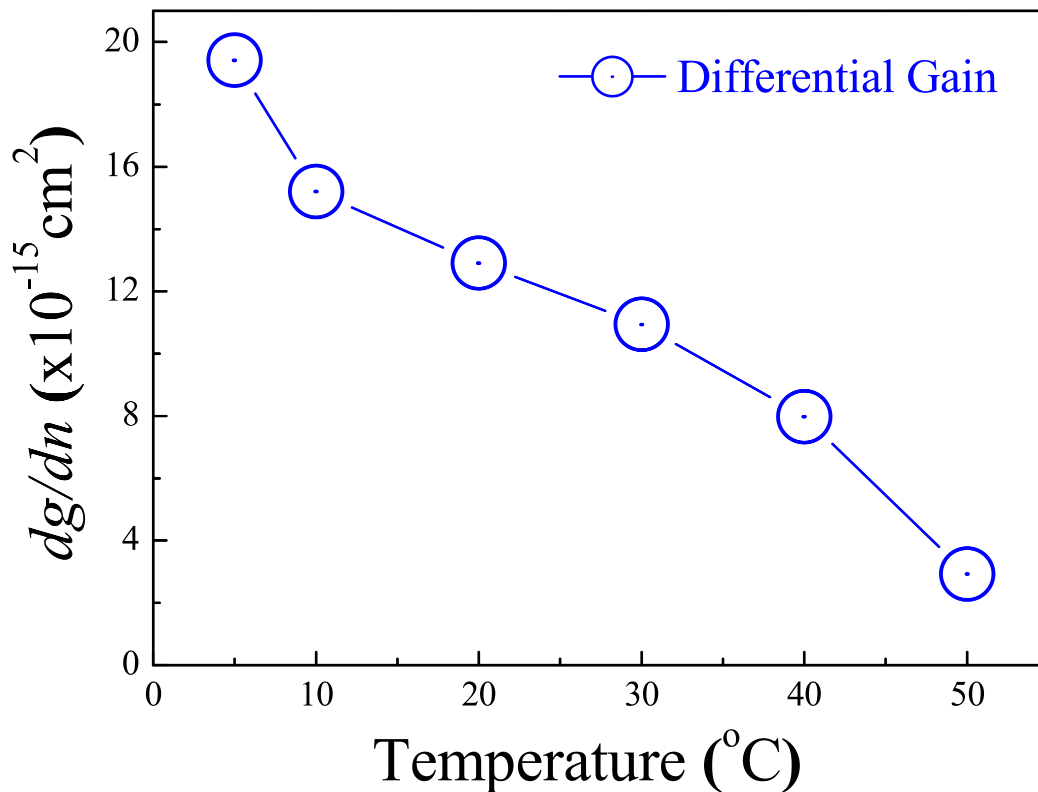

Figure 4.9 The plot of the differential gain at different temperatures.

From Equation (4.4), the intrinsic damping limited bandwidth $f_{3dB,damping}$ of the QD laser is 23 GHz at 5 °C and 8.9 GHz at 50 °C, which is limited by the carrier-capture time and modal gain via the *K*-factor [16, 85]. This implies that the 1.3 μm InAs/InGaAs QD lasers can potentially operate at very high frequencies. However, our experimental data showed a much lower bandwidth. This lower bandwidth could be caused by the serious hole thermalization due to the closely spaced hole-levels in 1.3 μm InAs/InGaAs QDs. Considering the relationship between the bandwidth and the resonance frequency, the saturation of the bandwidth could be attributed to the thermal effects (i.e. the thermal saturation of photon number (S_o) at roll-over current injection due to the self-heating). The resonance frequency related to the differential gain, the photon density, the photon lifetime, and the gain compression is based on the following equation:

$$f_r^2 \approx \frac{v_g (dg/dn) S_o}{4\pi^2 \tau_p (1+\varepsilon S_o)} \tag{4.5}$$

where S_o is the photon density, dg/dn is the differential gain, and τ_p is the photon lifetime. Using the parameters deduced from the measurements, the photon lifetime was determined to be 7.4 ps and was found not to be strongly temperature-dependent. Possibly, the saturation of the bandwidth is caused by a saturation of the photon density. A saturation of the photon density could be caused, possibly, by the strong gain compression. Meanwhile, the gain compression factor ε was in the order of 10^{-16} cm^3 and showed a relatively weak dependence on the temperature (refer to Fig. 4.7 (hollow circle)). The $\varepsilon \cdot S_o$ product was less than 0.1, which suggests that the effect of the gain compression on the resonance frequency was relatively small. By noting that the laser junction temperature under continuous-wave operation became very high when the output power started to saturate, it can be concluded that the photon density saturated at a high injection current because of a rapid increase in the threshold current. Possibly, the severe thermal effects could explain this since the internal junction temperature increased significantly with a small increase of the injection current. At relatively small damping effects, the thermal-limited bandwidth ($f_{3dB,thermal}$) is related to f_r by [69]:

$$f_{3dB,thermal} = \sqrt{1+\sqrt{2}}\, f_{r,\max} \tag{4.4}$$

where $f_{r,max}$ is the maximum resonance frequency at a constant temperature. The $f_{r,max}$ of 6.6 GHz at 5 °C and 2.5 GHz at 50 °C would give a thermal-limited bandwidth of 10 GHz and 3.9 GHz at 5 °C and 50 °C (refer to square symbols in Fig. 4.6), respectively. This suggests that the main limitation on the bandwidth might be due to the decrease in the differential gain, which may result from the thermal effects related to the carrier thermalization in the multi-stack QDs. The origin of the

temperature-dependent differential gain is currently under investigation.

Finally, the calculated intrinsic damping-limited bandwidth (squares) and thermal-limited bandwidth (circles) are shown for comparison with the experimental results $f_{3dB,measured}$ (triangles) in Fig. 4.6. The thermal-limited $f_{3dB,thermal}$ is in close agreement with the experimental results, indicating that the thermal effects limited the bandwidth measured in this study.

4.4 Summary

In conclusion, we studied the influence of the thermal effects on the small signal modulation characteristics of undoped InAs/InGaAs QD lasers. The roles of the temperature-dependent differential gain and the nonlinear gain compression factor in determining the frequency bandwidth were investigated. The calculation of the temperature-dependent bandwidth of the undoped QD laser showed a close agreement between the thermal-limited bandwidth and the measurement results. The bandwidth of the undoped InAs/InGaAs QD lasers was limited mainly by thermal effects, which may have resulted from carrier thermalization in the undoped QD laser structure. The incorporation of *p*-type modulation doping might improve the QD laser performance by reducing the thermal effects.

Chapter 5: Effects of *P*-doping and Rapid Thermal Annealing on the Two-State Lasing Behaviours of QD Lasers

Based on the literature reviews regarding the *p*-doping technique and QD intermixing, it is expected that both *p*-doping and proper thermal annealing can improve the gain characteristics of the QD laser. We believe that a study of the integration of these two methods will lead to a more complete picture on how *p*-doping and annealing can affect the lasing performances, specifically the two-state gain competition between the GS and the ES. This picture will be helpful for the development of high-speed QD lasers for uncooled telecommunication applications. Therefore, in this chapter, we investigate the effects of *p*-doping and annealing on the two-state competition in 1.3 μm InAs/InGaAs QD lasers.

5.1 Introduction

Since the first QD laser was developed about 15 years ago, the performance of the QD laser has improved significantly. As discussed in Chapter 2, due to the delta-like DOS in QDs, QD lasers have several advantages compared to conventional QW devices: extremely low threshold current densities, high internal efficiency, decreased temperature sensitivity, and emission wavelengths suitable for telecom applications (i.e. 1.3 μm and 1.55 μm) [8, 47, 50]. However, the high-speed modulation performance of QD lasers is generally poorer compared to the performance of QW lasers due to several factors such as the slow carrier capture/inter-level-relaxation mechanism and the closely spaced hole energy states in

the QDs. Compared to a less than 1 ps relaxation time in QWs [86], the reported relaxation times in QDs are typically in the range of 1-100 ps [87, 88].

In a spontaneous emission device, the impact of the slow relaxation time could be neglected. However, in a laser, the stimulated radiative emission rate is much faster than it is in a spontaneous emission device, so the effect of the relatively slow relaxation time may become significant [89]. Therefore, the slow inter-level relaxation of the carriers, combined with the limited DOS, leads to the easy occurrence of ES lasing in QD lasers [89-91]. Simultaneous GS and ES lasing, so called two-state lasing, may occur at a certain injected current levels. This simultaneous GS and ES lasing is undesirable since ES lasing reduces the GS lasing efficiency and thus degrades the device performance [92]. In order to achieve a larger bandwidth for telecommunication purposes, a short cavity length (≤ 1 mm) is required. Unfortunately, the occurrence of ES lasing is inevitable in lasers with short cavity lengths (i.e. ES lasing will eventually surpass GS lasing and dominate as the injected current and/or the operation temperature keeps increasing while the GS lasing gradually vanishes). To improve the high-speed performance of QD lasers for uncooled telecommunication applications, it is thus important to delay the onset of ES lasing to a higher injection current or operating temperature in short cavity lasers. However, only a few reports on the suppression of ES lasing in QD lasers exist [93].

Rapid thermal annealing (RTA) and *p*-doping are commonly used to improve the optical characteristics of QDs. The RTA process might result in the intermixing of the QD with the surrounding matrix, and the difference between the inter-level energy is expected to be smaller [94]. This will lead to a faster inter-level relaxation of carriers from the ES to the GS [60], and, consequently, to the possible suppression of ES lasing. Marcinkevicius *et al.* [30] reported that the RTA process improves the

dynamic characteristics by resulting in a faster carrier capture/relaxation mechanism. On the other hand, *p*-doping improves the gain properties and the temperature sensitivity behaviour of QD lasers [8, 47]. Many theoretical and experimental investigations [8, 45, 46, 49, 50, 95-99] have been conducted on the *p*-type modulation doping effect in QD laser gain. The theoretical studies [8] have shown obvious enhancements in the modal gain and the -3dB bandwidth of the *p*-doped QD lasers due to the large number of built-in excess holes in the QD active region, which saturate the energy levels in the valence band (VB) and reduce the thermal hole broadening. Furthermore, Masse *et al.* [49] recently show that *p*-doping can also reduce the effect of gain saturation and, thus, can allow GS lasing up to higher operating temperatures.

Recognizing that both RTA and *p*-doping could delay the onset of ES lasing, the study of both methods will lead to a more complete picture on how annealing and *p*-doping can affect the two-state competition in QD lasers. However, to the best of our knowledge, no publications have considered the effects of both methods on the competition between GS and ES lasing (i.e. two-state competition) in 1.3 μm QD lasers. Therefore, in this chapter, we investigate the effects of annealing and *p*-doping on the two-state competition in 1.3 μm InAs/InGaAs QD lasers.

5.2 Temperature-Dependent Study

The ten-layer InAs/InGaAs QD laser structure used in this experiment was described in Chapter 3 (Section 3.1). The undoped and *p*-doped InAs/InGaAs QD lasers have similar structures. The doping density in the *p*-doped QDs is 5.0×10^{17} cm^{-3}. The QD samples were capped with 200 nm of SiO_2 deposited by plasma enhanced chemical vapour deposition (PECVD) before annealing. For the samples

investigated in this work, the growth temperature for (Al)GaAs is 580 °C. Therefore, the annealing temperature should be higher than 580 °C for the annealing to take effect. The annealing process was then performed in N_2 ambient at 600 °C, 650 °C, and 700 °C at a constant annealing time of 15 s using a rapid thermal processor. After the annealing process, the PL intensity has been measured to predict the QD performance before the fabrication processes. As compared to the as-grown sample, PL intensity reduction and an obvious wavelength shift of ~4 nm have been observed for the 650 °C annealed sample. The PL intensity reduction and the blueshift become more obvious for the 700 °C annealed sample. The investigation of how annealing time affects the QD performance has been done by the previous research members in our group [100]. It has been found that increasing the annealing time has similar effects as increasing the annealing temperature. Therefore, the QD laser performance would be deteriorated with annealing temperature higher than 600 °C or annealing time longer than 15 s due to the reduction of PL intensity and wavelength shift. Generally, the blueshift of the emission wavelength will be larger and the structural changes to the dots will be more significant with a higher annealing temperature and a longer annealing time [33]. Subsequently, the as-grown, 600 °C, and 650 °C annealed samples were processed into 4-μm-wide RWG lasers and cleaved into individual laser bars [100].

The temperature-dependent light output power-current (*P-I*) measurement was carried out from 10 °C to 120 °C using a thermoelectric temperature controller. The logarithmic values of the threshold current densities ($\ln(J_{th})$) of the undoped and *p*-doped devices measured as a function of temperature are shown in Figs. 5.1 and 5.2, respectively.

As shown in Fig. 5.1, the characteristic temperatures (T_o) for the undoped

as-grown, 600 °C annealed and 650 °C annealed lasers were 98.7 K, 185.2 K and 41.8 K, respectively. The temperature investigated ranged from 10 °C to 45 °C since ES lasing started to dominate in the undoped 650 °C annealed laser after 50 °C. Among all the undoped QD lasers, the results showed that the 600 °C annealed laser had a better T_o than the as-grown one while the 650 °C annealed one had a poorer T_o than the as-grown one. Furthermore, the 600 °C annealed laser demonstrated lasing up to 120 °C while no lasing was observed for as-grown and 650 °C annealed lasers from 90 °C onwards. Most importantly, the undoped 600 °C annealed laser showed the lowest threshold current density among all the six samples throughout the measured temperature range from 10 °C to 120 °C. This could be due to the effective removal of nonradiative recombination centres by RTA [32].

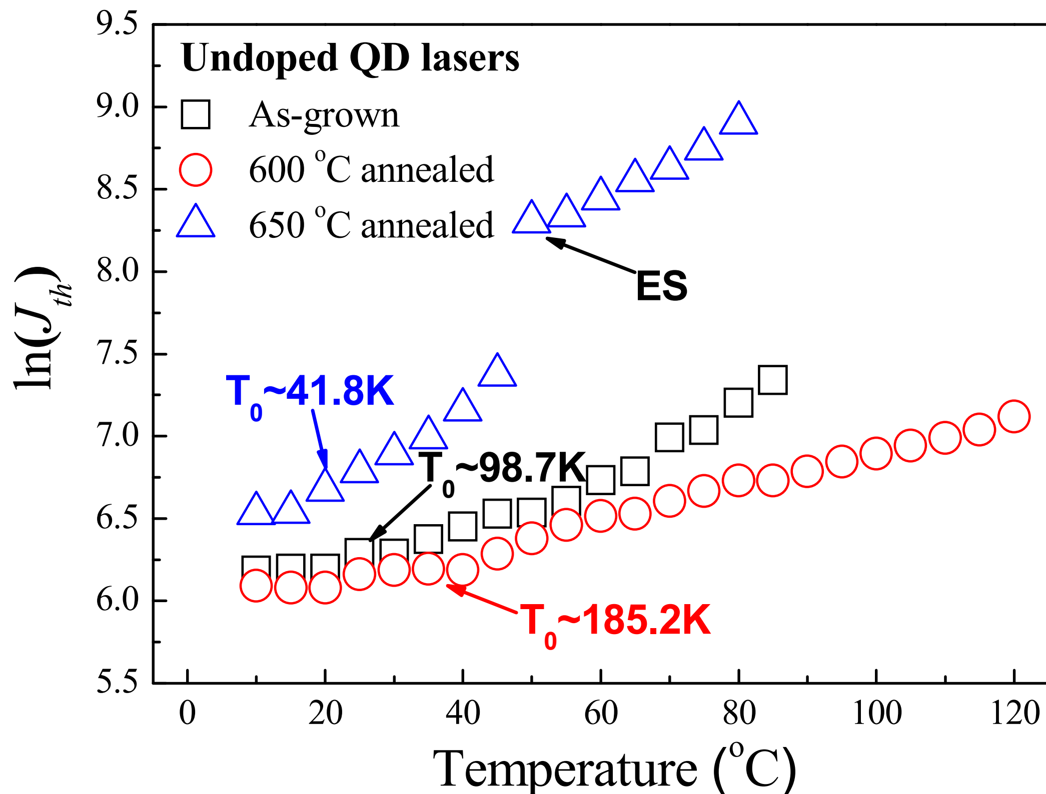

Figure 5.1 The plot of ln(J_{th}) versus the temperature of the undoped as-grown (open square), 600 °C annealed (open circle), and 650 °C annealed (open triangle)

QD lasers.

For the *p*-doped lasers, as shown in Fig. 5.2, all three types of *p*-doped lasers exhibited infinite T_o in the temperature range of 10-65 °C. This infinite T_o could be explained by the increase in Auger recombination and by the improved carrier thermalization with increasing temperature. The Auger recombination increases the threshold current. However, improved carrier thermalization with increasing temperature decreases the threshold current by increasing the efficiency of the radiative recombination due to the thermal escape of carriers from the dots and their transfer into deeper levels (larger dots) [49]. In the *p*-doped lasers, the electrostatic attraction of the excess holes increased the effective barrier for electron escape and thus limited the electron thermalization until a higher temperature compared to the undoped device. This resulted in a much larger T_o [50]. ES-dominated lasing started at 105 °C and 90 °C in the *p*-doped as-grown and 650 °C annealed QD lasers, respectively. No lasing was observed in the *p*-doped 650 °C annealed QD laser from 100 °C onwards. However, GS lasing dominated up to 120 °C in the *p*-doped 600 °C annealed QD laser. Therefore, *p*-doping clearly delayed the onset of ES lasing and sustained GS lasing to higher temperatures in QD lasers. In agreement with the work of Shchekin *et al.* [8], the introduction of the *p*-type doping increased the absolute value of J_{th} around room temperature (RT). Although *p*-doping increased the J_{th} of the device, it also improved the hole thermalization and carrier relaxation. This potentially resulted in an improved modulation speed and differential gain [98]. In addition, the 600 °C annealed laser showed the lowest J_{th} among all the *p*-doped samples.

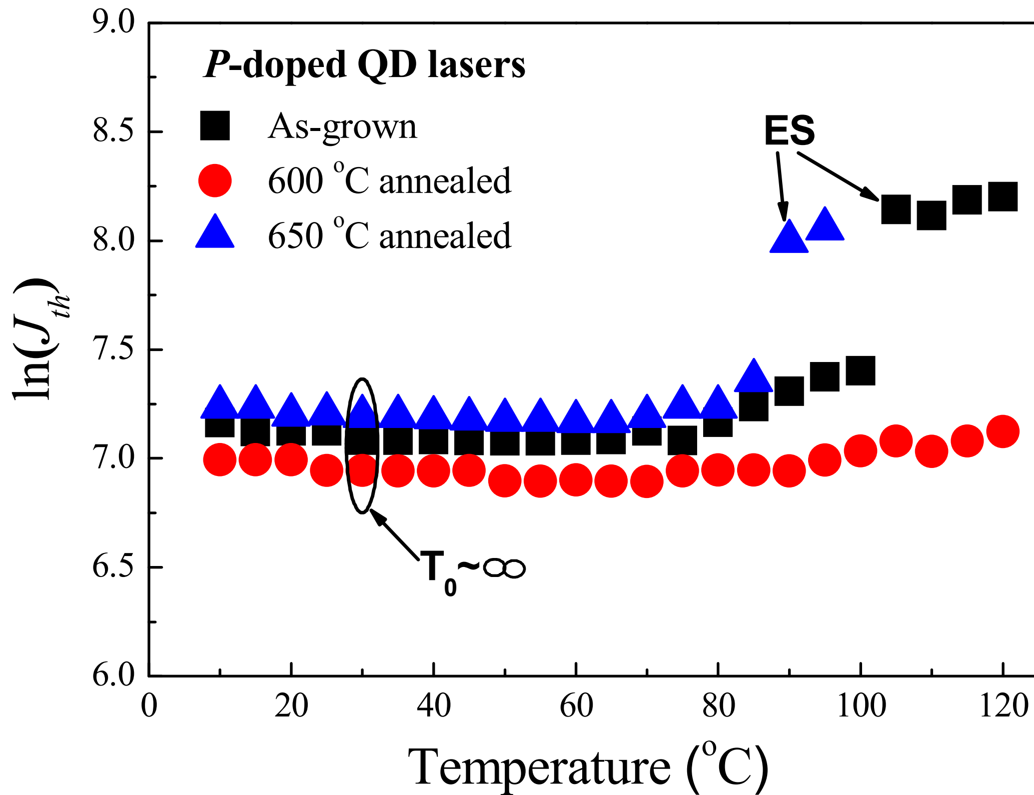

Figure 5.2 The plot of ln(J_{th}) versus the temperature of the *p*-doped as-grown (square), 600 °C annealed (circle), and 650 °C annealed (triangle) QD lasers.

5.3 Cavity-Dependent Study

In this study, we cleaved the fabricated QD lasers into different cavity lengths (1-4 mm) and characterized them under continuous-wave (CW) operation at RT. The internal quantum efficiency (η_i) and the internal optical loss (α_i) were extracted from a plot of the reciprocal of external differential quantum efficiency (η_d^{-1}) versus the cavity length (L) for the undoped and *p*-doped QD lasers, (see Figs. 5.3 and 5.4, respectively). The values of η_i and α_i for the six samples investigated in this chapter are summarized and depicted in Table 5.1.

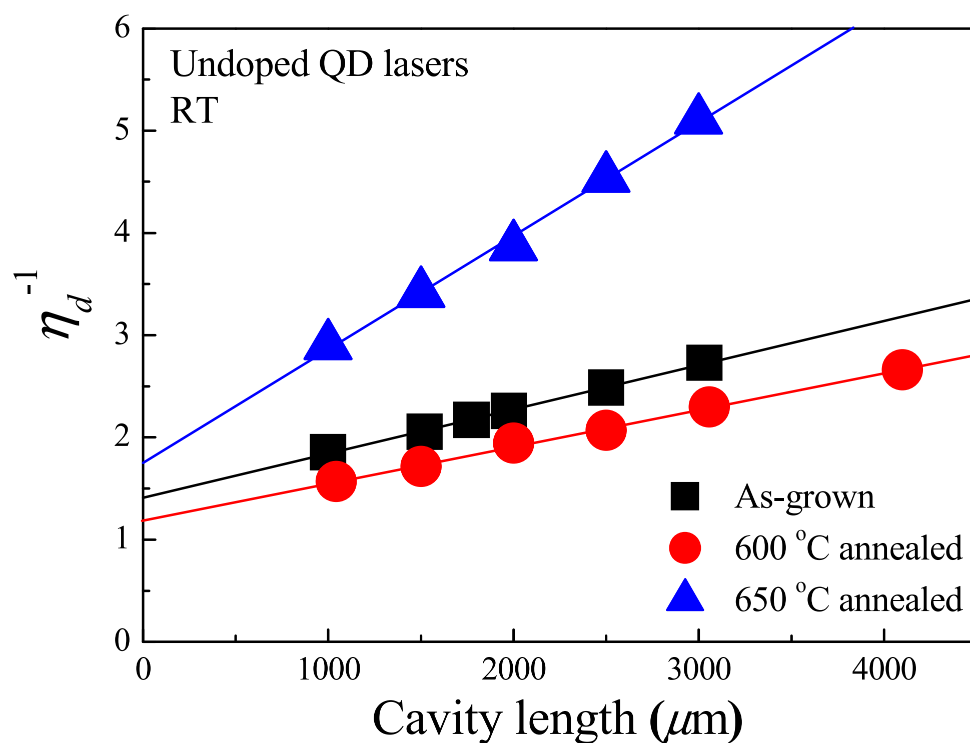

Figure 5.3 The plot of η_d^{-1} against L for the undoped as-grown, 600 °C annealed and 650 °C annealed QD lasers at RT.

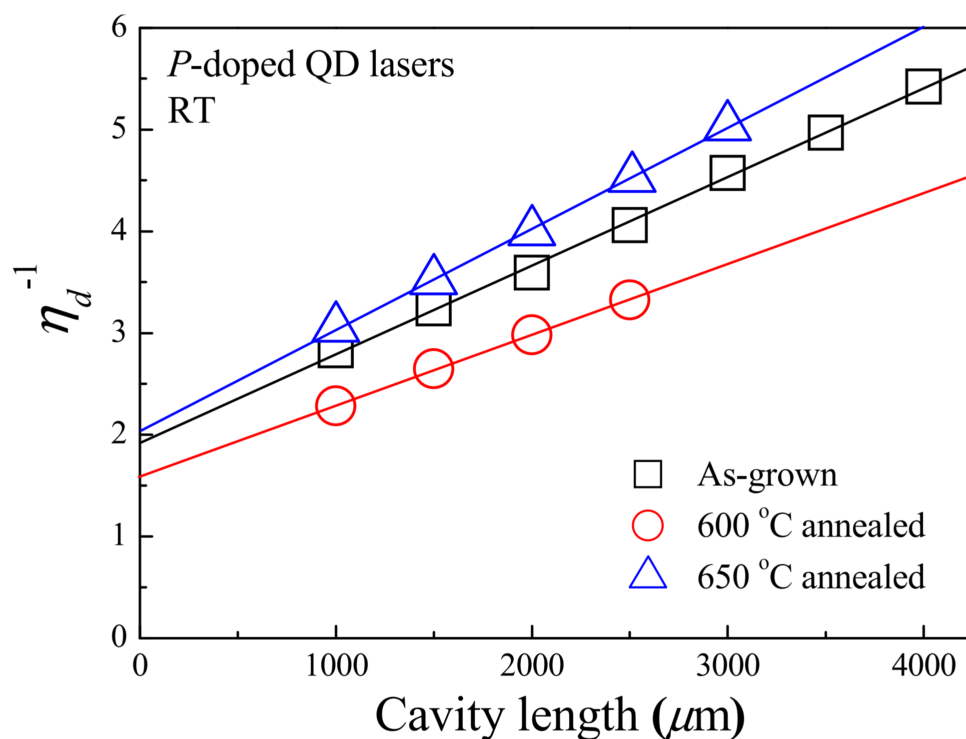

Figure 5.4 The plot of η_d^{-1} against L for the *p*-doped as-grown, 600 °C annealed and 650 °C annealed QD lasers at RT.

Table 5.1 The internal quantum efficiency (η_i) and the internal optical loss (α_i) of the six QD laser samples.

Sample Description	η_i (%)	α_i (cm^{-1})
undoped as-grown	71.2	3.57
undoped 600 °C annealed	83.9	3.3
undoped 650 °C annealed	57.3	7.25
p-doped as-grown	52.1	5.18
p-doped 600 °C annealed	62.6	4.94
p-doped 650 °C annealed	49.1	5.55

Although *p*-doping can improve the characteristic temperature, it has drawbacks in the laser internal quantum efficiency and in the internal optical loss due to the inter-valence band absorption (IVBA) [49] and the nonradiative recombination [50]. Comparing the samples under the same annealing conditions (refer to Figs. 5.3 and 5.4), the differential efficiency of the *p*-doped QD laser was generally poorer than that of the undoped QD laser due to the presence of a larger internal optical loss in the *p*-doped QD laser. Therefore, the characteristics of the undoped 600 °C annealed QD laser will be preferred in low-power communications and in emerging areas such as on-chip communications due to its low threshold, high efficiency, and low loss. On the other hand, the characteristics of the *p*-doped 600 °C annealed QD laser will be preferred in uncooled fibre optic applications due to its infinite characteristic temperature.

Compared to the as-grown QD lasers (undoped, *p*-doped), the improvement in the internal quantum efficiency of the 600 °C annealed QD lasers (undoped 600 °C annealed, *p*-doped 600 °C annealed) could be attributed to the removal of grown-in defects (acting as nonradiative recombination centres) due to the low-temperature growth (~485 °C) required for our QDs [32, 101]. A faster inter-level relaxation is

also expected in the 600 °C annealed QDs. Shi *et al.* [90] showed that the external quantum efficiency of the GS decreases almost linearly with the increase in the inter-level relaxation time. A fast inter-level relaxation is favourable for the GS lasing and leads to a higher GS capture efficiency in QDs and, thus, to a higher external differential quantum efficiency. When the inter-level relaxation becomes slower, the carriers captured into the ES cannot relax to the GS immediately and continue to fill up the ES [90]. The ES lasing will occur when the population inversion for the transition between the ES electrons and the GS holes is satisfied [90]. Consequently, the higher efficiency in the 600 °C annealed QD samples indicated a lower wetting layer (WL) carrier occupation probability and a higher GS capture efficiency, which might be due to the faster inter-level relaxation and the increase in radiative efficiency induced by RTA [32, 101]. However, the 650 °C annealed laser (undoped 650 °C annealed, *p*-doped 650 °C annealed) showed the poorest internal efficiency and internal optical loss among the QD lasers with the same doping condition. This could be attributed to the carrier leakage due to the relatively high annealing temperature of 650 °C. The group-III atoms intermixing mechanisms modify the composition potential from an abrupt interface to a graded one, leading to a shallower confinement potential (thus resulting in carrier leakage) [55, 61]. The threshold current of the GS lasing ($I_{th,GS}$), the characteristic temperature, and the efficiency of the undoped 650 °C annealed QD laser showed more obvious degradation compared to these characteristics of the *p*-doped 650 °C annealed QD laser. Therefore, it seems that the *p*-doped samples were more resistant to annealing. A possible explanation for this resistance could be the higher interstitial concentration in the *p*-doped QD samples, which may suppress the effects of annealing [61, 94].

5.4 QDs Gain Characteristics

The modal gain and electroluminescence (EL) spectra measurements were performed with an optical spectrum analyzer (OSA) at room temperature (RT) for QD lasers with cavity lengths of 1 mm. The details of the experimental set-up were explained in Chapter 3. The net modal gain ($G_{net}=G-\alpha_i$) was extracted from the amplified spontaneous emission (ASE) spectra using the Hakki-Paoli method [73]. By measuring the modulation depth of the Fabry-Perot (FP) resonances in the ASE spectra, G_{net} was determined using Equation (3.1). The measurements were performed from below the GS lasing threshold to above the ES lasing threshold.

Figure 5.5 depicts the net modal gain spectra of the undoped as-grown QD laser device at a series of injection current levels near the ES lasing threshold. When the injection current is low, as shown in Fig. 5.5 (a), only the GS lasing was observable with the maximum GS net modal gain pinned at its threshold value (~11.3 cm^{-1}). The ES modal gain, on the other hand, revealed a negative value for the whole wavelength range investigated. The ES modal gain increased following the increase in the injection current (see Fig. 5.5 (b)-(c)). Once the injection current was above the ES lasing threshold ($I_{th,ES}$), which was 12.3×$I_{th,\mathrm{GS}}$, the value of the maximum ES net modal gain was pinned at its threshold value (see Fig. 5.5 (c)-(d)). The net modal gain G_{net} was the gain available to overcome the mirror losses ($1/L\cdot\ln(1/R)$) in a laser with a cavity length of L and a facet reflectivity of R. Therefore, if both the GS and the ES net modal gains reach saturation, they saturate at the same maximum value, which is equal to the mirror loss of the laser. In contrast, as shown in Fig. 5.5 (c)-(d), in our samples the GS modal gain decreased as the injection current increased further. In the case of a high injection current, the GS transition did not have enough gain to perform the lasing operation, leaving the ES as the only surviving lasing peak (see Fig. 5.5 (d)).

The observations from the modal gain spectra clearly show the competition between GS and ES lasing in the as-grown QD laser device.

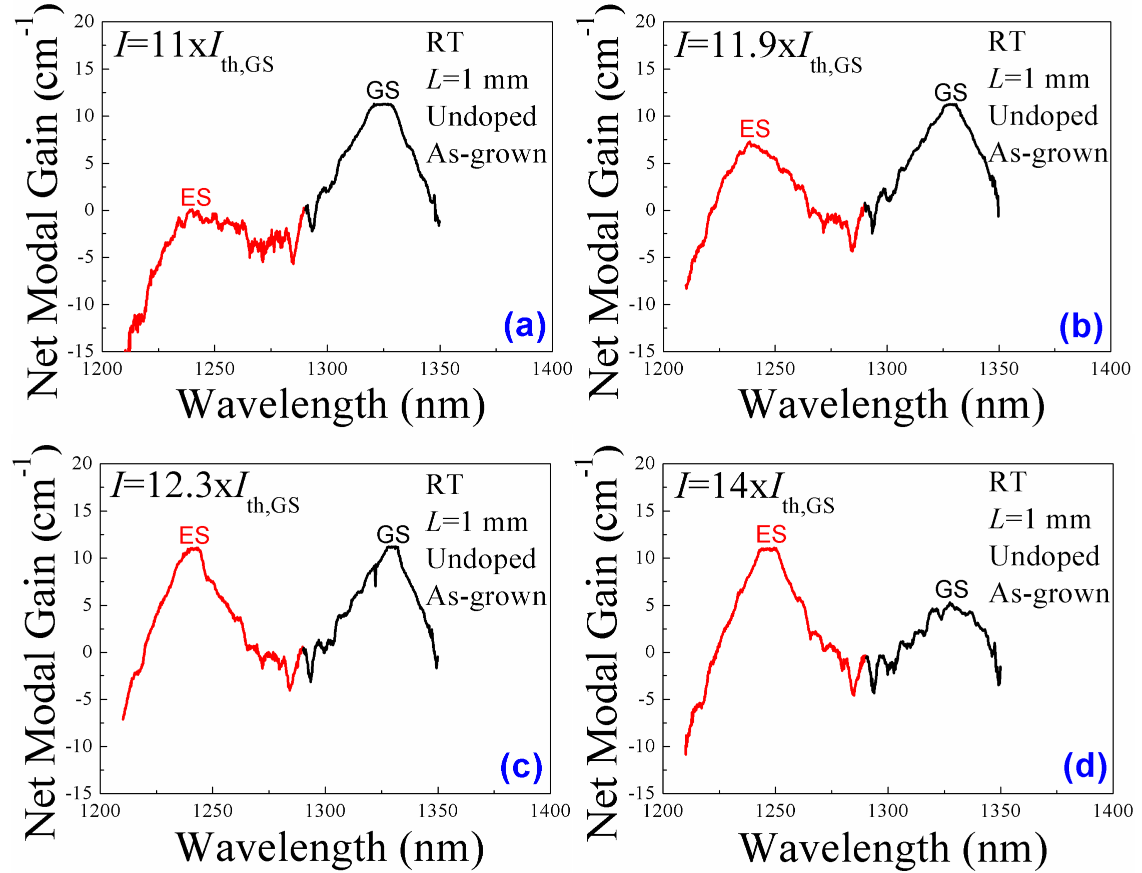

Figure 5.5 The net modal gain spectra as a function of the wavelength for the undoped as-grown QD laser with injection currents at (a) I=11×$I_{th,\mathrm{GS}}$, (b) I=11.9×$I_{th,\mathrm{GS}}$, (c) I=12.3×$I_{th,\mathrm{GS}}$, and (d) I=14×$I_{th,\mathrm{GS}}$.

Figure 5.6 depicts the net modal gain spectra as a function of the wavelength for the undoped 600 °C annealed QD laser device at a series of injection current levels near the ES lasing threshold. As shown in Fig. 5.6 (a)-(c), the ES modal gain increased following an increase in the injection current. The value of the maximum ES net modal gain was obtained at 17.2×$I_{th,\mathrm{GS}}$ (as shown in Fig. 5.6 (c)-(d)).

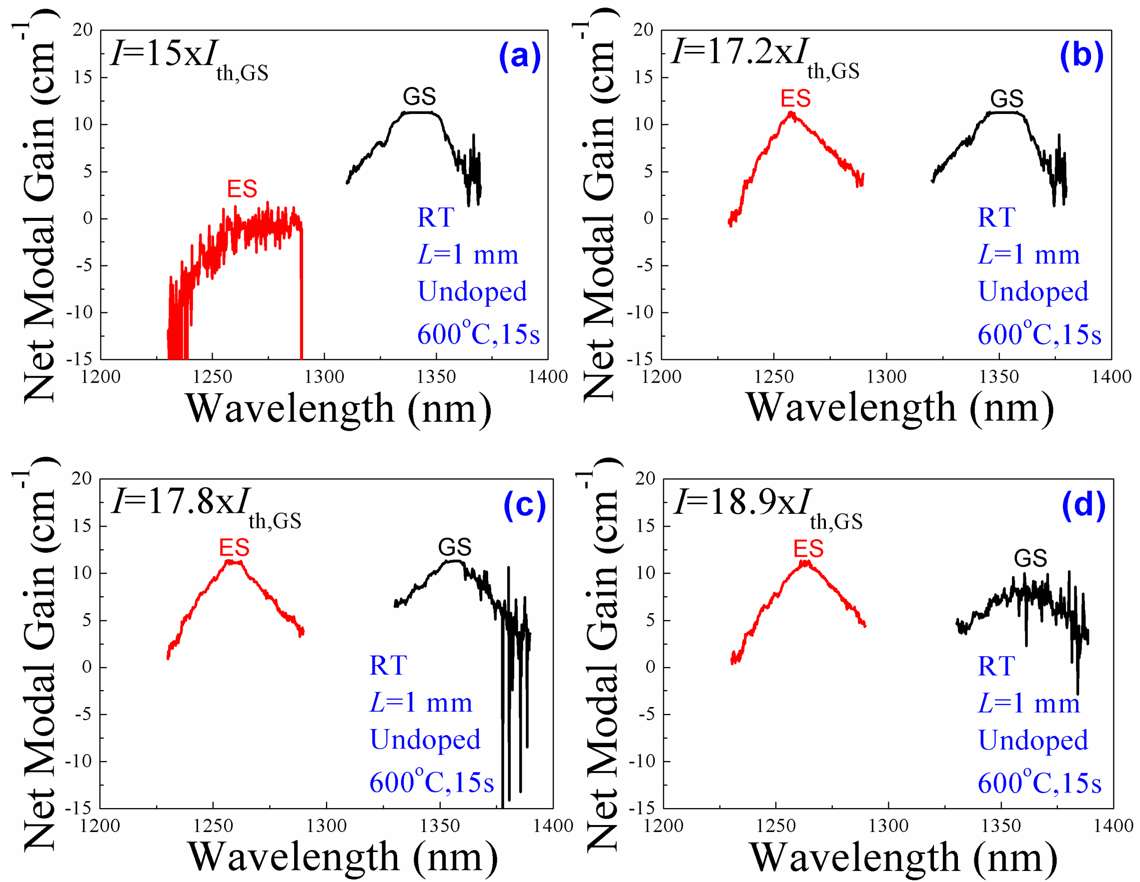

Figure 5.6 The net modal gain spectra as a function of the wavelength for the undoped 600 °C annealed QD laser with injection currents at (a) I=15×$I_{th,\mathrm{GS}}$, (b) I=17.2×$I_{th,\mathrm{GS}}$, (c) I=17.8×$I_{th,\mathrm{GS}}$, and (d) I=18.9×$I_{th,\mathrm{GS}}$.

Figure 5.7 depicts the net modal gain spectra as a function of the wavelength for the undoped 650 °C annealed QD laser device at a series of injection current levels near the ES lasing threshold. As shown in Fig. 5.7 (a)-(c), the ES modal gain increased following an increase in the injection current. The value of the maximum ES net modal gain was obtained at 5.4×$I_{th,\mathrm{GS}}$ (as shown in Fig. 5.7 (c)-(d)).

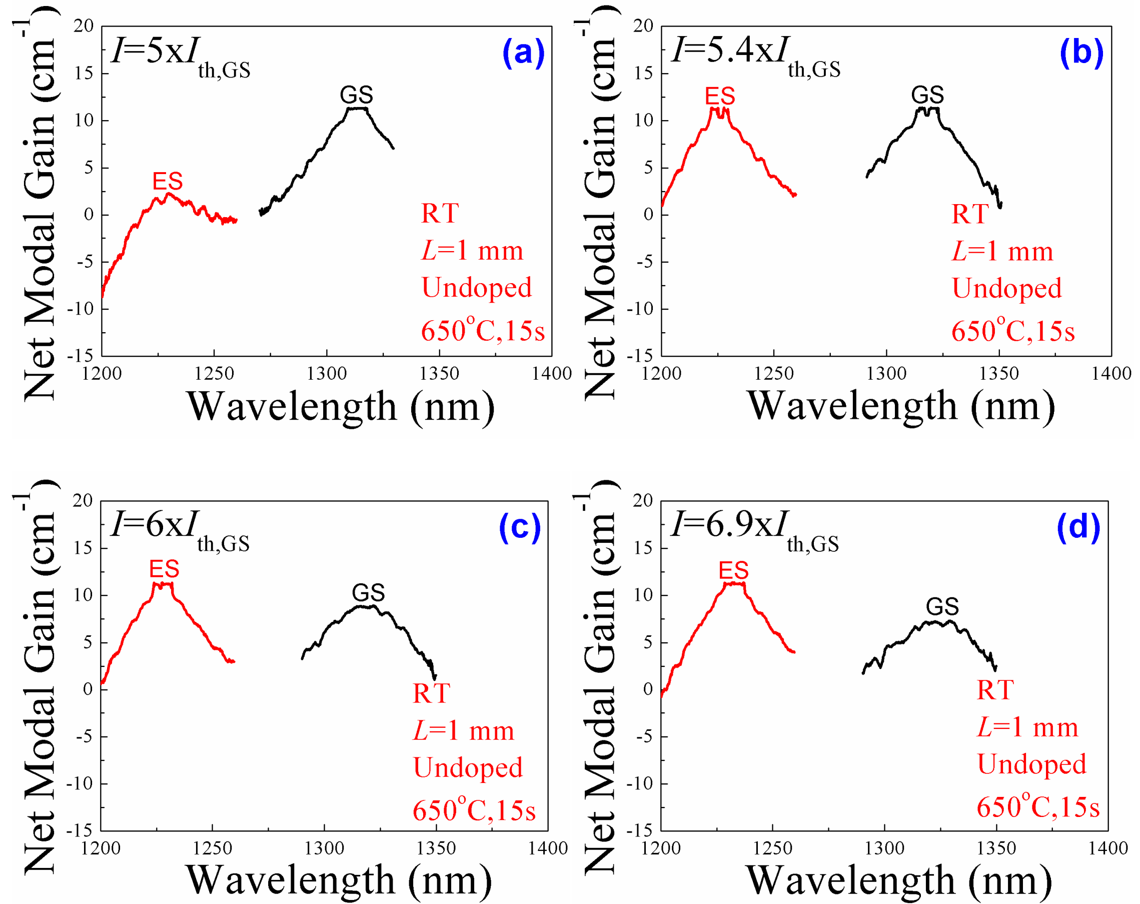

Figure 5.7 The net modal gain spectra as a function of the wavelength for the undoped 650 °C annealed QD laser with injection currents at (a) I=5×$I_{th,\mathrm{GS}}$, (b) I=5.4×$I_{th,\mathrm{GS}}$, (c) I=6×$I_{th,\mathrm{GS}}$, and (d) I=6.9×$I_{th,\mathrm{GS}}$.

The measured peak net modal gain of GS (solid symbols) and ES (open symbols) lasing as a function of the normalized injection current (with respect to the GS threshold current of each sample) for the undoped QD samples at room temperature are summarized in Figs. 5.8 to 5.10. In comparison, Figs. 5.11 to 5.13 show this for the *p*-doped QD samples. Before the onset of ES lasing, the GS net modal gain reached its maximum (~11.3 cm^{-1}) for all QD laser samples since they had the same cavity length of ~1 mm. Then the GS net modal gain started to decrease at a certain current level since fewer carriers relaxed from the ES to the GS at high

excitation conditions. At the same time, the gain of ES lasing increased rapidly with an increasing injection current. The ES reached transparency when the GS started saturating, further demonstrating the thermal distribution of the carriers. However, the undoped and *p*-doped QD samples with the same annealing condition exhibited different gain behaviours, which will be explained in detail in the following sections.

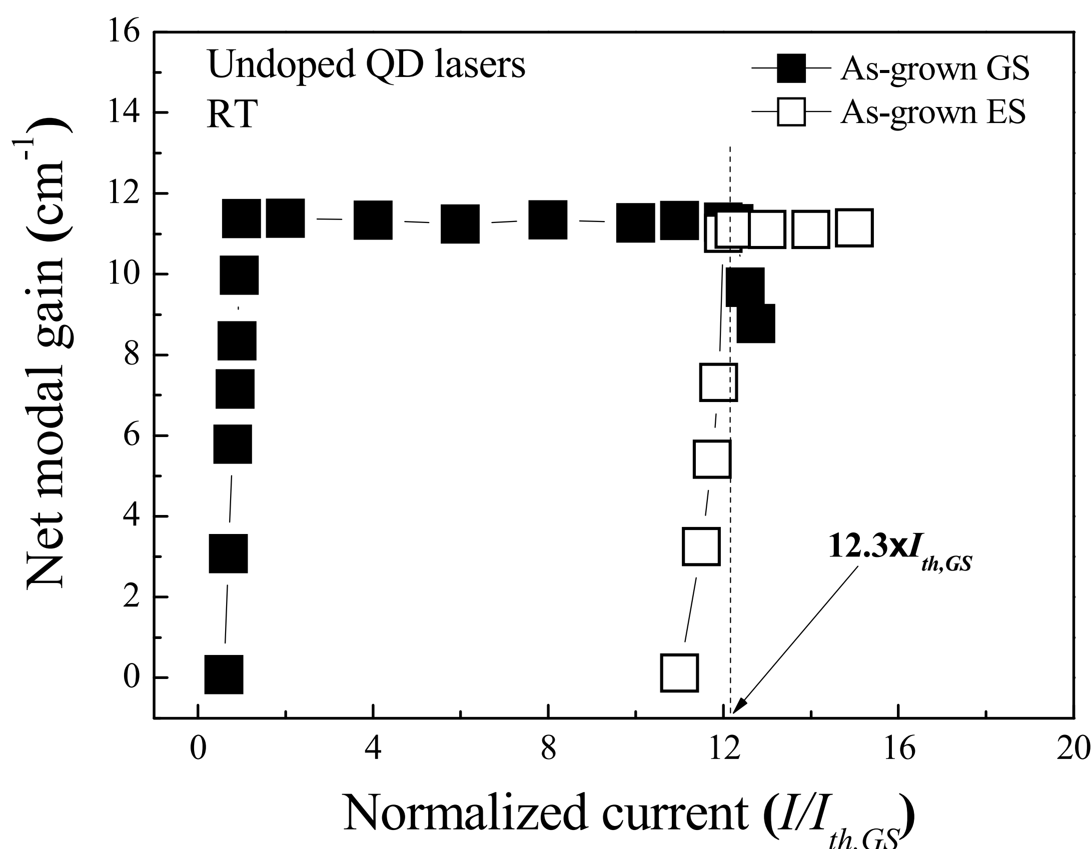

Figure 5.8 The maximum net modal gain of the GS (solid square) and the ES (open square) emissions versus a normalized injection current for the undoped as-grown QD laser at RT.

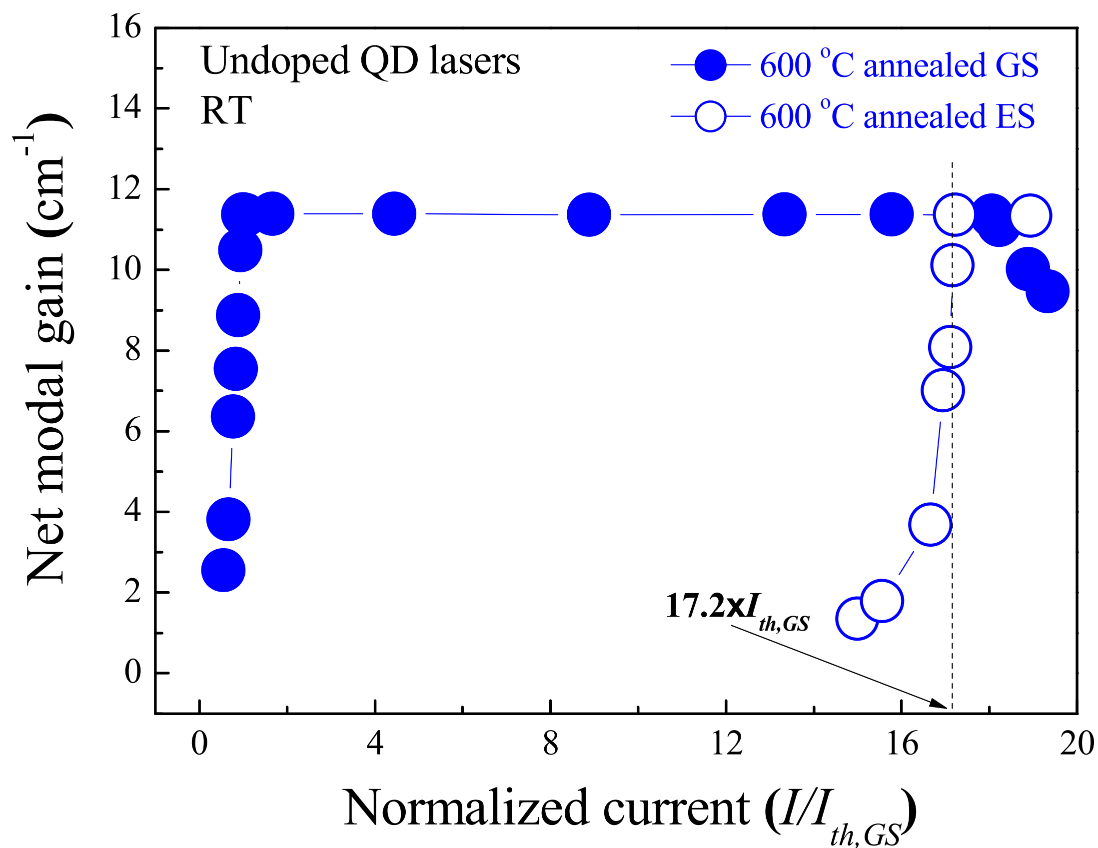

Figure 5.9 The maximum net modal gain of the GS (solid circle) and the ES (open circle) emissions versus a normalized injection current for the undoped 600 °C annealed QD laser at RT.

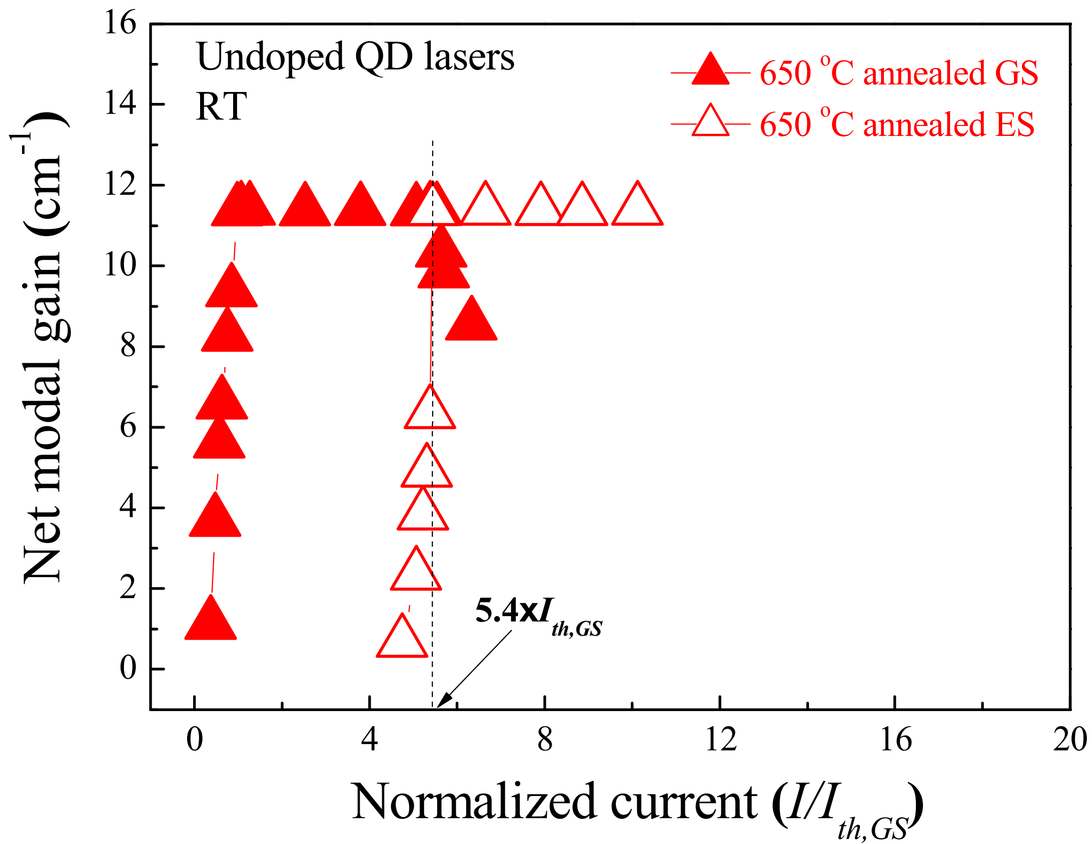

Figure 5.10 The maximum net modal gain of the GS (solid triangle) and the ES (open triangle) emissions versus a normalized injection current for the undoped 650 °C annealed QD laser at RT.

In the undoped QD lasers (refer to Figs. 5.8-5.10), the GS modal gain started to decrease at 12.3×$I_{th,GS}$, 18×$I_{th,GS}$ and 5.4×$I_{th,GS}$ for the as-grown, 600 °C annealed and 650 °C annealed QD lasers, respectively. The ES gain reached its maximum value at 12.3×$I_{th,GS}$, 17.2×$I_{th,GS}$ and 5.4×$I_{th,GS}$ for the as-grown, 600 °C annealed and 650 °C annealed lasers, respectively.

The $I_{th,ES}$ of the undoped as-grown, 600 °C annealed and 650 °C annealed QD lasers were 241 mA, 301 mA and 172 mA, respectively. The $I_{th,GS}$ of the undoped as-grown, 600 °C annealed and 650 °C annealed QD lasers were 19.6 mA, 17.5 mA and 31.7 mA, respectively.

In comparison, in the *p*-doped QD lasers (refer to Fig. 5.11-5.13), the GS modal gain started to decrease at 6.5×$I_{th,GS}$, 8×$I_{th,GS}$ and 3.7×$I_{th,GS}$ for the as-grown, 600 °C annealed and 650 °C annealed QD lasers, respectively. The ES gain reached its maximum value at 5.8×$I_{th,GS}$, 7×$I_{th,GS}$ and 3.6×$I_{th,GS}$ for the as-grown, 600 °C annealed and 650 °C annealed QD lasers, respectively.

The $I_{th,ES}$ of the *p*-doped as-grown, 600 °C annealed and 650 °C annealed QD lasers were 274 mA, 277 mA, and 192 mA, respectively. The $I_{th,GS}$ of the *p*-doped as-grown, 600 °C annealed and 650 °C annealed QD lasers were 47.5 mA, 39.6 mA, and 53.5 mA, respectively.

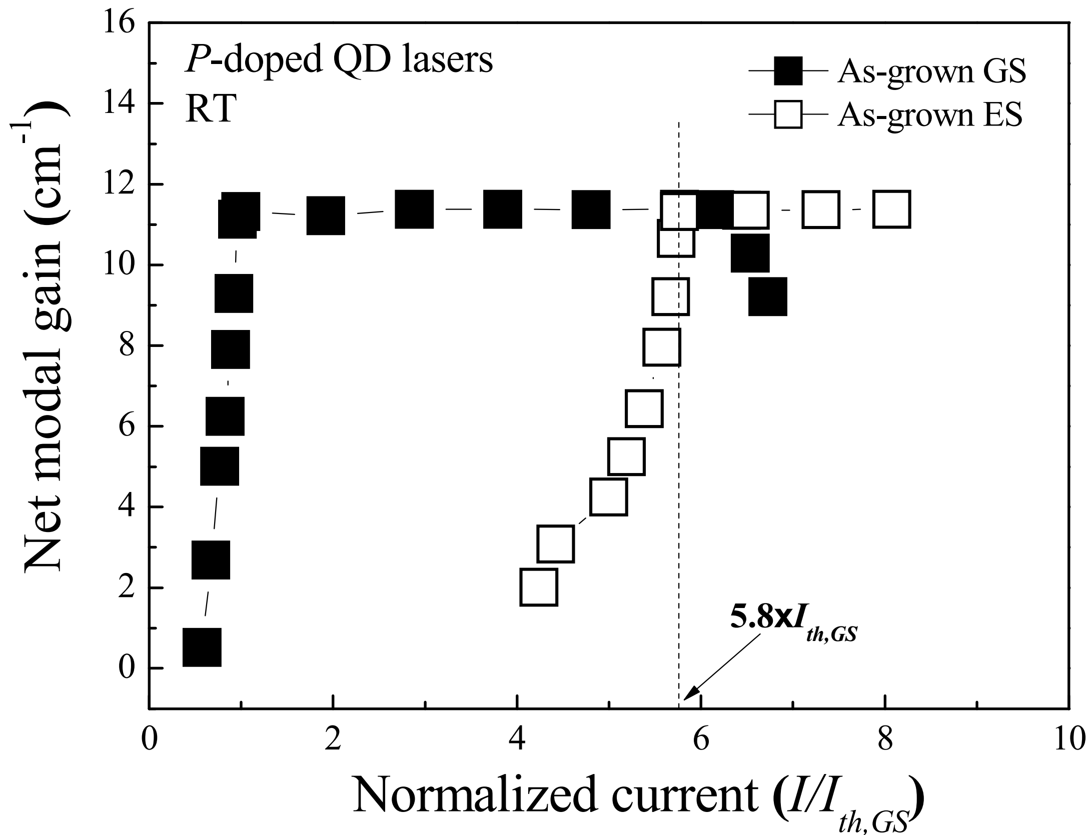

Figure 5.11 The maximum net modal gain of the GS (solid square) and the ES (open square) emissions versus a normalized injection current for the *p*-doped as-grown QD laser at RT.

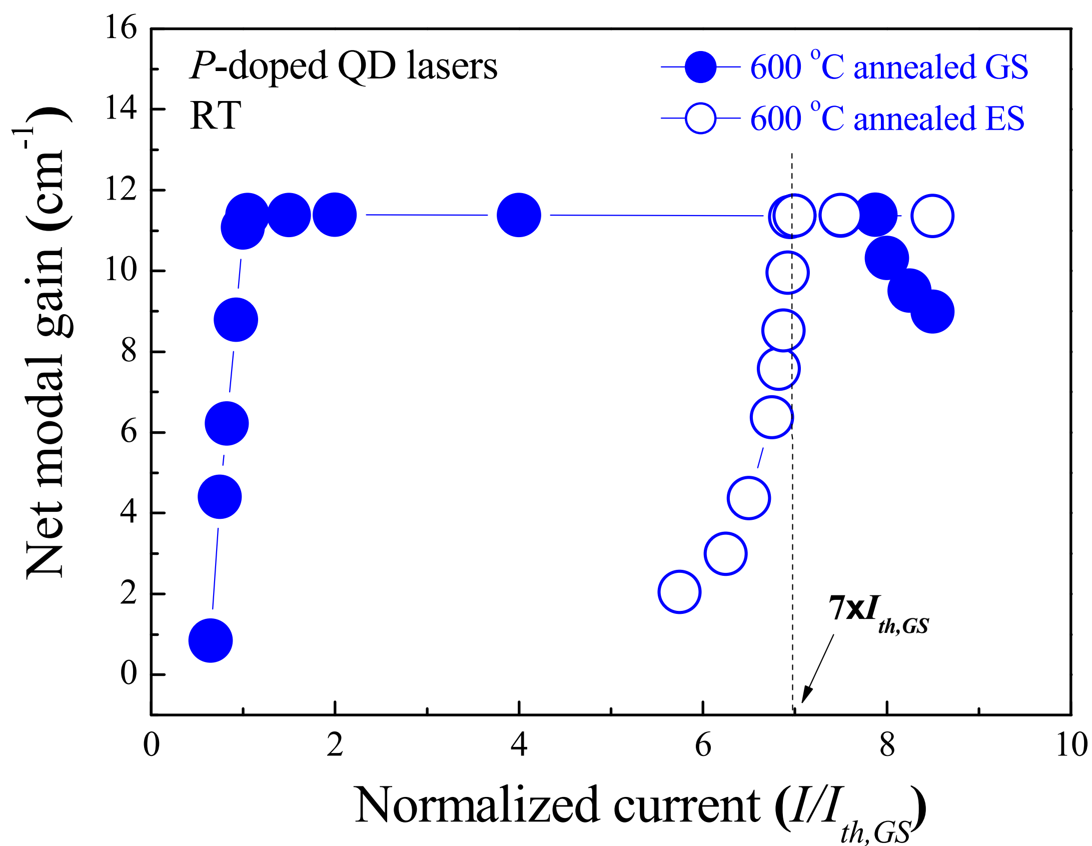

Figure 5.12 The maximum net modal gain of the GS (solid circle) and the ES (open circle) emissions versus a normalized injection current for the *p*-doped 600 °C annealed QD laser at RT.

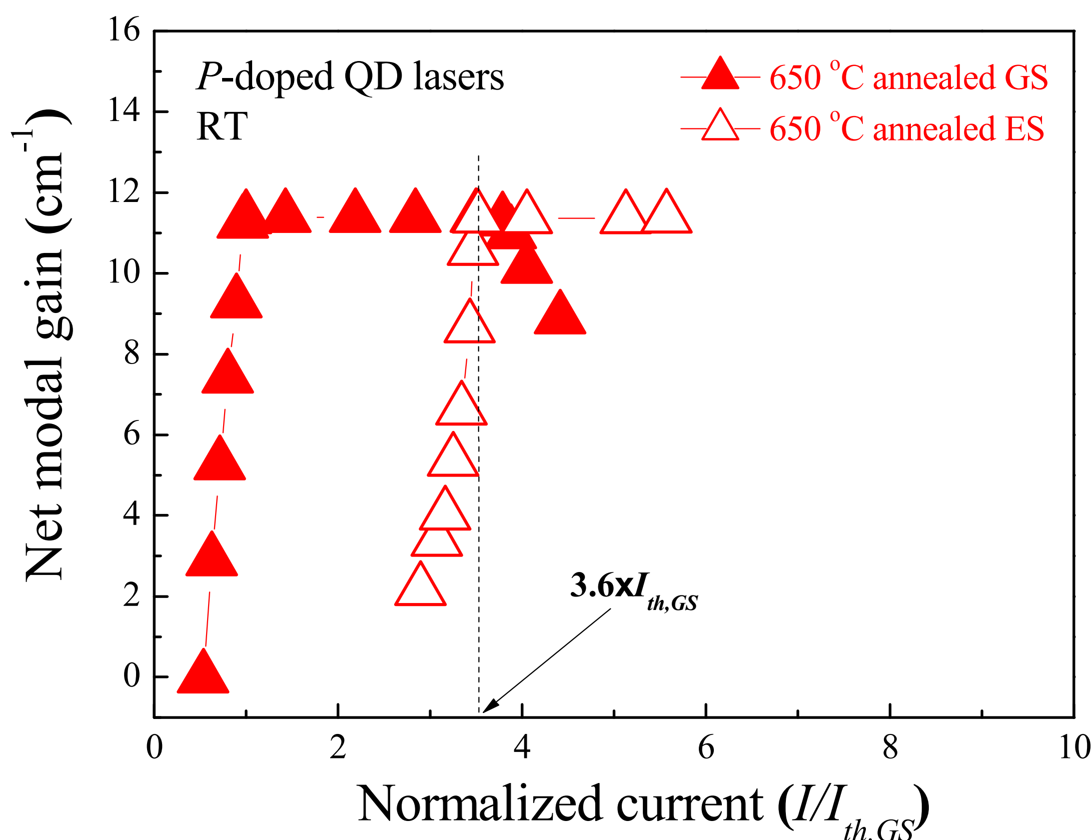

Figure 5.13 The maximum net modal gain of the GS (solid triangle) and the ES (open triangle) emissions versus a normalized injection current for the *p*-doped 650 °C annealed QD laser at RT.

Figures 5.14 and 5.15 show the EL spectra captured around the GS threshold for the undoped and *p*-doped QD lasers. The lasing wavelengths at the GS threshold were 1296.5 nm, 1295.6 nm, and 1290.2 nm for the undoped as-grown, 600 °C annealed and 650 °C annealed QD lasers. In addition, the lasing wavelengths were 1300.1 nm, 1299.5 nm, and 1297.0 nm for the *p*-doped as-grown, 600 °C annealed and 650 °C annealed QD lasers. A blueshift of 6 nm (i.e. ~0.5% of the centre wavelength) in the undoped 650 °C annealed QD sample and a blueshift of 3 nm in the *p*-doped 650 °C annealed QD sample compared to each as-grown QD sample was observed. This result suggests the onset of In-Ga intermixing at the annealing temperature of 650 °C.

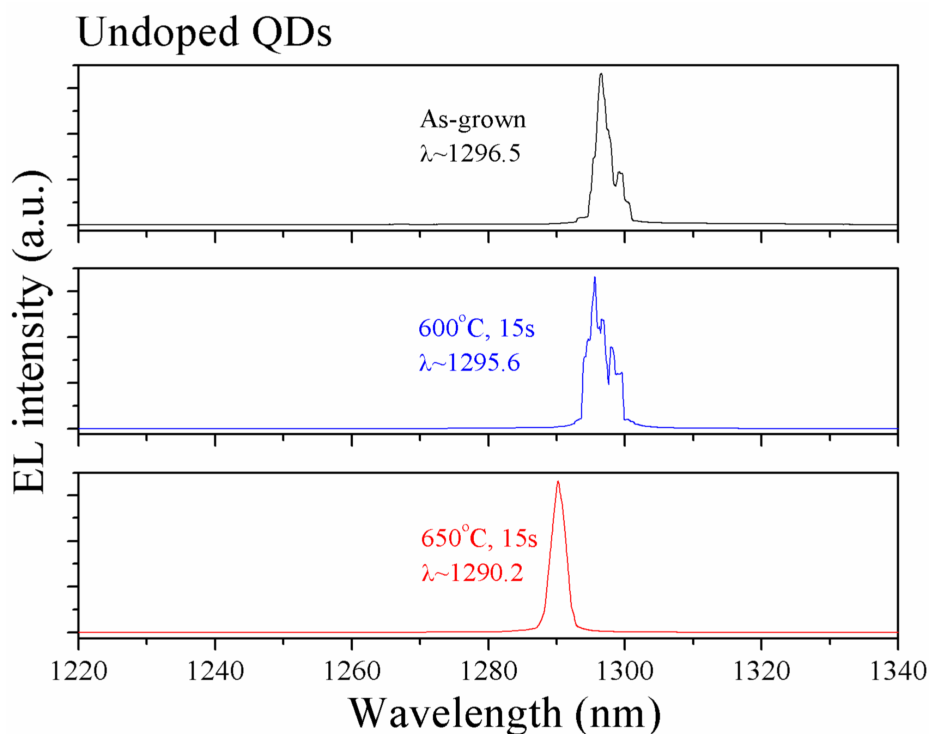

Figure 5.14 The EL spectra of the undoped QD lasers under an injection current level around the GS threshold.

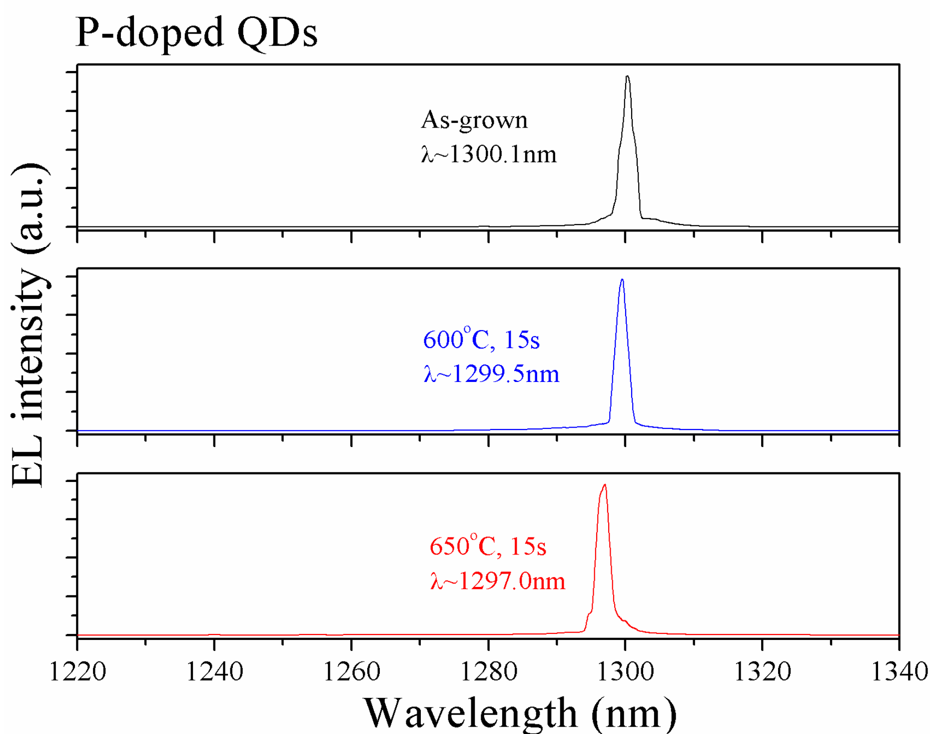

Figure 5.15 The EL spectra of the *p*-doped QD lasers under an injection current level around the GS threshold.

In the as-grown QD samples, the $I_{th,ES}$ was increased from 241 mA in the undoped QD laser to 277 mA in the *p*-doped QD laser. By comparing the absolute values of the $I_{th,ES}$, this implies that the QD laser can be driven harder before the gain switches from the GS to the ES with the presence of *p*-doping, which is consistent with the work of Smowton *et al.* [47]. We observed that the ES gain in the undoped as-grown, undoped 650 °C annealed and *p*-doped 650 °C annealed QD lasers reached its maximum value at approximately the point that the GS gain started to decrease, showing that the GS and the ES transitions competed for the same carriers [92]. However, in the case of the *p*-doped as-grown, *p*-doped 600 °C annealed and the undoped 600 °C annealed QD lasers, the GS gain remained at its maximum for a while before decreasing after the ES lasing reached the maximum modal gain.

These phenomena have not been reported before. This might be explained as the larger number of electrons in the conduction band (CB) waiting for recombination in the *p*-doped as-grown and the *p*-doped 600 °C annealed QDs due to the electrostatic attraction of excessive holes. For the undoped 600 °C annealed QD laser, the reason might be the faster carrier relaxation mechanism from the ES to the GS after annealing [60]. Therefore, a larger number of available states in the CB promises the population inversion of the ES without sacrificing the GS gain of the QDs. However, these phenomena have not been observed in undoped 650 °C annealed and *p*-doped 650 °C annealed QD lasers. The degradation of the gain performance in the 650 °C annealed lasers could be attributed to the carrier leakage from the shallower interdiffused QD potential due to the relatively high annealing temperature [61].

We also noticed that the $I_{th,ES}$ in the *p*-doped 600 °C annealed QD laser (i.e. 277 mA) was lower than that in the undoped 600 °C annealed QD laser (i.e. 301 mA). This could be due to the smaller annealing induced effects for the *p*-doped QD

samples since the interstitial concentration is higher [61]. This implies that the optimum annealing temperature to enhance the GS and to suppress the ES for the *p*-doped QDs could be slightly higher than that for the undoped QDs (600 °C). As such, smaller temperature steps (between 600 °C and 650 °C) would be required to determine the optimum annealing conditions.

5.5 Structural Investigation by TEM Study

We speculated that, after annealing, (i) a very small degree of In-Ga interdiffussion between the QD and its surrounding barrier layer might have occurred in the 650 °C annealed QDs, and (ii) the dot shape may have experienced a very small degree of change (less than 0.1 nm). In order to clarify the structural changes of the dots, cross-sectional transmission electron microscope (TEM) measurements were performed on the as-grown, 600 °C and 650 °C annealed QD samples and these measurements are shown in Fig. 5.16.

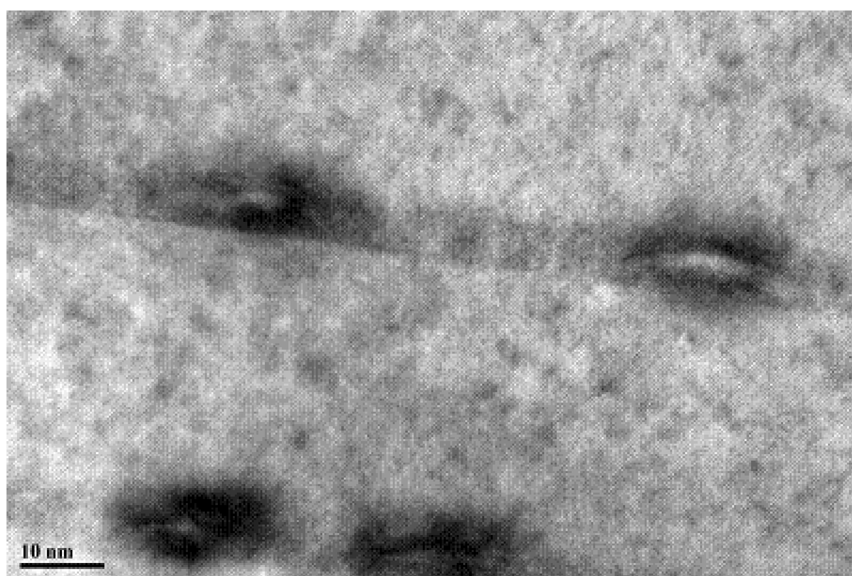

(a)

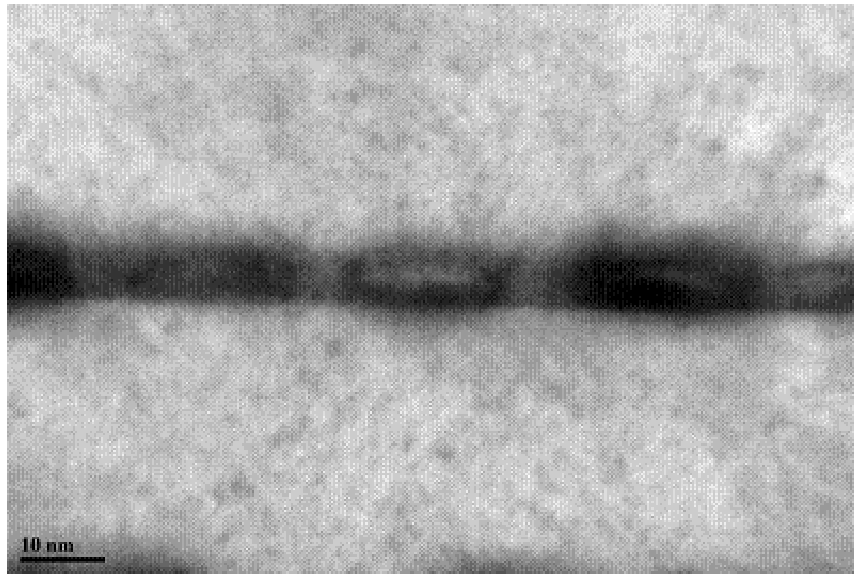

(b)

(c)

Figure 5.16 The TEM images of the (a) as-grown, (b) 600 °C annealed and (c) 650 °C annealed QDs.

However, from the lasing spectra of the undoped QD lasers shown in Fig. 5.14, the largest wavelength change after annealing should be the undoped 650 °C annealed QD laser with a wavelength change of 6 nm. Therefore, a less than 0.5% change of wavelength existed between the undoped 650 °C annealed QD laser and the

undoped as-grown QD laser. This means that only a very small degree of change (i.e. <0.1 nm) occurred in the 650 °C annealed QDs, which may not be observable in the TEM images. We expect that the Indium diffusion or the change of dot shape might not be obvious in the TEM images because there is only a 0.5% change in the wavelength.

5.6 Summary

The effects of *p*-doping and annealing on the two-state gain competition of the 1.3 μm InAs/InGaAs QD lasers were investigated in this chapter. In comparison with the as-grown QD lasers, both the undoped and the *p*-doped QD lasers exhibited enhancement (suppression) in GS (ES) lasing for the QD samples annealed at 600 °C for 15 s and suppression (enhancement) in GS (ES) lasing for the QD samples annealed at 650 °C for 15 s. We believe that the enhancement of GS lasing is due to the removal of nonradiative recombination centres upon annealing at 600 °C. This removal reduces the relaxation time and increases the relaxation efficiency. The suppression of GS lasing for the QD lasers annealed at the higher temperature (i.e. 650 °C) is believed to be due to carriers leaking out from the shallower interdiffused QD potential. This carrier leakage implies that there is an optimum annealing condition such that GS (ES) lasing can be effectively enhanced (suppressed). In addition, the optimum annealing condition has been determined to be at 600 °C for 15 s. For QD lasers annealed under the same conditions, the *p*-doped QD lasers were found to exhibit infinite characteristic temperatures and could sustain GS lasing to higher operating temperatures compared to the undoped ones. However, the differential efficiency and the internal optical loss of the *p*-doped QD lasers were poorer than that of the undoped ones. Therefore, a tradeoff exists in the QD laser

performances and the choice of undoped or *p*-doped QD lasers will depend on the application. We believe that these findings will be beneficial to researchers working on high-speed QD lasers for uncooled telecommunication applications.

Chapter 6: Effects of Rapid Thermal Annealing on the High-Speed Characteristics of Intrinsic QD Lasers

In Chapter 5, we investigated the annealing effects on the gain characteristics of the undoped QD lasers. A significant improvement of the ground state (GS) lasing was demonstrated upon optimum annealing (i.e. 600 °C for 15 s). This suggests that postgrowth thermal annealing is a promising method to improve the device performance. Therefore, in this chapter, we investigate the effects of rapid thermal annealing (RTA) on the high-speed performances of 1.3 μm InAs/InGaAs QD lasers based on the optimum annealing condition. The temperature-dependencies of the internal quantum efficiency, the internal optical loss, the differential gain, and the nonlinear gain compression factor of the as-grown and annealed 1.3 μm QD lasers are studied.

6.1 Introduction

QD systems have been studied extensively in order to increase the high-speed operation of the semiconductor lasers. QDs have been proposed to increase the modulation speed as a result of their discrete energy levels and their 3-D carrier confinement. Since the differential gain is recognized as one of the crucial factors for the modulation speed of a QD laser [8, 15, 98, 102], the *p*-doping technique was proposed because it increases the differential gain and improves its temperature stability. However, due to the fact that a fraction of the holes provided by the doped barriers reside in the 2-D wetting layer (WL) valance band (VB) states [3, 15], the

results were disappointing since the differential gain only increased slightly.

Researchers have speculated that a slow carrier capture and relaxation, which has a direct impact on the differential gain, is one of the factors that limit the modulation speed of the QD lasers [102-104]. In addition, the QDs' stochastic size distribution may also limit the differential gain, thus limiting the modulation speed of the QD lasers [13].

Post-growth RTA has attracted significant interest since it is an effective method to improve the uniformity of the QDs [30, 32, 60]. At the material level, many researchers have observed that, upon annealing, there are reductions in the carrier lifetimes of both the QD ground state (GS) and the excited state (ES) [60] and a shorter photoluminescence (PL) rise time [30], which accounts for carrier transport in the barriers and carrier capture and relaxation in the QDs. On the contrary, reported results at the device level are significantly less. Furthermore, the existing works mainly report the static characteristics of annealed QDs [32, 33, 94]. To the best of our knowledge, no works have been published about the investigation of the dynamic characteristics (i.e. the differential gain factor (dg/dn) and the nonlinear gain compression factor (ε)) of the annealed QD lasers.

6.2 QD Laser Static Characteristics

Based on the discussion in Chapter 5, 1.3 μm InAs/InGaAs QD lasers with the optimum annealing condition (i.e. 600 °C 15 s) were selected to study the effects of post-growth RTA on the high-speed performance of QDs. The small-signal modulation response of the as-cleaved QD lasers was measured under a continuous-wave (CW) biasing condition using the equipment set-up described in Chapter 3 (Section 3.4.4.). The measurements were normalized to the frequency

response of the photoreceiver and the measurement system.

Figure 6.1 shows the temperature-dependent threshold current (I_{th}) for the as-grown and annealed QD lasers deduced from the temperature-dependent power-current measurements. The cavity length (L) of both the as-grown and the annealed laser chips was 1 mm. The characteristic temperatures (T_o) for the as-grown and annealed QD samples were 52.6 K and 123.4 K, respectively. At each temperature, the annealed samples showed a lower I_{th} than the as-grown samples. This lower I_{th} could be attributed to the removal of grown-in defects upon annealing since these defects act as non-radiative recombination centres in the QDs [32, 33, 94]. Furthermore, the annealed QD lasers exhibited lasing up to 95 °C while the as-grown QD lasers only lased up to 70 °C.

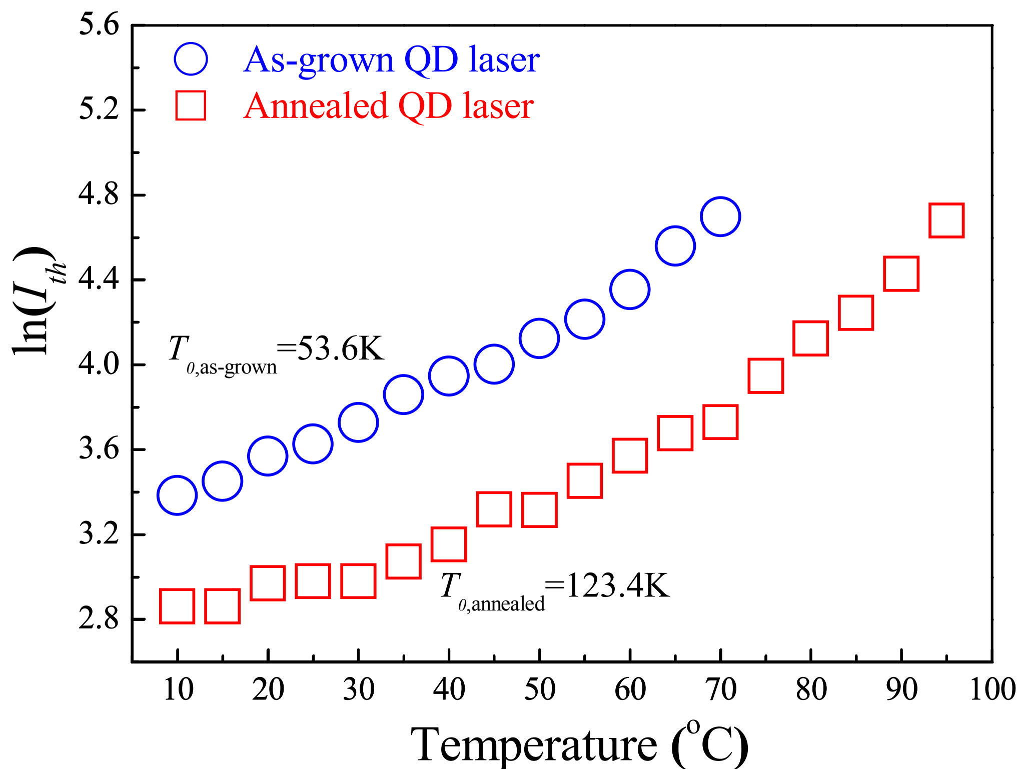

Figure 6.1 The plot of ln(I_{th}) versus temperature for the as-grown and annealed lasers with a 1 mm cavity length.

Figure 6.2 shows the PL spectra for the as-grown and annealed QD samples measured at 5 K. The significant increase (~26%) in the PL intensity after annealing was due to the sizable reduction in the material defectivity [61, 105], which was related to the diffusion and capture processes in the barrier. This increase is expected to result in an improvement in the device performance due to the increase in radiative efficiency as indicated by the improvement of the PL spectra [90]. The centre wavelength for the annealed QD samples was found to remain almost unchanged compared to the as-grown ones. This lack of change is attributed to the suppression of interdiffusion of indium atom under the strain field within or near QDs due to the relatively large number of stacking [31].

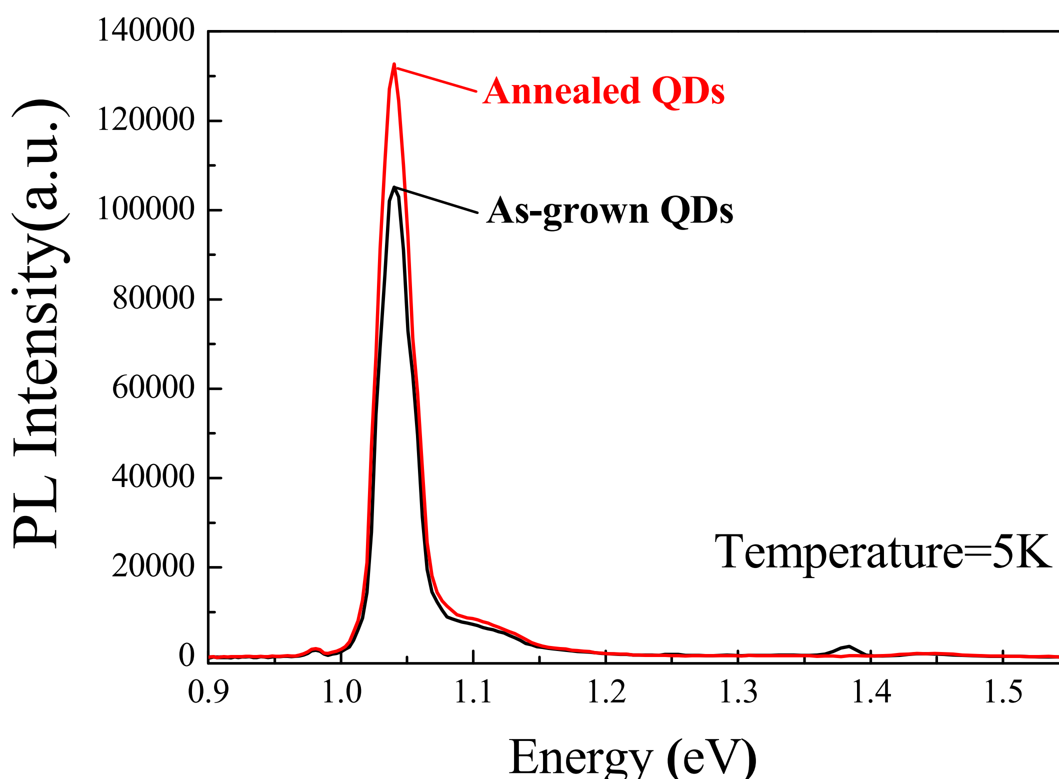

Figure 6.2 The plot of the PL spectra of the as-grown QD sample and the sample annealed at 600 °C for 15 s measured at 5 K.

The temperature-dependent emission wavelengths of the as-grown and annealed QD lasers at an injection current of 200 mA are shown in Fig. 6.3. As expected, the wavelength increased with temperature for both the as-grown and annealed QD lasers. However, the emission wavelength of the annealed QD lasers was slightly longer (~0.9 %) than that of the as-grown ones for a given temperature although such differences were not evident in the PL spectra in Fig. 6.2. At this point, since the threshold current of the annealed QD lasers was much lower than that of the as-grown ones, a higher I/I_{th} ratio was expected in the annealed QD samples at a given injection current (I) at each temperature. Therefore, the injected current of 200 mA in this case was 10 times the threshold current of the annealed QD lasers but it was only 6.7 times that of the as-grown ones at 10 °C. Consequently, the slight difference in the lasing wavelength might be due to the internal device heating as a result of the higher I/I_{th} ratio in the annealed QD lasers.

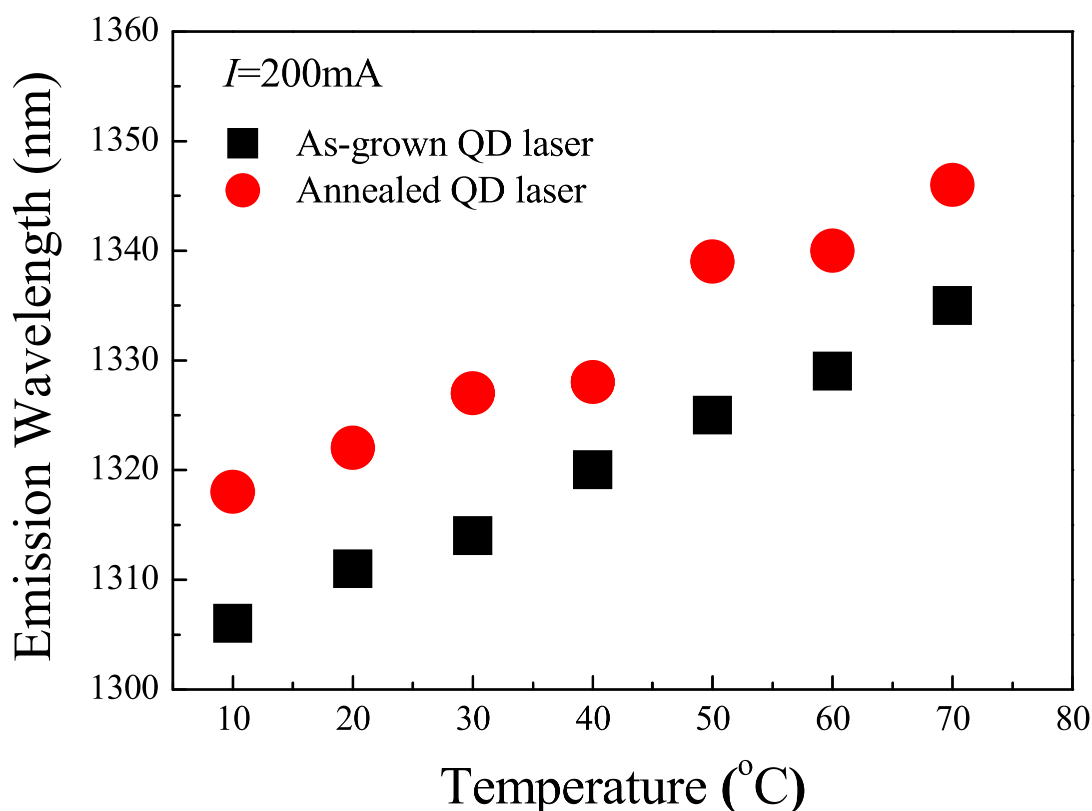

Figure 6.3 The temperature-dependent emission wavelength of the two devices.

In order to calculate the values of the differential gain (*dg/dn*) and the nonlinear gain compression factor (ε), the internal quantum efficiency (η_i) and internal optical loss (α_i) were determined by measuring the as-grown and annealed QD lasers with different cavity lengths (1-4 mm) at different temperatures [65, 96]. Figures 6.4 and 6.5 show the plot of the reciprocal of the external quantum efficiency (η_d^{-1}) versus the cavity length (L) at 10 °C and 70 °C from a batch of as-cleaved as-grown and annealed QD lasers, respectively. The values of η_i and α_i for the QD samples investigated in this chapter are summarized and depicted in Table 6.1. At each temperature, the internal quantum efficiency η_i of the annealed QD lasers was higher than that of the as-grown QD lasers while the internal optical loss α_i was slightly smaller compared to the as-grown QD lasers. This could be attributed to the reduction in defect density in the annealed QDs [100].

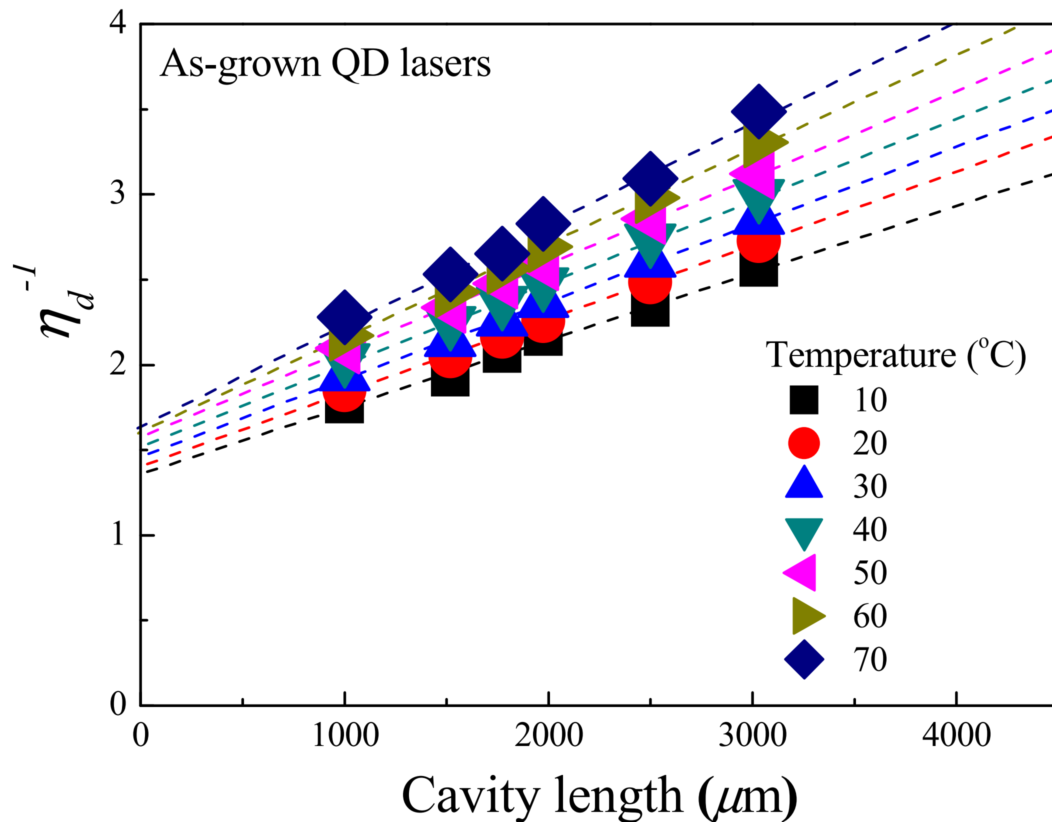

Figure 6.4 The plot of the reciprocal of external quantum efficiency η_d^{-1} as a function of the cavity length L for the as-grown QD lasers.

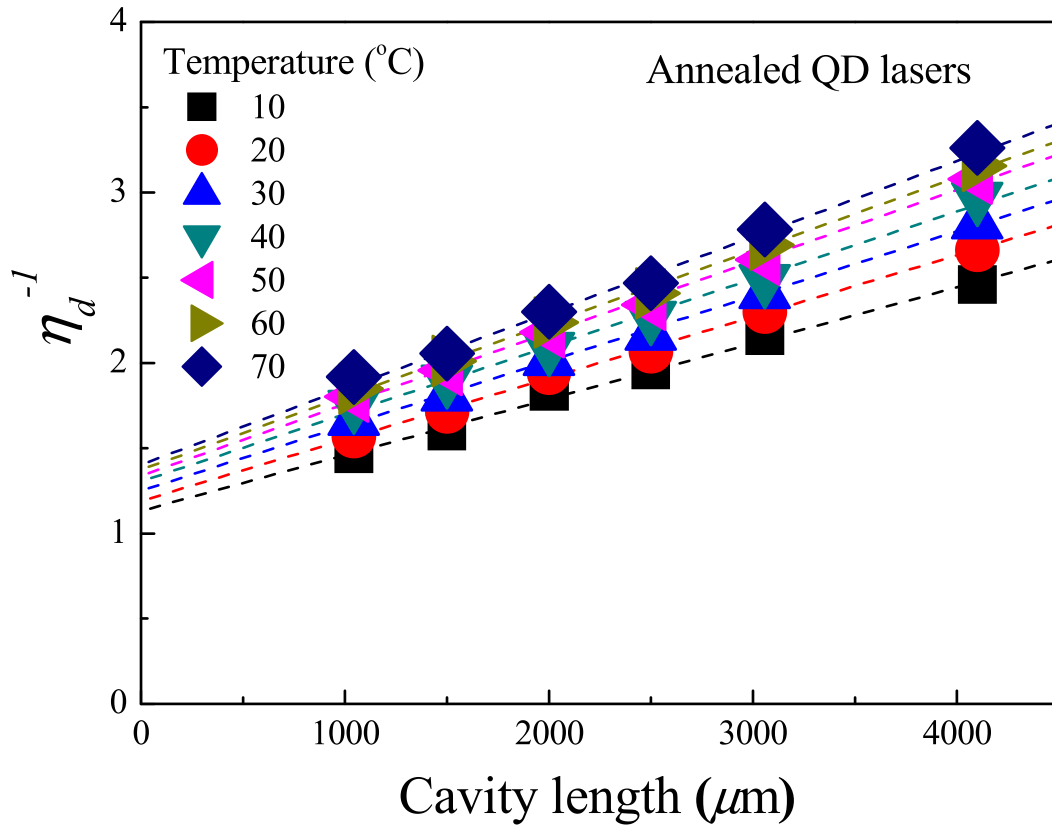

Figure 6.5 The plot of the reciprocal of external quantum efficiency η_d^{-1} as a function of the cavity length L for the annealed QD lasers.

Table 6.1 The internal quantum efficiency (η_i) and the internal optical loss (α_i) of the as-grown and annealed QD lasers at different temperatures.

	As-grown QDs		Annealed QDs	
Temperature	η_i (%)	α_i (cm^{-1})	η_i (%)	α_i (cm^{-1})
10 °C	73.6	3.34	88	3.29
20 °C	71.2	3.53	83.9	3.43
30 °C	62.6	3.26	80.1	3.46
40 °C	65.1	3.56	76.6	3.47
50 °C	63.4	3.69	74.9	3.57
60 °C	63	4.03	72.8	3.56
70 °C	60.9	4.12	71	3.61

6.3 Small Signal Modulation

Small-signal modulations were carried out at different temperatures to study the effects of annealing on the high-speed properties of the QD lasers. Figure 6.6 shows the small-signal response curves for the as-grown QD lasers measured at (a) 10 °C and (b) 70 °C. The bandwidth of the as-grown lasers was 8.2 GHz at 10 °C and 2.8 GHz at 70 °C. Figure 6.7 shows the small-signal response curves for the annealed QD lasers measured at (a) 10 °C and (b) 70 °C. The bandwidth for the annealed QD lasers was 8.5 GHz at 10 °C and 5.3 GHz at 70 °C. As such, the bandwidths of the as-grown QD lasers were more sensitive to the temperature compared to the bandwidths of the annealed QD lasers.

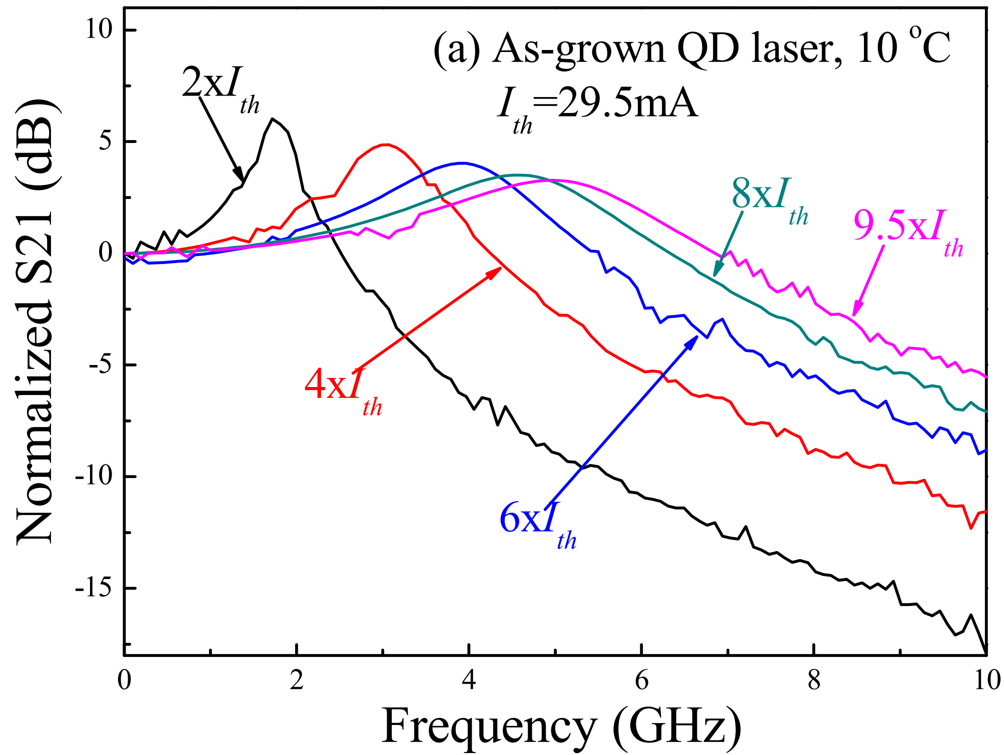

(a)

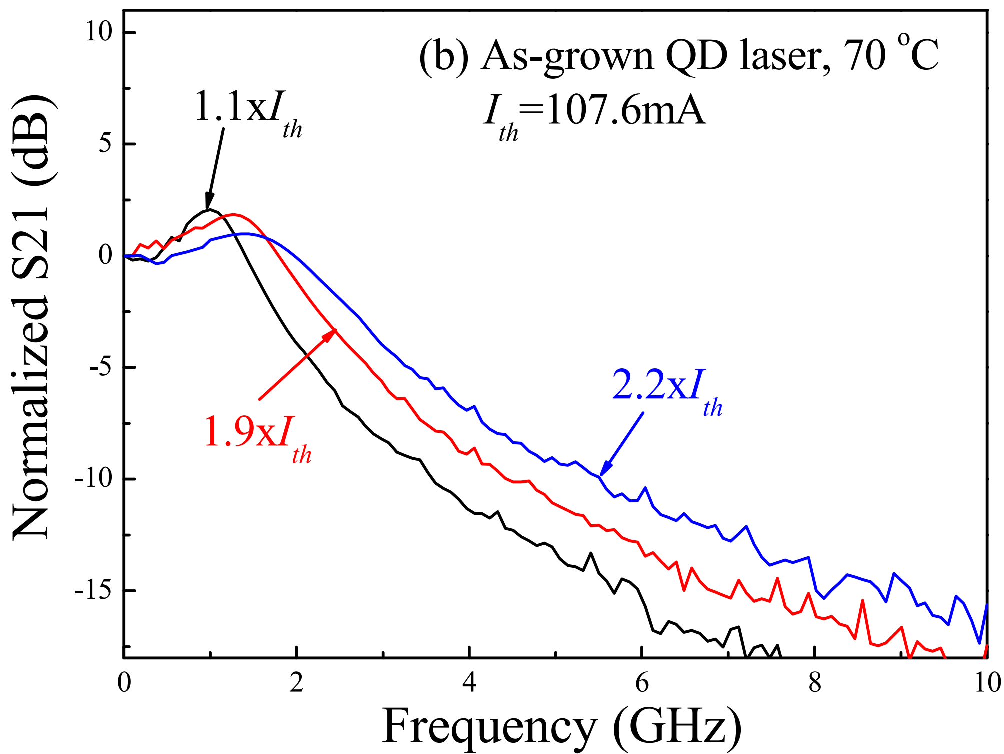

(b)

Figure 6.6 The frequency response curves for the as-grown QD lasers measured at (a) 10 °C and (b) 70 °C.

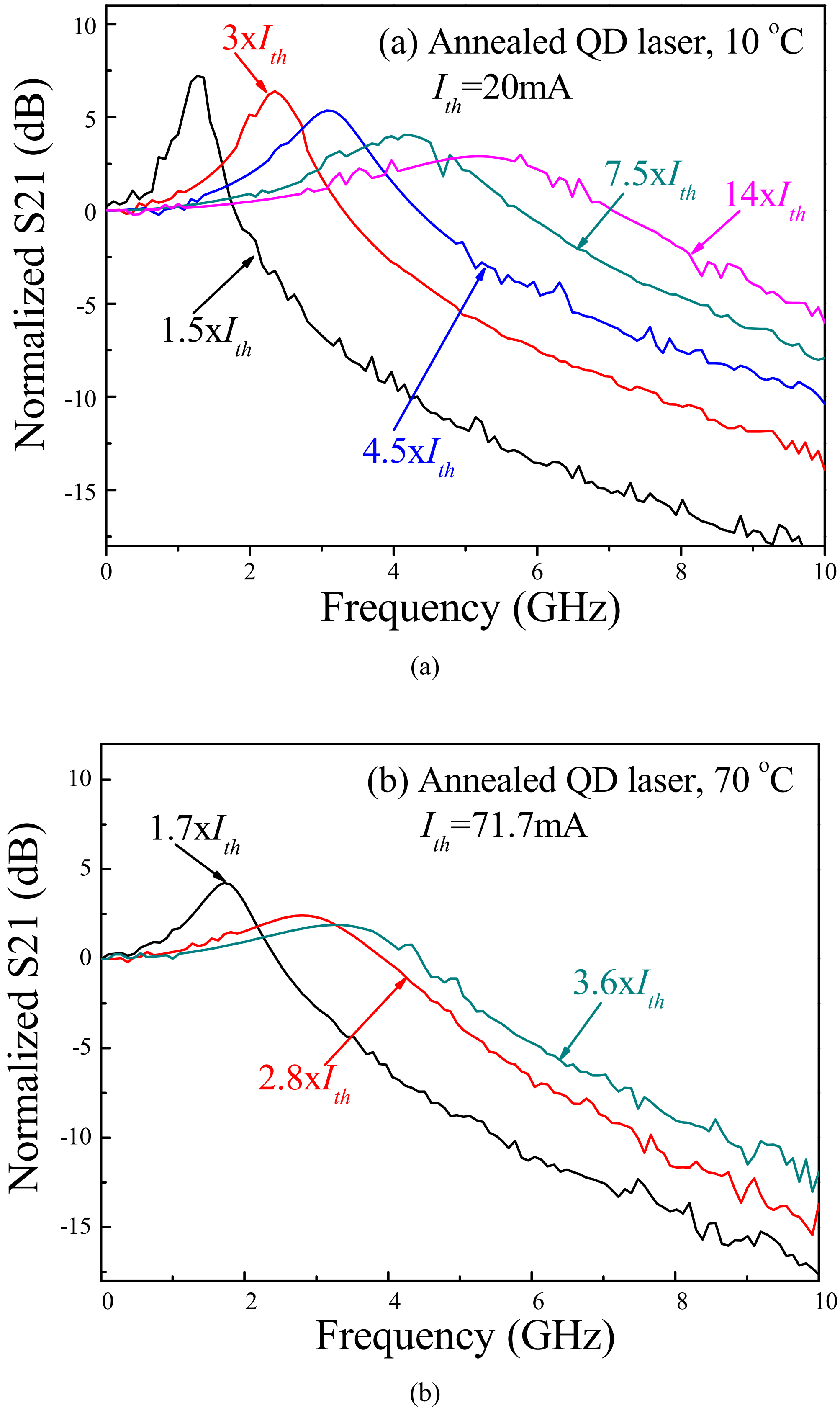

Figure 6.7 The frequency response curves for the annealed QD lasers measured at (a) 10 °C and (b) 70 °C.

Figure 6.8 shows the lasing spectra, measured at 70 °C, of the 1-mm-long as-grown and annealed QD lasers at 240 mA (i.e. 2.23×I_{th}) and 260 mA (i.e. 3.63×I_{th}), respectively. No ES lasing was observed in the annealed QD lasers while ES lasing started to appear at high injection currents for the as-grown QD lasers.

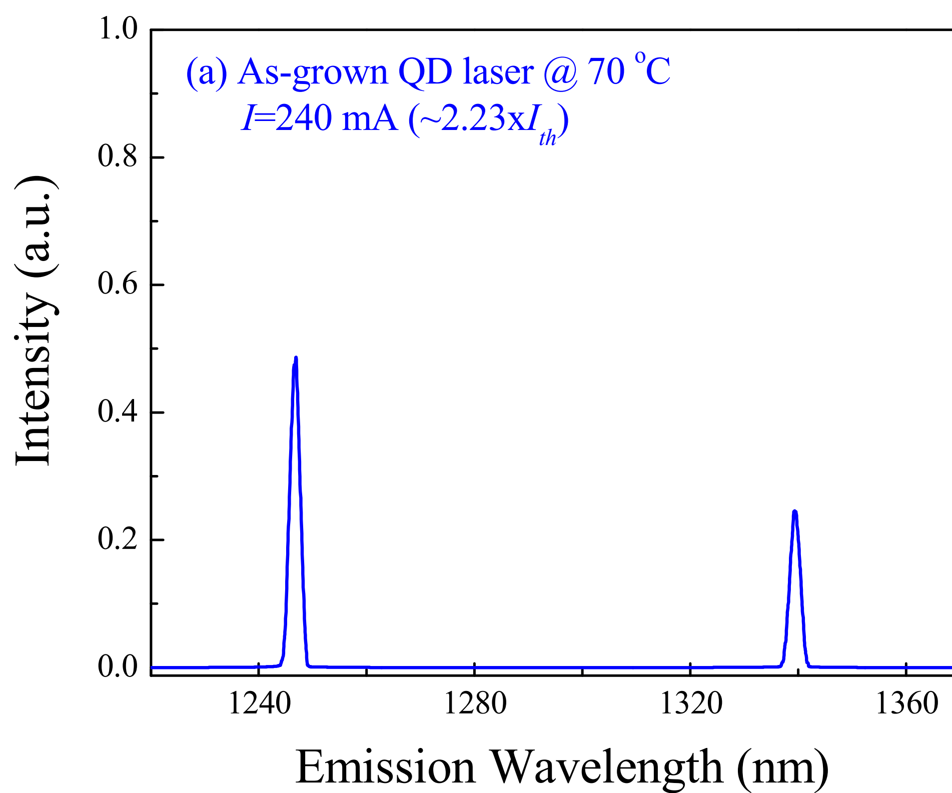

(a)

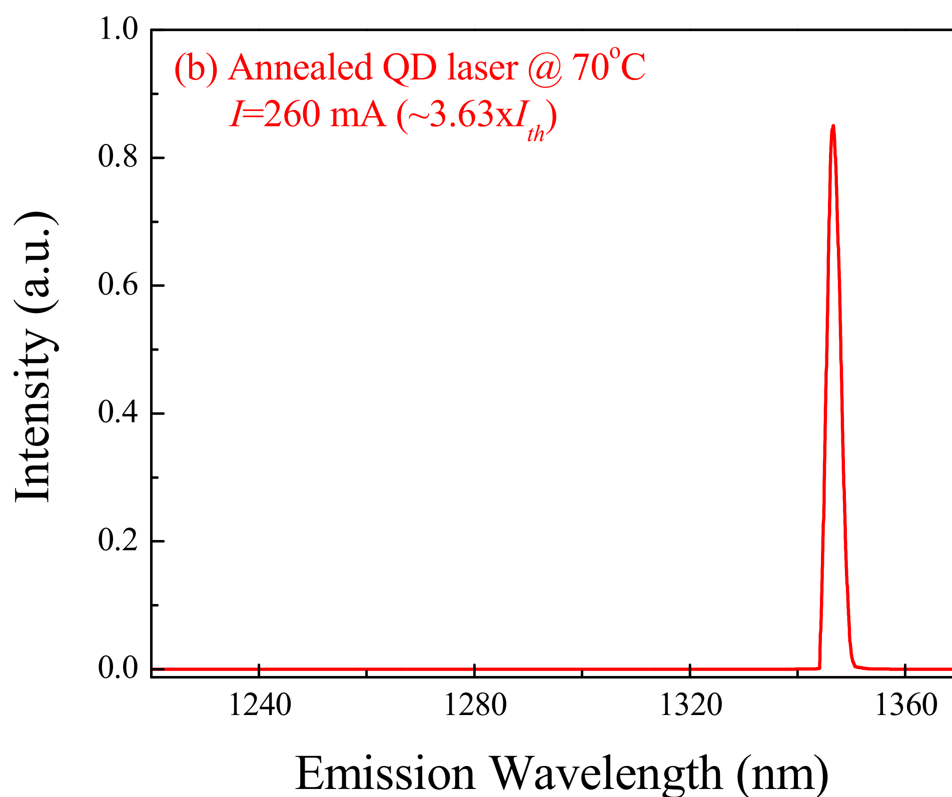

(b)

Figure 6.8 The emission wavelengths of the (a) as-grown and (b) annealed QD lasers at the corresponding injection currents at 70 °C.

The small-signal response curves were fitted with the modulation transfer function in order to extract the values of the damping rate γ and resonance frequency f_r at different bias currents [6, 69]:

$$M(f) \propto \frac{f_r^4}{\left(f_r^2 - f^2\right)^2 + \frac{f^2}{4\pi^2}\gamma^2} \tag{7.1}$$

According to the plot of f_r versus the square root of the normalized bias current $(I\text{-}I_{th})^{1/2}$, the slope (known as the *D*-factor or the modulation efficiency) was obtained. The value of the differential gain (*dg/dn*) was deduced from this slope. The relationship between f_r and γ defined the *K*-factor, which was used to determine the values of the nonlinear gain compression factor (ε).

With the values of the temperature-dependent η_i and α_i, the values of the temperature-dependent differential gain (*dg/dn*) were obtained and plotted in Fig. 6.9. The improvement in *dg/dn* upon annealing may have been caused by an effective reduction in the carrier transportation time at the barriers and by a decrease in the carrier capture and relaxation time into the QDs [30]. The trend of a decreasing *dg/dn* with an increasing temperature is expected. The degradation of *dg/dn* with temperature was almost doubled for the as-grown QD lasers compared to the annealed ones. Since the bandwidth was proportional to $(dg/dn)^{0.5}$ [69], the high-speed performance of the annealed QD lasers was expected to exhibit a better temperature stability compared to the as-grown QD lasers.

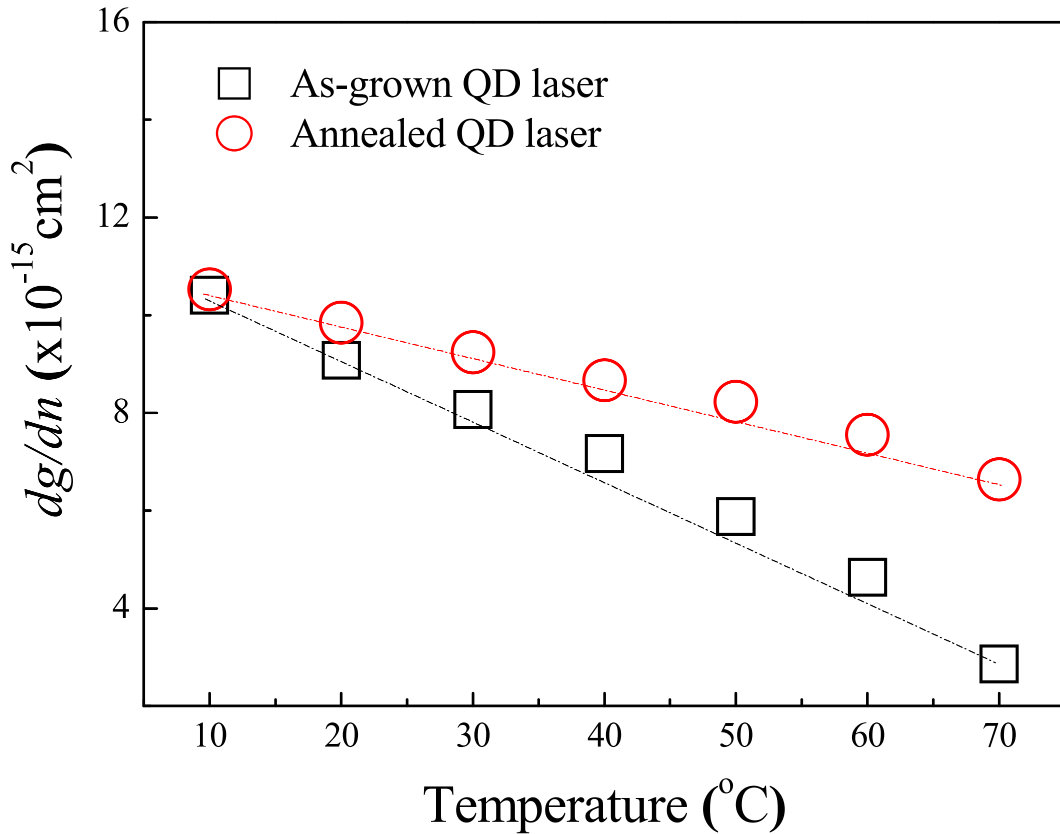

Figure 6.9 The temperature dependence of the differential gain for the as-grown and annealed QD lasers.

The temperature dependency of the nonlinear gain compression factor (ε) is shown in Fig. 6.10. Similarly, an improvement in the temperature stability is evident since the increase in ε with respect to temperature (i.e. $d\varepsilon/dT$) for the annealed QD lasers was only half of that of the as-grown ones. The gain compression in QDs was affected by the time needed to re-establish the intraband steady-state populations, which was limited, in turn, by the electron relaxation time of the InAs/InGaAs QD system [15]. Hence, the smaller values of ε in the annealed QDs might be due to a faster electron relaxation time. More importantly, since the gain compression factor limited the bandwidth of the QD lasers by affecting the K-factor [69], a smaller ε at a higher temperature thus translated to a larger bandwidth of the annealed QD lasers compared to the as-grown ones. The differential gain and the gain compression have

been shown to be limited by the intradot relaxation in the CB [15]. Therefore, the higher differential gain and the lower gain compression exhibited by the annealed QD laser were possibly due to a faster electron relaxation.

The carrier dynamics are important in determining the high-speed performance of the QD lasers. The observed improvement in the dynamic characteristics of the annealed QD lasers compared to the as-grown ones (more obvious at higher temperature) might be due to a more efficient carrier relaxation from the ES to the ground-state (GS) upon annealing. The mechanism where carriers relax from the barrier into the QDs first involves the carriers being captured into the ES followed by their relaxation from the ES to the GS. Similar capture-time-limited bandwidth at a high temperature was reported by Klotzkin *et al.* [85] and they found that the capture of electrons is more critical since its capture rate is slower than that of the holes. However, it was also found that the time required for the carriers to be captured from the barrier layer to the ES of QDs is faster than that required to the GS [106]. Since the ES was suppressed in the annealed QD lasers (as shown in Fig. 6.8), the carrier relaxation time from the ES to the GS is believed to be shortened for the annealed QDs [100].

Tong *et al.* [98] recently reported that the improvement of 1-3.4 GHz in the bandwidth could be expected from a 1 ps reduction in the relaxation time. Hence, the observed increase in the bandwidth of 0.3 GHz and 1.5 GHz at 10 °C and 70 °C, respectively, from the annealed QD laser might be due to a reduction in the relaxation time in the order of 10^{-1} ps.

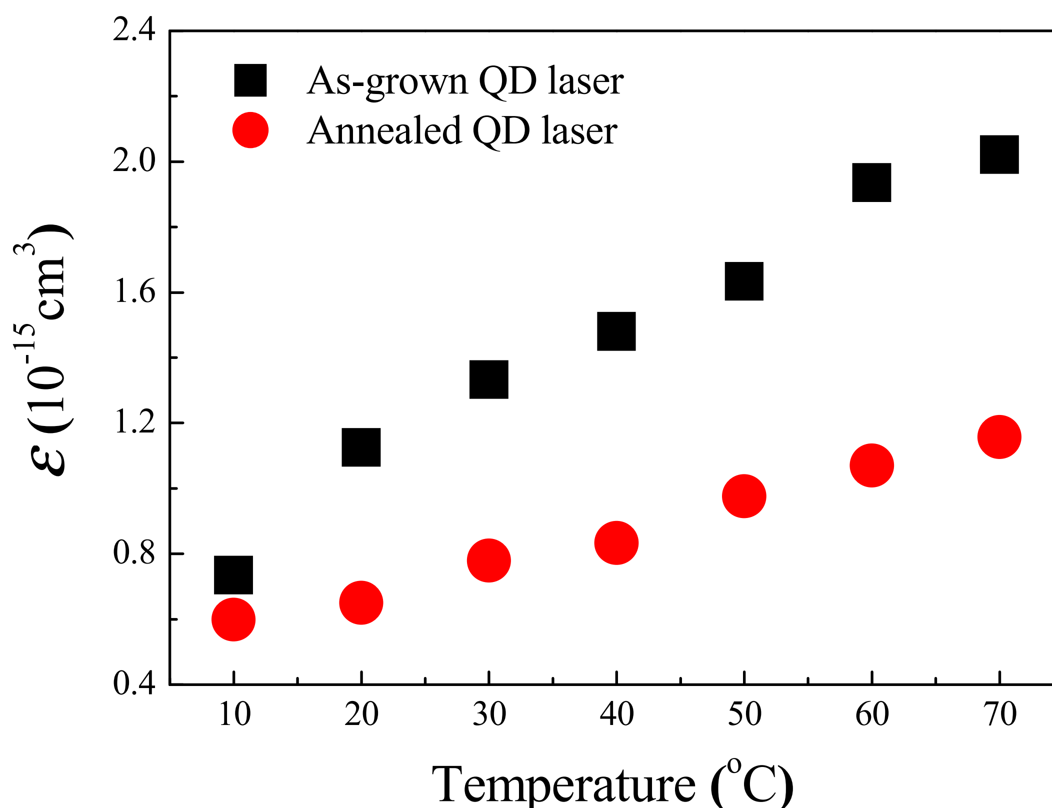

Figure 6.10 The temperature dependency of the nonlinear gain compression (ε) for the as-grown and annealed QD lasers.

6.4 Summary

In summary, we investigated the effects of post-growth RTA on the small signal modulation characteristics and the thermal stability of the 1.3 μm InAs/InGaAs QD lasers. The characteristic temperature was enhanced by a factor of 2.3 upon annealing. Excited state lasing was suppressed after the RTA process and the carrier capture and relaxation to the ground-state may have been enhanced after RTA. Compared to the as-grown QD laser, the differential gain was increased and the nonlinear gain compression was reduced in the annealed QD laser. More importantly, the temperature-stability of these two parameters was improved through RTA. This shows that the RTA process could improve the dynamic characteristics of the 1.3 μm

InAs/InGaAs QD lasers without the re-growth of the QD structure, which is significant for the development of uncooled high-speed QD lasers.

Chapter 7: Improved Ground-State High-Speed Characteristics of *P*-doped QD Lasers by Optimum Annealing

In Chapter 5, the effect of annealing and *p*-doping on the two-state lasing competition was studied. In addition, the effect of *p*-doping on the gain characteristics of QD lasers was investigated. Improved temperature stability and modal gain were demonstrated from the *p*-doped QDs. More importantly, GS (ES) lasing was enhanced (suppressed) through *p*-doping and optimum annealing. Since a faster carrier relaxation mechanism is expected in the annealed QDs, we need to clarify what the effect of annealing is on the high-speed performances of the QDs with *p*-doping. Therefore, in this chapter, we investigate the high-speed modulation characteristics of the 1.3 μm *p*-doped InAs/InGaAs QD lasers that consist of either as-grown QDs or annealed QDs with the optimum annealing condition.

7.1 Introduction

QDs are promising for realizing fast and stable laser sources in fibre optic applications due to their superior characteristics over conventional QW lasers. These superior characteristics include a low threshold current, a high internal efficiency, and an infinite characteristic temperature [49, 92]. However, the high-speed performance of QDs is generally poorer than that of QWs due to several factors: the slow inter-level relaxation of the carriers [90], the finite DOS, and the closely spaced hole energy levels [13]. The slow carrier relaxation rate, in combination with the limited DOS, will lead to early switching from GS lasing to ES lasing at high temperatures

and/or at high driving currents. This switching is undesirable since ES lasing reduces GS lasing efficiency due to the gain saturation of the GS transition. Due to the state filling effect in discrete quantum levels, this degrades the high-speed characteristics of the QD lasers [42, 92]. Furthermore, for high-speed modulation, a shorter cavity length is favoured. Unfortunately, the transition from GS to ES lasing occurs earlier in short cavity lasers (≤ 1 mm) due to the increased cavity loss compared to long cavity lasers [90]. Thus, to improve the high-speed performance of the QD lasers, we need to delay the onset of ES lasing.

P-doping of the QDs can reduce the effect of gain saturation and thus maintain GS lasing up to a higher operating temperature [49] and a potentially faster relaxation time [98]. On the other hand, rapid thermal annealing (RTA) might result in the intermixing of the QDs with the surrounding matrix and tunable inter-level energy. This may lead to a faster inter-level relaxation of the carriers [60] and, consequently, to the suppression of ES lasing and to an improved high-speed modulation efficiency. However, only a handful of publications on the effects of RTA on the GS modulation of the annealed *p*-doped QD lasers exist.

In this chapter, we investigate the effect of rapid thermal annealing on the GS modulation characteristics of 1.3 μm *p*-doped InAs/InGaAs QD lasers. Both the bandwidth and the modulation efficiency increase significantly upon optimum annealing.

7.2 QD Laser Small Signal Modulation

The choice of annealing conditions was determined from Chapter 5 [100]. Subsequently, the as-grown and annealed QD samples were processed into 4-μm-wide narrow RWG lasers [107]. The high-speed modulation of the as-cleaved

QD lasers was performed using the set-up described in Chapter 3 [101]. The spontaneous emission intensity of the device under different bias currents was obtained with an integrating sphere.

Figure 7.1 shows the frequency response of the as-grown QD laser device with a cavity length of 1 mm, measured at 10 °C. The threshold current (I_{th}) of the as-grown QD device was ~51.6 mA. The bandwidth increased gradually with the bias currents. The maximum bandwidth obtained was 7.73 GHz measured at 290 mA. The bandwidth obtained from purely GS lasing was 6.95 GHz at 280 mA. A slight increase of the bias current by 10 mA caused a significant increase of the bandwidth by 0.78 GHz (i.e. from 6.95 GHz to 7.73 GHz), which was likely due to the additional photons emitted by the ES lasing. Therefore, the bandwidth of 7.73 GHz for the as-grown QD laser included the bandwidth contribution from ES lasing. However, the bandwidth contributed from ES lasing was undesirable since the wavelength of interest for telecommunications is 1.3 μm.

Figure 7.2 shows the lasing spectra of the same as-grown QD laser at 10 °C. The ES lasing threshold ($I_{th,ES}$) of the as-grown QD device was 284 mA. At the bias current of 5.43×I_{th} (i.e. 280 mA), the QD laser emission wavelength was ~1318.8 nm and corresponded to the GS lasing (refer to Fig. 7.2 (a)). When the bias current was increased to 5.62×I_{th} (i.e. 290 mA), emission wavelengths of ~1227.4 nm and ~1320 nm existed simultaneously (refer to Fig. 7.2 (b)). The energy separation between the two states was ~71 meV. Thus, in the as-grown QD laser, GS lasing dominated at low bias currents while ES lasing dominated at higher bias currents.

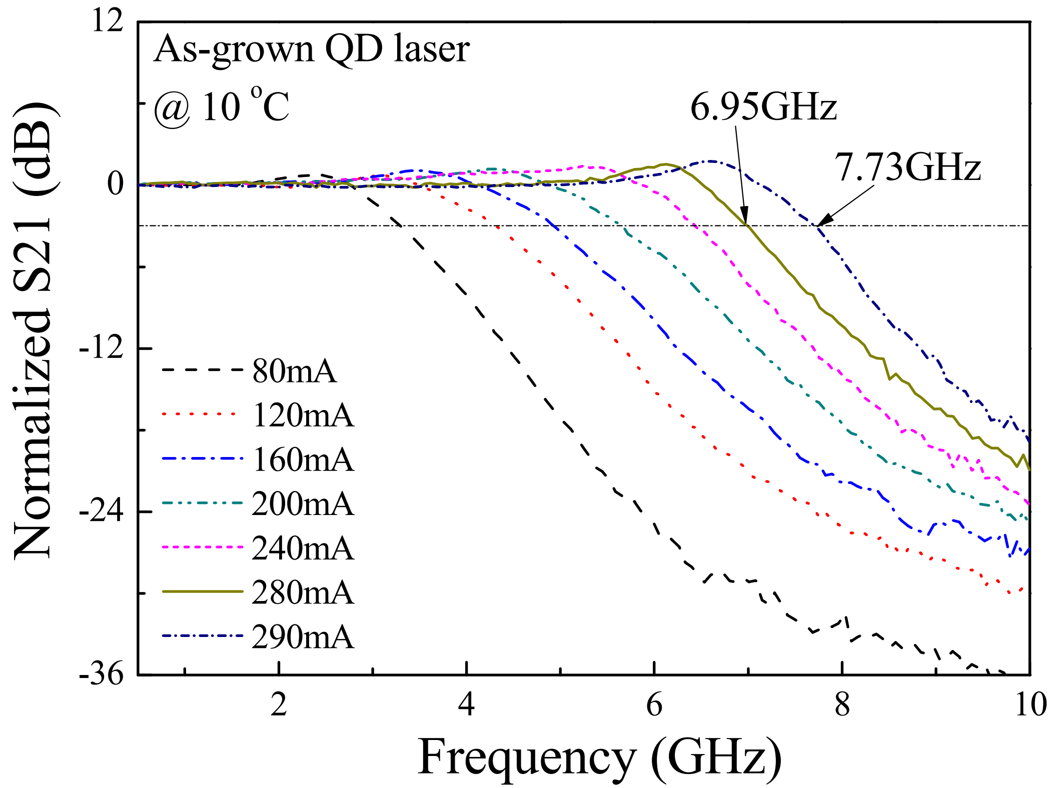

Figure 7.1 The frequency response of an as-grown QD laser with a cavity length of 1 mm, measured at 10 °C.

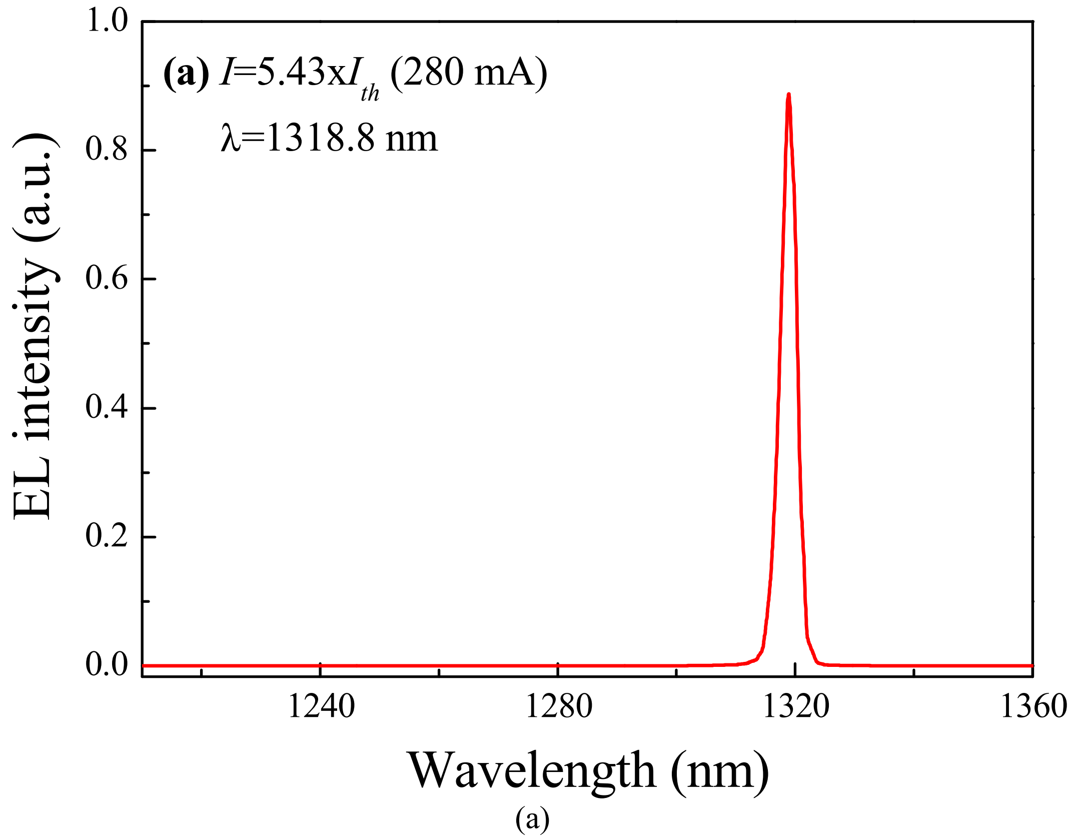

(a)

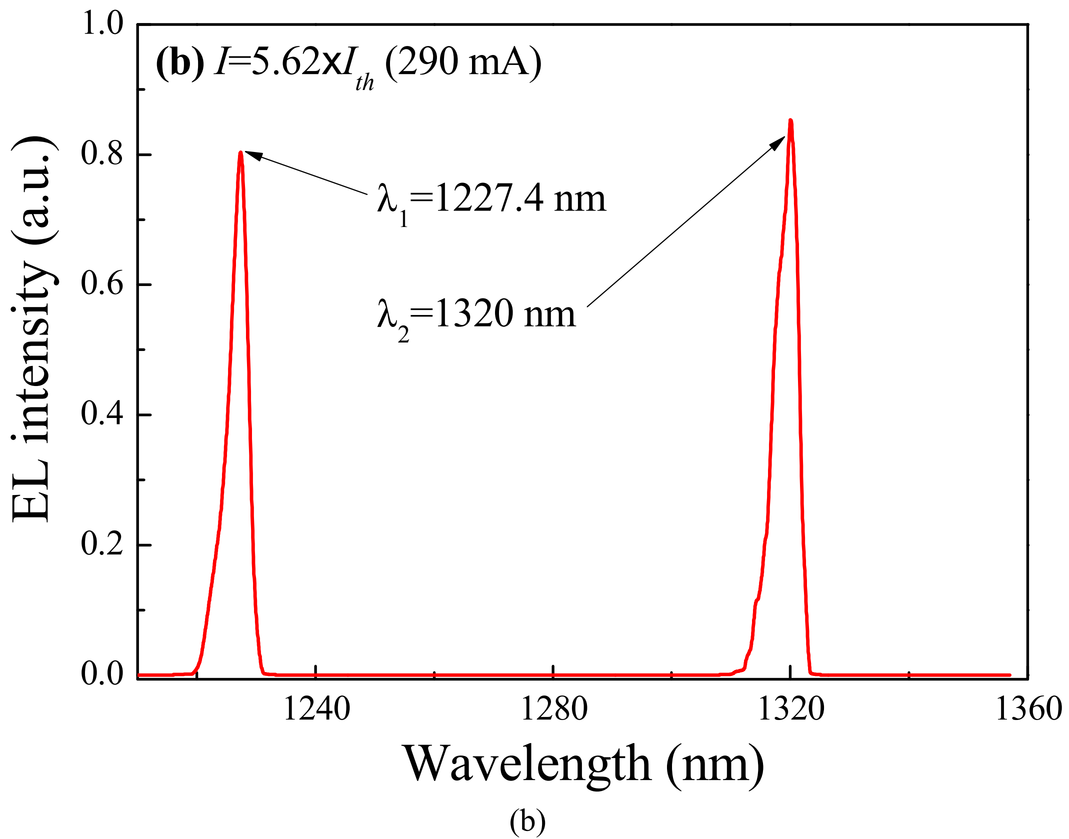

(b)

Figure 7.2 The lasing spectra of the same as-grown QD laser measured at (a) 280 mA and (b) 290 mA.

Figure 7.3 shows the frequency response for the 600 °C annealed QD laser device with a cavity length of 1 mm, measured at 10 °C. The I_{th} of the 600 °C annealed QD device was ~42.6 mA. The lasing spectrum of the 600 °C annealed QD device at 7.51×I_{th} (i.e. 320 mA) is shown in Fig. 7.4. The QD laser emission wavelength was ~1339.6 nm and corresponded to the GS lasing. Since the bandwidth saturated at a current greater than 320 mA, the maximum bandwidth obtained was 8.18 GHz. After annealing, an 18% improvement in the modulation bandwidth was achieved. No ES lasing was observed in the annealed QD laser at any of the bias current levels investigated. Therefore, the maximum bandwidth of 8.18 GHz for the 600 °C annealed QD device was purely from GS lasing. Comparing Fig. 7.2 (a) and Fig. 7.4, the difference in the GS wavelength may have been due to the carrier induced bandgap shrinkage [108] and the thermal induced emission wavelength shift [109-111]. At a fixed current injection above threshold, a higher I/I_{th} ratio was resultant in the annealed QD lasers than in the as-grown QD lasers due to the significant reduction of threshold current through optimum annealing (i.e. 42.6 mA for the annealed QD laser and 51.6 mA for the as-grown QD laser) [101]. The thermal effects may have become more dominant in affecting the wavelength due to annealing. The reasons behind this wavelength shift are currently under investigation.

By comparing Fig. 6.7 (a) and Fig. 7.3, it can be observed that the maximum bandwidth of the annealed undoped laser (i.e., 8.5 GHz) is larger than that of the annealed *p*-doped laser (i.e., 8.18 GHz). This could be attributed to the smaller annealing induced effects for the *p*-doped QD samples since the interstitial concentration is higher [61]. This implies that the optimum annealing temperature to maximize the modulation bandwidth for the *p*-doped QDs could be slightly higher than that for the undoped QDs. As such, smaller temperature steps (between 600 °C

and 650 °C) would be required to determine the optimum annealing condition for the *p*-doped QDs in the future.

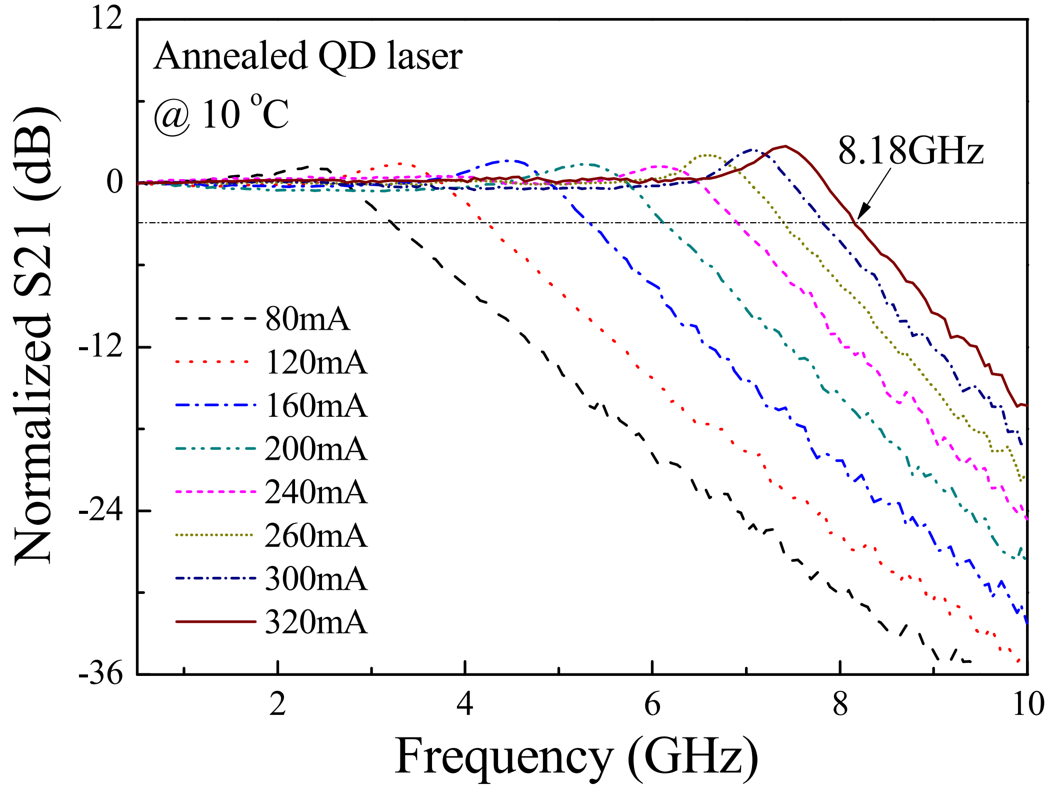

Figure 7.3 The frequency response of the 600 °C annealed QD laser with a 1-mm cavity length measured at 10 °C.

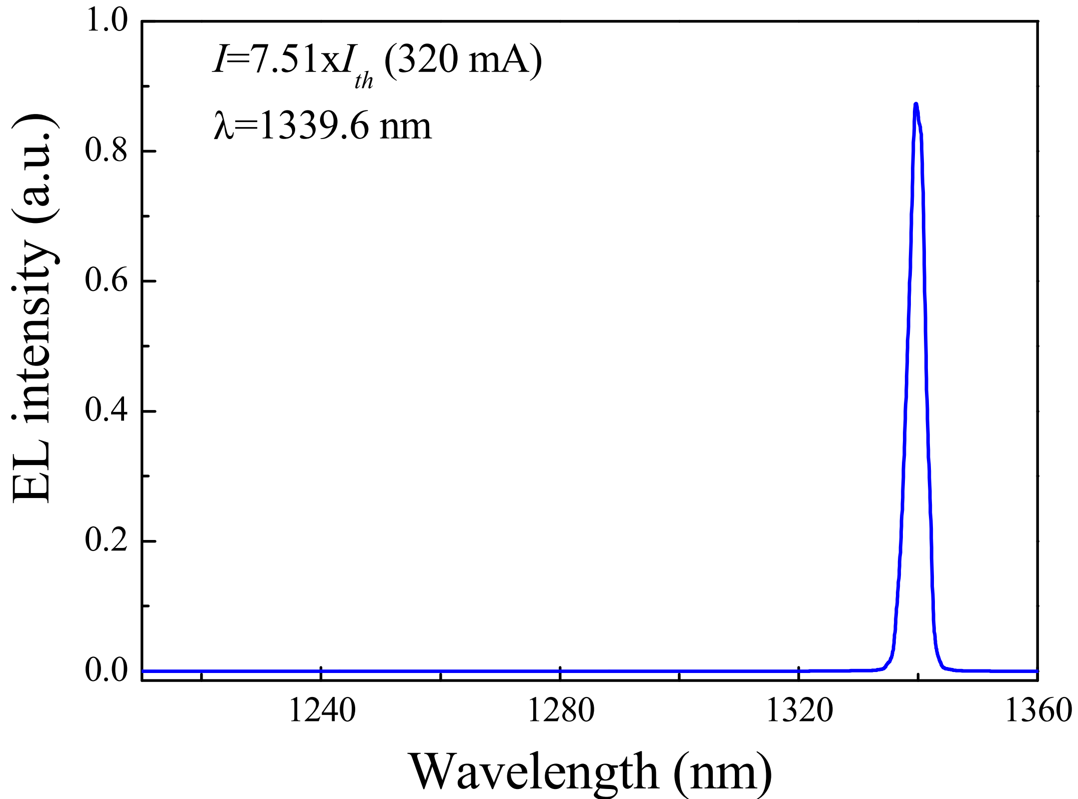

Figure 7.4 The lasing spectrum of the same annealed QD laser measured at 320 mA.

The measured bandwidths as a function of the normalized bias current $(I\text{-}I_{th})^{1/2}$ above threshold at 10 °C for the as-grown and 600 °C annealed QD lasers are summarized in Fig. 7.5. The solid symbols show the bandwidth for GS lasing while the hollow symbols show the bandwidth with the contribution of ES lasing for the as-grown QD laser at a higher bias current. The slope deduced from the bandwidth versus $(I\text{-}I_{th})^{1/2}$ (also known as the modulation efficiency) was ~0.33 GHz/mA$^{1/2}$ for the as-grown QD device at a low bias current. A sudden increase of the modulation efficiency occurred when ES lasing started to dominate. GS lasing dominated in the 600 °C annealed device throughout the measured bias current range while ES lasing was completely suppressed, even at higher bias currents. The modulation efficiency for the 600 °C annealed QD device was ~0.48 GHz/mA$^{1/2}$. Therefore, the modulation efficiency was increased by ~45% after the optimum RTA process.

Asryan *et al.* [104] showed that the slow carrier capture from the optical confinement layer into QDs can strongly limit the modulation bandwidth of a QD laser. Shi *et al.* [90] showed that a fast inter-level relaxation is favourable for GS lasing and leads to a higher QD GS capture efficiency. When the inter-level relaxation becomes slower, the carriers captured into the ES cannot relax to the GS immediately and they continue to occupy the ES. The ES lasing will occur when the population inversion for the transition between the ES electrons and the GS holes is satisfied. A higher modulation efficiency in the 600 °C annealed QD laser indicates a lower WL carrier occupation probability and a higher GS capture efficiency, which may be due to a faster inter-level relaxation induced by RTA [100].

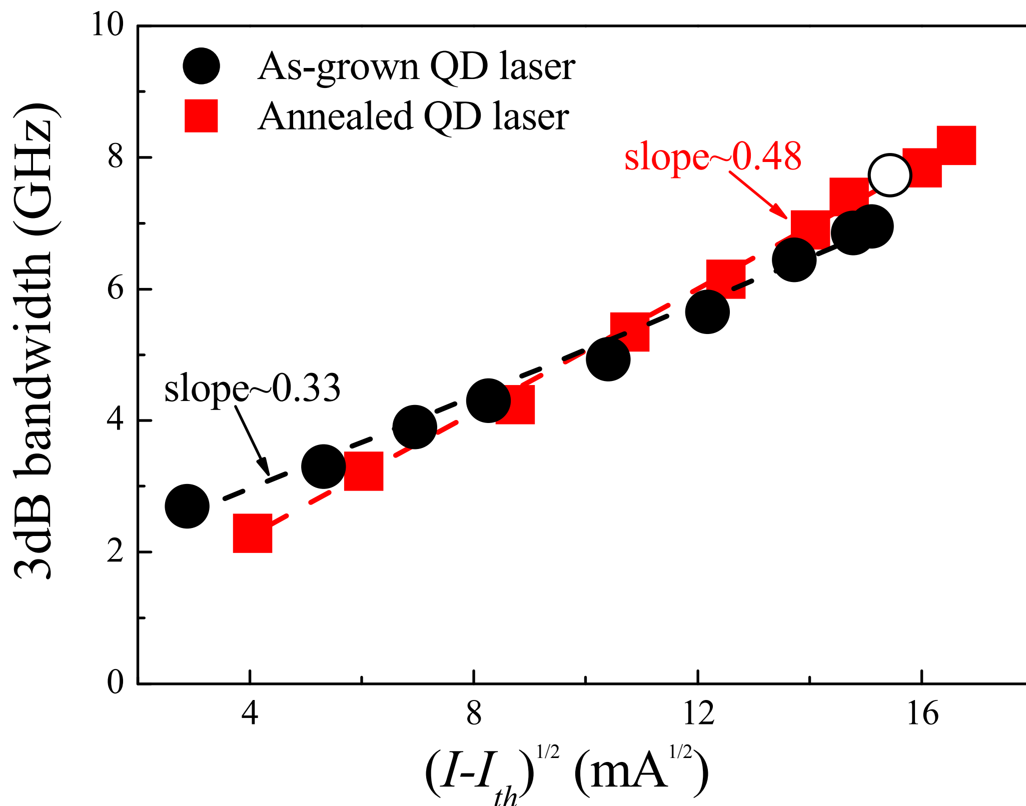

Figure 7.5 The measured bandwidth as a function of the normalized bias current $(I\text{-}I_{th})^{1/2}$ for the as-grown (circles) and annealed (squares) lasers at 10 °C. The hollow circle shows the bandwidth with ES lasing for the same as-grown QD laser.

7.3 Temperature-Dependent Characterization

Refer to Fig. 5.2 in Chapter 5, the logarithmic values of threshold current densities (ln(J_{th})) as a function of temperature for the as-grown and 600 °C annealed QD devices were shown. The T_o^1 for the as-grown and annealed QD lasers are obtained and shown in Figure 7.6. The as-grown QD laser exhibited a T_o^1~77.9 K from 70 °C to 100 °C. ES-dominated lasing started at 105 °C in the as-grown QD laser. However, in the annealed QD laser, GS lasing dominated throughout the measured temperature range, up to 120 °C. The annealed QD laser exhibited a T_o^1~249 K from 75 °C to 120 °C. As shown in Fig. 7.6, the threshold current was reduced compared to the as-grown QD laser and an improved T_o^1 for the annealed QD laser was demonstrated up to 120 °C. These improvements were possibly due to the reduction in Auger recombination in the annealed QDs since the Auger recombination increased the threshold current. In agreement with the work of Shchekin *et al.* [8], the modulation response of the QD laser is closely related to the threshold characteristics. Although QDs have been predicted to be modulated at very high frequencies theoretically, Deppe *et al.* [13] showed that the current densities required to reach these values should be considered. The low threshold current density of the annealed QD laser suggests that this device could be driven far above threshold and that it could reach a higher speed. Marko *et al.* [50] observed that Auger recombination is an important loss process in the 1.3 μm InAs/GaAs QD lasers around room temperature. Although *p*-doping of the QDs enhanced the gain, it also increased the threshold current, possibly due to an increased Auger recombination [45]. The improved characteristic temperature T_o, together with the reduced threshold current density in the annealed QD lasers, implies that the severe nonradiative Auger recombination was possibly reduced as a consequence of thermal annealing by reducing the defect

densities. This reduction potentially resulted in an improved carrier relaxation, thus promising high-speed modulation characteristics.

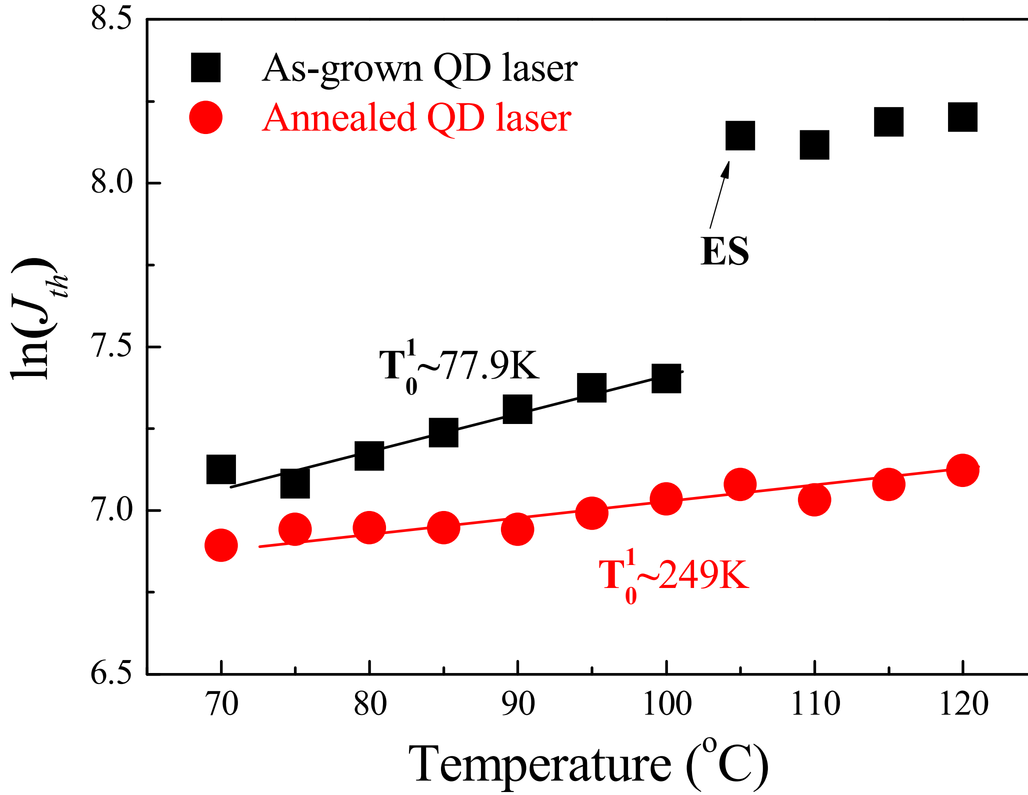

Figure 7.6 The plot of ln(J_{th}) versus temperature from 70 °C to 120 °C for the as-grown (square) and 600 °C annealed (circle) QD lasers.

7.4 Spontaneous Emission Measurement

In order to better understand the effects of RTA on the performance of the *p*-doped QD lasers, the total spontaneous emission intensity was measured by modulating the QD device in the unamplified region, where $I < I_{th}$. Over this limited range of I, we employed a general relationship between I and L_{sp}, where I was the injection current and L_{sp} was the total spontaneous emission intensity [112]:

$$\ln(I) \propto Z \ln(L_{sp}^{1/2}) \quad (7.1)$$

where $1 \leq Z \leq 3$, depending on the relative importance of nonradiative monomolecular recombination process due to defects or impurities (Z=1),

bimolecular radiative recombination process (Z=2) or nonradiative Auger recombination process (Z=3). Generally, $2 \leq Z \leq 3$ applies in InAs/GaAs QDs, especially in the *p*-doped QDs, due to the enhanced nonradiative Auger recombination process [113]. Figure 7.7 shows the plot of $\ln(I)$ versus $\ln(L_{sp}^{1/2})$ for the as-grown and 600 °C annealed QD devices with cavity length of 2 mm at room temperature. The I_{th} of the as-grown and 600 °C annealed QD laser is 93.6 mA and 81.8 mA, respectively. The gradient obtained is known as the Z value, which gives the information about the dominant recombination mechanism.

As shown in Fig. 7.7, the Z value reduced from 2.748 in the as-grown QD device to 2.217 in the annealed QD device. This suggests that the radiative recombination became more dominant than the Auger-related recombination processes resulting from the optimum annealing [112]. Therefore, the radiative recombination was enhanced after the 600 °C thermal annealing. The suppression of the nonradiative Auger recombination may also result in a smaller carrier lifetime and, thus, improved the high-speed modulation performances, which agrees well with our experimental results on the improved small signal modulation performances in the annealed QD lasers (as shown in Figs. 7.1, 7.3, and 7.5). Furthermore, our experimental results also demonstrated an improved quantum efficiency and a reduced internal optical loss in the 600 °C annealed QD lasers [100].

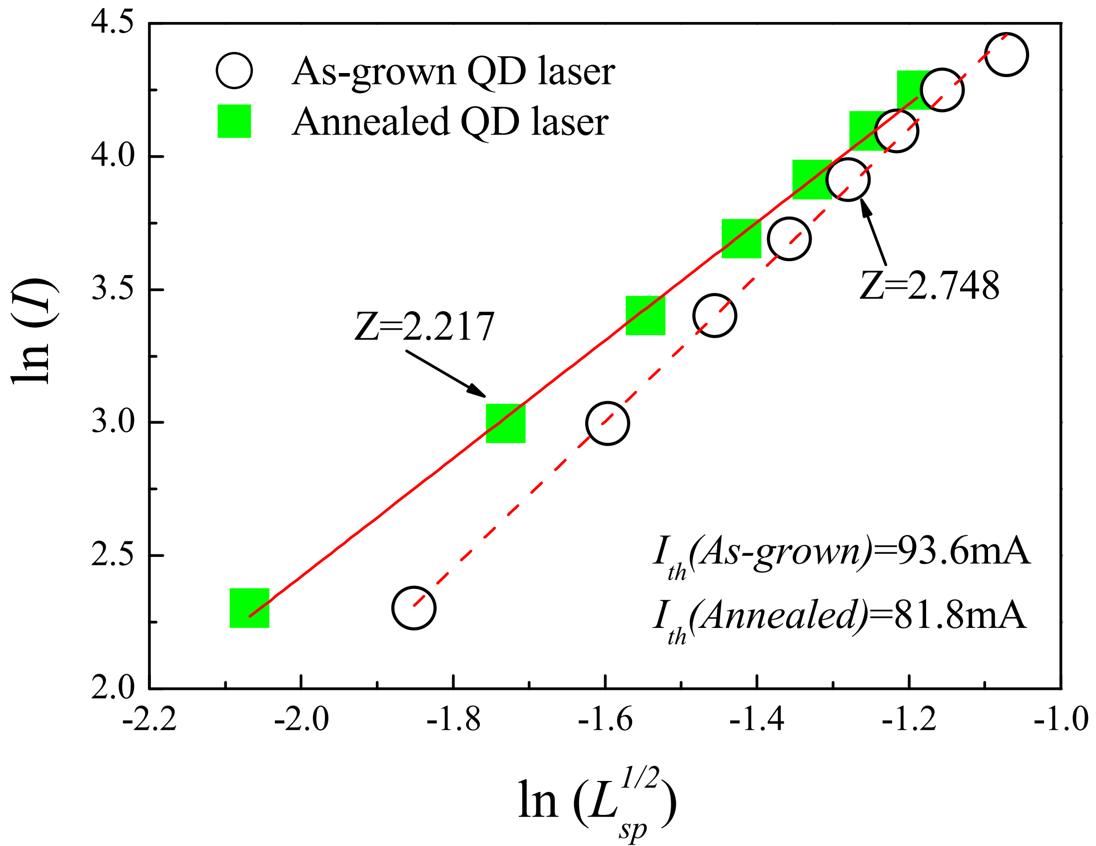

Figure 7.7 The plot of the logarithmic values of the injection current (ln(I)) versus the logarithmic values of the total spontaneous emission intensity (ln($L_{sp}^{1/2}$)) for the as-grown and 600 °C annealed QD devices with cavity length of 2 mm at room temperature. The I_{th} of the as-grown and 600 °C annealed QD laser is 93.6 mA and 81.8 mA, respectively.

7.5 Summary

In summary, we investigated the GS modulation characteristics of the 1.3 μm *p*-doped InAs/GaAs QD lasers that consisted of either as-grown or annealed QDs. Compared to the as-grown QD lasers, the annealed QD lasers exhibited ~18% improvement in the modulation bandwidth and ~45% improvement in the modulation efficiency. These observed improvements in the *p*-doped QDs were possibly due to (i) the removal of defects, which act as nonradiative recombination centres in the QD

structure, and (ii) the reduction in the Auger-related recombination processes upon annealing.

Chapter 8: Conclusions and Recommendations for Future Research

8.1 Conclusions

This research study investigated the characteristics of the ten-layer InAs/InGaAs QD lasers emitting at 1.3 μm grown on a GaAs substrate for uncooled high-speed optical communication systems. The study examined (i) the bandwidth limitations of the intrinsic QD lasers, (ii) the effects of *p*-doping on the gain properties and temperature-dependent characteristics of the QDs lasers, (iii) the effects of post-growth thermal annealing (RTA) on the gain competitions of the undoped and *p*-doped QDs lasers, and (iv) the high-speed characterization of the undoped and *p*-doped QD lasers based on optimum annealing conditions.

A high modulation bandwidth is the primary requirement for high-speed optical communication systems. Therefore, it becomes essential to identify the bandwidth limitations of the intrinsic ten-layer InAs/InGaAs QD lasers. In specific, the influence of damping and thermal effects on the high-speed characteristics of the 1.3 μm undoped InAs/InGaAs QD lasers with a narrow RWG structure were investigated in a wide temperature range. While the intrinsic damping-limited modulation bandwidth was as high as 23 GHz, the actual modulation bandwidth was limited by carrier thermalization under continuous-wave operations. The calculation of the temperature-dependent bandwidth of the undoped QD laser showed a close agreement between the thermal-limited bandwidth and the experimental results. The saturation of the resonance frequency was found to be the result of the thermal reduction in the differential gain, which may originate from carrier thermalization.

Therefore, the bandwidth of the intrinsic InAs/InGaAs QD lasers was limited mainly by thermal effects, which may have resulted from carrier thermalization in the undoped QD laser structure. Several methods were proposed to improve the bandwidth and the temperature-dependent characteristics of the 1.3 μm InAs/InGaAs QD lasers.

P-doping and post-growth rapid thermal annealing were introduced to improve the performance of the QD lasers. Specifically, the effects of annealing and *p*-doping on the two-state lasing competition in the 1.3 μm InAs/InGaAs QD lasers were studied by analyzing the modal gain competition from the below-ground-state (GS) to the above-excited-state (ES) thresholds. Both the structural and the optical performance changes in the QDs were investigated. In comparison to the as-grown QD lasers, both the undoped and the *p*-doped QD lasers exhibited enhancement (suppression) in GS (ES) lasing with annealing at 600 °C for 15 s and they exhibited suppression (enhancement) in GS (ES) lasing with annealing at 650 °C for 15 s. The enhancement of the GS lasing is believed to be due to the removal of nonradiative recombination centres, which reduces the carrier relaxation time and increases the relaxation efficiency. The suppression of GS lasing in the QD lasers annealed at a higher temperature (i.e. 650 °C) is believed to be due to carriers leaking out from the shallower interdiffused QD potential. This implies that the onset of ES lasing could be delayed significantly to a higher injection current with the optimum annealing conditions. The optimum annealing condition for the QD samples investigated in this research study was determined to be at 600 °C for 15 s.

Moreover, the effects of the *p*-doping technique on the gain performance and temperature-dependent behaviours of the 1.3 μm InAs/InGaAs QD lasers were studied. For the QDs lasers annealed under the same conditions, the *p*-doped QD lasers were

found to: (i) sustain GS lasing to a higher operating temperature and exhibit an infinite characteristic temperature T_o, and (ii) have a poorer differential efficiency and internal loss optical compared to the undoped QD lasers. Therefore, a tradeoff exists in the QD laser performances with/without *p*-doping. The choice of undoped or *p*-doped QDs will depend on the application that the lasers will be used in. The characteristics of the undoped QD lasers will be preferred in low-power communications and in emerging areas such as on-chip communications due to their low threshold, their high efficiency, and their low loss. On the other hand, the characteristics of the *p*-doped QD laser will be preferred in uncooled fibre optic applications due to their infinite characteristic temperature.

Eventually, following the successful improvement of the static characteristics by optimum thermal annealing performed on the 1.3 μm ten-layer InAs/InGaAs QD structures, a high-speed modulation characterization was performed on the undoped and *p*-doped QD lasers with an optimum annealing condition.

For the undoped QD lasers under optimum annealing condition, the characteristic temperature was enhanced by a factor of 2.3 upon optimum annealing. Temperature-dependent small signal modulation results demonstrated improvements in the temperature stability of the modulation bandwidth. The improvements were attributed to the following factors: (i) the increase in internal quantum efficiency due to defects removal and (ii) the reduction in the temperature dependency of the differential gain. The increase in the bandwidth at a high temperature from the annealed QD laser could be due to a reduction in the carrier relaxation time in the order of 10^{-1} ps. The carrier capture and their relaxation to GS may have been enhanced after RTA. The differential gain was increased and the nonlinear gain compression was reduced through optimum annealing. More importantly, the

temperature stability of the characteristic parameters was improved after RTA.

For the *p*-doped QD lasers, an almost 18% improvement in the modulation speed was obtained from the annealed QD lasers with reference to the as-grown QD lasers. In addition, the modulation efficiency of the annealed QD lasers improved by approximately 45% compared to the modulation efficiency of the as-grown ones. These observed improvements were due to: (i) the removal of defects, which act as nonradiative recombination centres in the QD structure, and (ii) the reduction in the Auger-related recombination processes in the *p*-doped QDs upon optimum annealing.

These encouraging results suggest that the RTA is an attractive approach to modify both the static and the dynamic characteristics of the 1.3 μm InAs/InGaAs QDs without re-growth of the structure if its condition is carefully designed. This finding will be beneficial for the development of high-speed QDs for uncooled optical communication networks.

8.2 Recommendations for Future Research

The future development of modulated 1.3 μm InAs/InGaAs QD lasers will strongly depend on the substantial improvement of the intrinsic QD modulation properties.

8.2.1 Further Investigations on the Intermixing Effects in QDs

This thesis demonstrated the study of RTA effects on the QD laser performance at relatively low annealing temperatures (i.e. 600 °C and 650 °C). The annealing time was fixed at 15 s to realize the device performance improvements after RTA. Additional annealing conditions, such as a higher annealing temperature (>700 °C) and a longer annealing time, could be introduced on the QD laser structure.

The study of QW intermixing based on various annealing conditions was

reported by Chen *et al.* [114] with a demonstration of unchanged static performances and a slight degradation of the dynamic properties for the InGaAs-InGaAsP QW lasers. Generally, the blueshift of the emission wavelength will be larger and the structural changes to the dots will be more significant with RTA with a higher annealing temperature and a longer annealing time. Normally, a reduction in the intersublevel energy spacing will be observed at a high annealing temperature [33]. The ability to tune the intersublevel spacing between the GS and the ES of the QDs is of interest for various device applications such as the realization of mid-infrared detectors and other devices based on intersubband transitions, broadband QD lasers, and QD superluminenscent light-emitting diodes [94]. Therefore, it will be interesting to perform systematic investigations on the changes in the QD laser characteristics with respect to these annealing conditions, especially with respect to the high-speed modulation characteristics.

In addition to the experimental investigations, a theoretical model should be developed to simulate the effects of thermal annealing on the structural and performance changes of the QDs. Guidance for the epitaxial growth of faster QD structures can only arise from a thorough understanding and modelling of the complete QD structure. Although the requirements for the modelling of QD lasers have been clarified in past years, no computationally feasible and complete dynamic model including crucial spectral and electronic features has been presented. Therefore, the modelling and the simulation of the QD lasers are important milestones for the next few years.

8.2.2 The Modulation of Short Cavity QD Lasers with a Coplanar Contact Structure

The QD laser investigated in this thesis is based on the narrow ridge waveguide structure. In order to perform high-speed modulation, the device needs to be bonded on a submount with Ground-Signal-Ground (G-S-G) contacts. The length of the bonding wire will become a constraint for the modulation speed of the short cavity length (<0.4 mm) QD lasers. In the future, the expected modulation bandwidth will be larger than 20 GHz for the high-speed modulation of short cavity length QD lasers. Therefore, it is necessary to optimize the device structure by fabricating the coplanar G-S-G contact pads on the device, which will enable direct high-frequency probing without any bonding steps [115]. Additional fabrication steps will be introduced.

In order to form the coplanar *p*- and *n*-contacts on the device, a large area mesa will be defined and etched by inductively coupled plasma (ICP) dry etching down to the *n*+-GaAs substrate. Subsequently, the whole structure will be planarized by spinning a thick layer of benzocyclobutene (BCB). The thick BCB layer will electively reduce the parasitic capacitance between the *p*-contact and the *n*+-substrate due to the increased separation and the low dielectric constant of BCB. This can be achieved by a careful design of the mask set and by the good control of the fabrication process.

In addition to the optimum annealing, a proper high-reflectivity (HR) facet coating design can be applied to the QD laser to suppress the ES lasing in the short cavity length QD lasers [93].

8.2.3 Investigation of the Effect of Device Structure on the High-speed Modulation of QD Lasers

The ridge height, which is controlled by the etch depth during fabrication, is an important parameter for the lateral spreading current to achieve a low threshold current in the ridge waveguide edge emitting lasers [116]. The dependence of the characteristic parameters, such as threshold current density and external quantum efficiency, on the ridge height of the ridge waveguide edge emitting QW lasers has been studied by Liu *et al.* [117]. Since the ridge height has a significant effect on the device performance of the narrow ridge waveguide lasers, it will be interesting to investigate effects of the ridge height on the performances of the narrow ridge waveguide QD lasers. However, there only few studies on the effect of the ridge height on the static and dynamic properties of the narrow ridge waveguide QD lasers exist [118].

Further investigations could focus on the high-speed modulation behaviours of the narrow ridge waveguide QD lasers. A systematic study should be performed on the effects of the ridge height on the modal gain, the differential gain, the modulation bandwidth, the K-factor, and the gain compression of the narrow ridge waveguide QD lasers. The temperature-dependent modulation characteristics should also be studied for the realization of the future development of uncooled high-speed optical communication systems.

Author's Publications

1. **H. X. Zhao**, S. F. Yoon, C. Y. Ngo, and R. Wang, "Improved Ground-state Modulation Characteristics in 1.3 μm InAs/GaAs Quantum Dot Lasers by Rapid Thermal Annealing," *Nanoscale Res. Lett.*, vol. 6, no. 382, Apr 2011.

2. **H. X. Zhao**, S. F. Yoon, C. Y. Ngo, R. Wang, Q. Cao, and C. Y. Liu, "Effects of Annealing and *p*-doping on the Two-state Competition in 1.3 μm InAs/GaAs Quantum Dot Lasers," *IEEE Trans. Nanotechnol.,* vol, 10, no, 6, pp.1211-1213, Mar 2011.

3. **H. X. Zhao**, S. F. Yoon, C. Z. Tong, C. Y. Liu, R. Wang and Q. Cao, "Thermal Effects and Small Signal Modulation of 1.3-μm InAs/GaAs Self-Assembled Quantum-Dot Lasers," *Nanoscale Res. Lett.*, vol. 6, no. 37, Sep 2010.

4. **H. X. Zhao,** S. F. Yoon, C. Y. Ngo, R. Wang, C. Z. Tong, C. Y. Liu, and Q. Cao, "Effects of thermal annealing on the dynamic characteristics of InAs/GaAs quantum dot lasers," *Photonics Journal, IEEE.*, vol. 2, no. 4, pp. 630-635, Aug 2010.

5. **H. X. Zhao**, S. F. Yoon, C. Y. Ngo, and R. Wang, "The effects of thermal annealing on the photoluminescence and DC characteristics of 1.3 μm *p*-doped InAs/InGaAs/GaAs quantum dot lasers," *Physica Status Solidi (c)*., vol. 9, no 2, pp. 326-329, 2012.

6. **H. X. Zhao**, S. F. Yoon, C. Y. Ngo, and R. Wang, "Improved Ground State Characteristics of 1.3 μm InAs/GaAs Quantum Dot Lasers by Optimum Rapid Thermal Annealing," in *The 38th International Symposium on Compound Semiconductors (ISCS)*, Germany, May 2011.

7. **H. X. Zhao**, R. Wang, Q. Cao, C. Y. Liu, C. Z. Tong, S. M. L. Nai, J. Wei, and S. F. Yoon, "Quantum dot laser diode with native oxide injection current confinement: static and dynamic properties," in *International Conference on Materials for Advanced Technologies.*, Singapore, Symp O. A01953-04208. Jun 2009.

8. R. Wang, S. F. Yoon, **H. X. Zhao**, and C. Y. Liu, "Self-Heating Effect on Modal Gain of 1.3 μm InAs/GaAs QD Lasers with Different p-Doping Levels,"

Photonics Journal, IEEE., vol. 3, no, 4, pp. 713-717, Jul 2011.

9. R. Wang, S. F. Yoon, **H. X. Zhao**, and C. Y. Ngo, "Geometrical Effects on Characteristic Temperature and Modal Gain of InAs/GaAs Quantum Dot Lasers," *IEEE Photonics Technol. Lett.*, vol. 23, pp. 863-865, Apr 2011.

10. C. Y. Ngo, S. F. Yoon, S. Y. Lee, **H. X. Zhao**, R. Wang, D. R. Lim, Vincent Wong, and S. J. Chua, "Electroabsorption Characteristics of Single-Mode 1.3-μm InAs–InGaAs–GaAs Ten-Layer Quantum-Dot Waveguide," *IEEE Photonics Technol. Lett.,* vol. 22, no. 23, pp. 1717-1719, Dec 2010.

11. R. Wang, S. F. Yoon, **H. X. Zhao**, C. Z. Tong, C. Y. Liu, and Q. Cao, "Temperature Dependent Study on Modal Gain and Differential Gain of 1.3 μm InAs/GaAs QD Lasers with Different *p*-Doping Levels," *IEEE Photonics Technol. Lett.,* vol. 22, no. 14, pp. 1045-1047, Jul 2010.

12. R. Wang, C. Z. Tong, S. F. Yoon, C. Y. Liu, **H. X. Zhao**, and Q. Cao, "Temperature Characteristics of Gain Profiles in 1.3 μm *p*-doped and Undoped InAs/GaAs Quantum Dot Lasers," *IEEE Electron. Device Lett.,* vol. 30, pp. 1311-1313, Dec 2009.

13. Q. Cao, S. F. Yoon, C. Z. Tong, C. Y. Ngo, C. Y. Liu, R. Wang, and **H. X. Zhao**, "Two-state competition in 1.3-μm multilayer InAs/InGaAs quantum dot lasers," *Appl. Phys. Lett.,* vol. 95, pp. 191101, Nov 2009.

14. R. Wang, S. F. Yoon, **H. X. Zhao**, C. Z. Tong, C. Y. Liu, and a. Q. Cao, "Doping effect on two-state lasing in 1.3 μm InAs/GaAs quantum dot lasers," in *Semiconductor Laser Conference (ISLC), 2010 22nd IEEE International*, Kyoto, Japan, 2010, pp. 73-74.

15. C. Y. Liu, S. F. Y, R. Wang, Q. Cao, and **H. X. Zhao**, "Design the distributed bragg reflectors for short-cavity edge emitting quantum dot lasers by transfer matrix method and FDTD," in *International Conference on Materials for Advanced Technologies*, Singapore, 2009.

16. C. Y. Liu, S. F. Y, R. Wang, Q. Cao, and **H. X. Zhao**, "Comparison of optical properties from GaAs-based 1.3 μm InAs quantum dot lasers and InGaAsN quantum well lasers," in *International Conference on Materials for Advanced Technologies*, Singapore, 2009.

Bibliography

[1] P. W. Shumate, "Fiber-to-the-home: 1977-2007," *J. Lightwave Technol.,* vol. 26, pp. 1093-1103, 2008.

[2] N. N. Ledentsov, "Quantum dot laser," *Semicond. Sci. Technol.,* vol. 26, pp. 014001-1-014001-8, Jan 2011.

[3] S. Fathpour, Z. Mi, and P. Bhattacharya, "Small-signal modulation characteristics of *p*-doped 1.1- and 1.3-μm quantum-dot lasers," *IEEE Photonics Technol. Lett.,* vol. 17, pp. 2250-2252, 2005.

[4] S. Ghosh, S. Pradhan, and P. Bhattacharya, "Dynamic characteristics of high-speed $In_{0.4}Ga_{0.6}As$/GaAs self-organized quantum dot lasers at room temperature," *Appl. Phys. Lett.,* vol. 81, pp. 3055-3057, 2002.

[5] S. M. Kim, Y. Wang, M. Keever, and J. S. Harris, "High-frequency modulation characteristics of 1.3-μm InGaAs quantum dot lasers," *IEEE Photonics Technol. Lett.,* vol. 16, pp. 377-379, 2004.

[6] M. Sugawara, N. Hatori, M. Ishida, H. Ebe, and Y. Arakawa, "Recent progress in self-assembled quantum-dot optical devices for optical telecommunication: temperature-insensitive 10Gbs^{-1} directly modulated lasers and 40Gbs^{-1} signal-regenerative amplifiers," *J. Phys. D: Appl. Phys.,* vol. 38, pp. 2126-2134, 2005.

[7] K. Kamath, J. Phillips, H. Jiang, J. Singh, and P. Bhattacharya, "Small-signal modulation and differential gain of single-mode self-organized $In_{0.4}Ga_{0.6}As$/GaAs quantum dot lasers," *Appl. Phys. Lett.,* vol. 70, pp. 2952-2954, 1997.

[8] O. B. Shchekin and D. G. Deppe, "The role of *p*-type doping and the density of states on the modulation response of quantum dot lasers," *Appl. Phys. Lett.,* vol. 80, pp. 2758-2760, Apr 2002.

[9] H. Su and L. F. Lester, "Dynamic properties of quantum dot distributed feedback lasers: high speed, linewidth and chirp," *J. Phys. D-Appl. Phys.,* vol. 38, pp. 2112-2118, Jul 2005.

[10] D. R. Matthews, H. D. Summers, P. M. Smowton, and M. Hopkinson, "Experimental investigation of the effect of wetting-layer states on the gain–current characteristic of quantum-dot lasers," *Appl. Phys. Lett.,* vol. 81, pp. 4904-4906, 2002.

[11] J. Urayama, T. B. Norris, H. Jiang, J. Singh, and P. Bhattacharya, "Temperature-dependent carrier dynamics in self-assembled InGaAs quantum dots," *Appl. Phys. Lett.,* vol. 80, pp. 2162-2164, Mar 2002.

[12] D. G. Deppe, S. Freisem, H. Huang, and S. Lipson, "Electron transport due to inhomogeneous broadening and its potential impact on modulation speed in *p*-doped quantum dot lasers," *J. Phys. D: Appl. Phys. ,* vol. 38, pp. 2119-2125, 2005.

[13] D. G. Deppe, H. Huang, and O. B. Shchekin, "Modulation characteristics of quantum-dot lasers: The influence of *p*-type doping and the electronic density

of states on obtaining high speed," *IEEE J. Quantum Electron.,* vol. 38, pp. 1587-1593, 2002.

[14] Z. Mi, P. Bhattacharya, and S. Fathpour, "High-speed 1.3 μm tunnel injection quantum-dot lasers," *Appl. Phys. Lett.,* vol. 86, pp. 153109-1-153109-3, 2005.

[15] A. Fiore and A. Markus, "Differential gain and gain compression in quantum-dot lasers," *IEEE J. Quantum Electron.,* vol. 43, pp. 287-294, 2007.

[16] M. Ishida, N. Hatori, T. Akiyama, K. Otsubo, Y. Nakata, H. Ebe, M. Sugawara, and Y. Arakawa, "Photon lifetime dependence of modulation efficiency and K factor in 1.3 μm self-assembled InAs/GaAs quantum-dot lasers: Impact of capture time and maximum modal gain on modulation bandwidth," *Appl. Phys. Lett.,* vol. 85, pp. 4145-4147, 2004.

[17] P. F. Xu, T. Yang, H. M. Ji, Y. L. Cao, Y. X. Gu, Y. Liu, W. Q. Ma, and Z. G. Wang, "Temperature-dependent modulation characteristics for 1.3 μm InAs/GaAs quantum dot lasers," *J. Appl. Phys.,* vol. 107, pp. 013102-1-013102-5, Jan 2010.

[18] M. Sugawara, K. Mukai, and H. Shoji, "Effect of phonon bottleneck on quantum-dot laser performance," *Appl. Phys. Lett. ,* vol. 71, pp. 2791-2793, 1997.

[19] S. Fathpour, Z. Mi, and P. Bhattacharya, "High-speed quantum dot lasers," *J. Phys. D: Appl. Phys.,* vol. 38, pp. 2103–2111, 2005.

[20] J. H. Marsh, "Quantum Qell Intermixing " *Semicond. Sci. Technol.,* vol. 8, pp. 1136-1155, Jun 1993.

[21] N. Yamada and J. S. Harris, "Strained InGaAs/GaAs Single Quantum-Well Lasers with Saturable Absorbers Fabricated by Quantum-Well Intermixing," *Appl. Phys. Lett.,* vol. 60, pp. 2463-2465, May 1992.

[22] J. Ko, E. R. Hegblom, Y. Akulova, B. J. Thibeault, and L. A. Coldren, "Low-threshold 840-nm laterally oxidized vertical-cavity lasers using AlInGaAs-AlGaAs strained active layers," *IEEE Photonics Technol. Lett.,* vol. 9, pp. 863-865, 1997.

[23] J. H. Teng, J. R. Dong, S. J. Chua, R. Yin, B. C. Foo, B. Z. Wang, and Y. J. Wang, "Elimination of mode grouping in InGaAsP/InP ridge waveguide laser using quantum-well intermixing," *Appl. Phys. Lett.,* vol. 88, p. 011109, 2006.

[24] A. O. Kosogov, P. Werner, U. Gosele, N. N. Ledentsov, D. Bimberg, V. M. Ustinov, A. Y. Egorov, A. E. Zhukov, P. S. Kop'ev, N. A. Bert, and I. A. Zh, "Structural and optical properties of InAs-GaAs quantum dots subjected to high temperature annealing," *Appl. Phys. Lett.,* vol. 69, pp. 3072-3074, 1996.

[25] R. Leon, K. Yong, C. Jagadish, M. Gal, J. Zou, and D. J. H. Cockayne, "Effects of interdiffusion on the luminescence of InGaAs/GaAs quantum dots," *Appl. Phys. Lett.,* vol. 69, pp. 1888-1890, 1996.

[26] S. Fafard, Z. R. Wasilewski, C. N. Allen, D. Picard, M. Spanner, J. P. McCaffrey, and P. G. Piva, "Manipulating the energy levels of semiconductor quantum dots," *Phys. Rev. B.,* vol. 59, pp. 15368-15373, 1999.

[27] R. Leon, S. Fafard, P. G. Piva, S. Ruvimov, and Z. Liliental-Weber, "Tunable intersublevel transitions in self-forming semiconductor quantum dots," *Phys.*

Rev. B, vol. 58, pp. 4262-4265, Aug 1998.

[28] D. Bhattacharyya, A. Saher Helmy, A. C. Bryce, E. A. Avrutin, and J. H. Marsh, "Selective control of self-organized $In_{0.5}Ga_{0.5}As$-GaAs quantum dot properties: quantum dot intermixing," *J. Appl. Phys.,* vol. 88, pp. 4619-4622, 2000.

[29] J. F. Chen, C. H. Yang, R. M. Hsu, and U. S. Wang, "Influence of thermal annealing on the electron emission of InAs quantum dots containing a misfit defect state," *J. Appl. Phys.,* vol. 105, pp. 063705-1-063705-9, 2009.

[30] S. Marcinkevicius and R. Leon, "Carrier capture and escape in $In_xGa_{1-x}As$/GaAs quantum dots: Effects of intermixing," *Phys. Rev. B,* vol. 59, pp. 4630-4633, 1999.

[31] J. Tatebayashi, Y. Arakawa, N. Hatori, H. Ebe, M. Sugawara, H. Sudo, and A. Kuramata, "InAs/GaAs self-assembled quantum-dot lasers grown by metalorganic chemical vapor deposition - Effects of postgrowth annealing on stacked InAs quantum dots," *Appl. Phys. Lett.,* vol. 85, pp. 1024-1026, Aug 2004.

[32] H. S. Djie, Y. Wang, B. S. Ooi, D. N. Wang, J. C. M. Hwang, G. T. Dang, and W. H. Chang, "Defect annealing of InAs-InAlGaAs quantum-dash-in-asymmetric-well laser," *IEEE Photonics Technol. Lett.,* vol. 18, pp. 2329-2331, Nov-Dec 2006.

[33] H. S. Djie, Y. Wang, D. Negro, and B. S. Ooi, "Postgrowth band gap trimming of InAs/InAlGaAs quantum-dash laser," *Appl. Phys. Lett.,* vol. 90, pp. 031101-1-031101-3, Jan 2007.

[34] R. Dingle and C. H. Henry, "Quantum effects in heterostructure lasers " US Patent: 3982207, 1976.

[35] Y. Arakawa and H. Sakaki, "Multidimensional quantum well lasers and temperature dependence of its threshold current," *Appl. Phys. Lett.,* vol. 40, pp. 939-941, 1982.

[36] http://www-opto.e-technik.uni-ulm.de/lehre/cs/index.html, available online on Nov. 25, 2009.

[37] N. Kirstaedter, N. N. Ledentsov, M. Grundmann, D. Bimberg, V. M. Ustinov, S. S. Ruvimov, M. V. Maximov, P. S. Kopev, Z. I. Alferov, U. Richter, P. Werner, U. Gosele, and J. Heydenreich, "Low threshold, large To injection laser emission from (InGa)As quantum dots," *Electron. Lett.,* vol. 30, pp. 1416-417, Aug 1994.

[38] K. Kamath, P. Bhattacharya, T. Sosnowski, T. Norris, and J. Phillips, "Room-temperature operation of $In_{0.4}Ga_{0.6}As$/GaAs self-organised quantum dot lasers," *Electron. Lett.,* vol. 32, pp. 1374-1375, 1996.

[39] N. N. Ledentsov, V. A. Shchukin, M. Grundmann, N. Kirstaedter, J. Bohrer, O. Schmidt, D. Bimberg, V. M. Ustinov, A. Y. Egorov, A. E. Zhukov, P. S. Kopev, S. V. Zaitsev, N. Y. Gordeev, Z. I. Alferov, A. I. Borovkov, A. O. Kosogov, S. S. Ruvimov, P. Werner, U. Gosele, and J. Heydenreich, "Direct formation of vertically coupled quantum dots in Stranski-Krastanow growth," *Phys. Rev. B,* vol. 54, pp. 8743-8750, Sep 1996.

[40] P. G. Eliseev, H. Li, G. T. Liu, A. Stintz, T. C. Newell, L. F. Lester, and K. J. Malloy, "Ground-state emission and gain in ultralow-threshold InAs-InGaAs quantum-dot lasers," *IEEE J. Sel. Top. Quantum Electron.,* vol. 7, pp. 135-142, Mar-Apr 2001.

[41] O. G. Schmidt, N. Kirstaedter, N. N. Ledentsov, M. H. Mao, D. Bimberg, V. M. Ustinov, A. Y. Egorov, A. E. Zhukov, M. V. Maximov, P. S. Kopev, and Z. I. Alferov, "Prevention of gain saturation by multi-layer quantum dot lasers," *Electron. Lett.,* vol. 32, pp. 1302-1304, Jul 1996.

[42] H. Y. Liu, D. T. Childs, T. J. Badcock, K. M. Groom, I. R. Sellers, M. Hopkinson, R. A. Hogg, D. J. Robbins, D. J. Mowbray, and M. S. Skolnick, "High-performance three-layer 1.3-μm InAs-GaAs quantum-dot lasers with very low continuous-wave room-temperature threshold currents," *IEEE Photonics Technol. Lett.,* vol. 17, pp. 1139-1141, Jun 2005.

[43] A. Salhi, L. Martiradonna, G. Visimberga, V. Tasco, L. Fortunato, M. T. Todaro, R. Cingolani, A. Passaseo, and M. De Vittorio, "High-modal gain 1300-nm In(Ga)As-GaAs quantum-dot lasers," *IEEE Photonics Technol. Lett.,* vol. 18, pp. 1735-1737, 2006.

[44] S. S. Mikhrin, A. R. Kovsh, I. L. Krestnikov, A. V. Kozhukohov, D. A. Livshits, N. N. Ledentsov, Y. M. Shernyakov, I. I. Novikov, M. V. Maximov, V. M. Ustinov, and Z. I. Alferov, "High power temperature-insensitive 1.3 µm InAs/InGaAs/GaAs quantum dot lasers," *Semicond. Sci. Technol.,* vol. 20, pp. 340-342, 2005.

[45] S. Fathpour, Z. Mi, P. Bhattacharya, A. R. Kovsh, S. S. Mikhrin, I. L. Krestnikov, A. V. Kozhukhov, and N. N. Ledentsov, "The role of Auger recombination in the temperature-dependent output characteristics T_0=infinity of *p*-doped 1.3 μm quantum dot lasers," *Appl. Phys. Lett.,* vol. 85, pp. 5164-5166, 2004.

[46] I. C. Sandall, P. M. Smowton, J. D. Thomson, T. Badcock, D. J. Mowbray, H. Y. Liu, and M. Hopkinson, "Temperature dependence of threshold current in p-doped quantum dot lasers," *Appl. Phys. Lett.,* vol. 89, pp. 151118-1-151118-3, 2006.

[47] P. M. Smowton, I. C. Sandall, H. Y. Liu, and M. Hopkinson, "Gain in *p*-doped quantum dot lasers," *J. Appl. Phys.,* vol. 101, pp. 013107-1-013107-7, Jan 2007.

[48] K. W. Sun, A. Kechiantz, B. C. Lee, and C. P. Lee, "Ultrafast carrier capture and relaxation in modulation-doped InAs quantum dots," *Appl. Phys. Lett.,* vol. 88, pp. 163117-1-163117-3, Apr 2006.

[49] N. F. Masse, S. J. Sweeney, I. P. Marko, A. R. Adams, N. Hatori, and M. Sugawara, "Temperature dependence of the gain in *p*-doped and intrinsic 1.3 μm InAs/GaAs quantum dot lasers," *Appl. Phys. Lett.,* vol. 89, pp. 191118-1-191118-3, Nov 2006.

[50] I. P. Marko, N. F. Masse, S. J. Sweeney, A. D. Andreev, A. R. Adams, N. Hatori, and M. Sugawara, "Carrier transport and recombination in *p*-doped and intrinsic 1.3 μm InAs/GaAs quantum-dot lasers," *Appl. Phys. Lett.,* vol. 87, pp. 211114-1-211114-3, Nov 2005.

[51] Y. Q. Wei, J. S. Gustavsson, A. Haglund, P. Modh, M. Sadeghi, S. M. Wang, and A. Larsson, "High-frequency modulation and bandwidth limitations of GaInNAs double-quantum-well lasers," *Appl. Phys. Lett.,* vol. 88, pp. 051103-1-051103-3, 2006.

[52] P. Bhattacharya, S. Ghosh, Sameer Pradhan, J. Singh, Z. K. Wu, J. Urayama, K. Kim, and T. B. Norris, "Carrier dynamics and high-speed modulation properties of tunnel injection InGaAs–GaAs quantum-dot lasers," *IEEE J. Quantum Electron.,* vol. 39, pp. 952-962, 2003.

[53] O.B. Shchekin, J. Ahn, and D. G. Deppe, "High temperature performance of self-organised quantum dot laser with stacked *p*-doped active region," *Electron. Lett.,* vol. 38, pp. 712-713, 2002.

[54] D. R. Matthews, H. D. Summers, P. M. Smowton, and M. Hopkinson, "Experimental investigation of the effect of wetting-layer states on the gain-current characteristic of quantum-dot lasers," *Appl. Phys. Lett.,* vol. 81, pp. 4904-4906, 2002.

[55] O. Gunawan, H. S. Djie, and B. S. Ooi, "Electronics states of interdiffused quantum dots," *Phys. Rev. B.,* vol. 71, pp. 205319-1-205319-10, 2005.

[56] H. S. Djie, O. Gunawan, D. N. Wang, B. S. Ooi, and J. C. M. Hwang, "Group-III vacancy induced $In_xGa_{1-x}As$ quantum dot interdiffusion," *Phys. Rev. B,* vol. 73, pp. 155324-1-155324-6, Apr 2006.

[57] J. H. Marsh, D. Bhattacharyya, A. S. Helmy, E. A. Avrutin, and A. C. Bryce, "Engineering quantum-dot lasers," *Physica E-Low-Dimensional Systems & Nanostructures,* vol. 8, pp. 154-163, Aug 2000.

[58] F. Heinrichsdorff, M. Grundmann, O. Stier, A. Krost, and D. Bimberg, "Influence of In/Ga intermixing on the optical properties of InGaAs/GaAs quantum dots," *J. Cryst. Growth,* vol. 195, pp. 540-545, Dec 1998.

[59] N. Perret, D. Morris, L. Franchomme-Fosse´, R. Coˆte´, S. Fafard, V. Aimez, and J. Beauvais, "Origin of the inhomogenous broadening and alloy intermixing in InAs/GaAs self-assembled quantum dots," vol. 62, pp. 5092-5099, 2000.

[60] S. Malik, E. C. Le Ru, D. Childs, and R. Murray, "Time-resolved studies of annealed InAs/GaAs self-assembled quantum dots," *Phys. Rev. B.,* vol. 63, pp. 155313-1-155313-6, Apr 2001.

[61] Q. Cao, S. F. Yoon, C. Y. Liu, and C. Z. Tong, "Effects of rapid thermal annealing on optical properties of *p*-doped and undoped InAs/InGaAs dots-in-a-well structures," *J. Appl. Phys.,* vol. 104, pp. 033522-1-033522-6, Aug 2008.

[62] V. M. Ustinov, A. E. Zhukov, A. Y. Egorov, and N. A. Maleev, *Quantum dot lasers* New York: Oxford university Press, 2003.

[63] N. N. Ledentsov, V. M. Ustinov, A. Y. Egorov, A. E. Zhukov, M. V. Maksimov, I. G. Tabatadze, and P. S. Kopev, "Optical-properties Of Heterostructures with InGaAs-GaAs Quantum Clusters," *Semiconductors,* vol. 28, pp. 832-834, Aug 1994.

[64] S. L. Chuang, *Physics of optoelectronic devices*. New York: Wiley, 1995.

[65] L. V. Asryan, "Limitations on standard procedure of determining internal loss and efficiency in quantum dot lasers," *J. Appl. Phys.,* vol. 99, pp. 013102-1-013102-4, Jan 2006.

[66] M. Sugawara, *Self-assembled InGaAs/GaAs quantum dots* vol. 60: Academic Press, 1999.

[67] L. V. Asryan and S. Luryi, "Tunneling-injection quantum-dot laser: ultrahigh temperature stability," *IEEE J. Quantum Electron.,* vol. 37, pp. 905-910, 2001.

[68] Kjebon., R. Schatz, S. Lourdudoss, S. Nilsson, and B. Stdnacke, "Modulation response measurements and evaluation of MQW InGaAsP lasers of various designs," *SPIE,* vol. 2684, pp. 138-156, 1996.

[69] L. A. Coldren and S. W. Corzine., "Diode lasers and photonic integrated circuits ": Wiley, 1995.

[70] C. Y. Liu, S. F. Yoon, S. Z. Wang, W. J. Fan, Y. Qu, and S. Yuan, "Fabrication of high-performance InGaAsN ridge waveguide lasers with pulsed anodic oxidation," *IEEE Photonics Technol. Lett.,* vol. 16, pp. 2409-2411, 2004.

[71] C. Y. Liu, S. F. Yoon, W. J. Fan, A. Uddin, and S. Yuan, "Ridge-width dependence on high-temperature continuous-wave operation of native oxide-confined InGaAsN triple-quantum-well lasers," *IEEE Photonics Technol. Lett.,* vol. 18, pp. 791-793, Mar-Apr 2006.

[72] S. Yuan, C. Jagadish, Y. Kim, Y. Chang, H. H. Tan, R. M. Cohen, M. Petravic, L. V. Dao, M. Gal, M. C. Y. Chan, E. H. Li, J. S. O, and P. S. Zory, "Anodic-oxide-induced intermixing in GaAs-AlGaAs quantum-well and quantum-wire structures," *IEEE J. Sel. Top. Quantum Electron.,* vol. 4, pp. 629-635, Jul-Aug 1998.

[73] B. W. Hakki and T. L. Paoli, "Gain spectra In GaAs double-heterostructure injection lasers," *J. Appl. Phys.,* vol. 46, pp. 1299-1306, Sep 1975.

[74] H. Y. Liu, I. R. Sellers, M. Gutierrez, K. M. Groom, W. M. Soong, M. Hopkinson, J. P. R. David, R. Beanland, T. J. Badcock, D. J. Mowbray, and M. S. Skolnick, "Influences of the spacer layer growth temperature on multilayer InAs/GaAs quantum dot structures," *J. Appl. Phys.,* vol. 96, pp. 1988-1992, Aug 2004.

[75] *Microwave Office 2001*: Applied Wave Research, 2001.

[76] O. B. Shchekin and D. G. Deppe, "Low-threshold high-T_o 1.3-μm InAs quantum-dot lasers due to *p*-type modulation doping of the active region," *IEEE Photonics Technol. Lett.,* vol. 14, pp. 1231-1233, 2002.

[77] D. Y. Cong, A. Martinez, K. Merghem, A. Ramdane, J. G. Provost, M. Fischer, I. Krestnikov, and A. Kovsh, "Temperature insensitive linewidth enhancement factor of *p*-type doped InAs/GaAs quantum-dot lasers emitting at 1.3μm," *Appl. Phys. Lett.,* vol. 92, pp. 191109-1-191109-3, 2008.

[78] D. W. Xu, S. F. Yoon., and C. Z. Tong, "Self-consistent analysis of carrier confinement and output power in 1.3-μm InAs-GaAs quantum-dot VCSELs," *IEEE J. Quantum Electron.,* vol. 44, pp. 879-885, 2008.

[79] K. Mukai, Y. Nakata, K. Otsubo, M. Sugawara, N. Yokoyama, and H. Ishikawa, "1.3-μm CW lasing characteristics of self-assembled InGaAs-GaAs

quantum dots," *IEEE J. Quantum Electron.,* vol. 36, pp. 472-478, 2000.

[80] P. Gyoungwon, O. B. Shchekin, and D. G. Deppe, "Temperature dependence of gain saturation in multilevel quantum dot lasers," *IEEE J. Quantum Electron.,* vol. 36, pp. 1065-1071, 2000.

[81] M. T. Todaro, A. Salhi, L. Fortunato, R. Cingolani, A. Passaseo, M. De Vittorio, P. Della Casa, F. Ghiglieno, and L. Bianco, "High-performance directly modulated 1.3-μm undoped InAs/InGaAs quantum-dot lasers," *IEEE Photonics Technol. Lett.,* vol. 19, pp. 191-193, 2007.

[82] N. Kirstaedter, O. G. Schmidt, N. N. Ledentsov, D. Bimberg, V. M. Ustinov, A. Y. Egorov, A. E. Zhukov, M. V. Maximov, P. S. Kopev, and Z. I. Alferov, "Gain and differential gain of single layer InAs/GaAs quantum dot injection lasers," *Appl. Phys. Lett.,* vol. 69, pp. 1226-1228, Aug 1996.

[83] J. Kim and S. L. Chuang, "Theoretical and experimental study of optical gain, refractive index change, and linewidth enhancement factor of *p*-doped quantum-dot lasers," *IEEE J. Quantum Electron.,* vol. 42, pp. 942-952, Sep-Oct 2006.

[84] M. Kuntz, N. N. Ledentsov, D. Bimberg, A. R. Kovsh, V. M. Ustinov, A. E. Zhukov, and Y. M. Shernyakov, "Spectrotemporal response of 1.3 μm quantum-dot lasers," *Appl. Phys. Lett.,* vol. 81, pp. 3846-3848, 2002.

[85] D. Klotzkin and P. Bhattacharya, "Temperature dependence of dynamic and DC characteristics of quantum-well and quantum-dot lasers: a comparative study," *J. Lightwave Technol.,* vol. 17, pp. 1634-1642, 1999.

[86] M. C. Tatham, J. F. Ryan, and C. T. Foxon, "Time-resolved raman measurements of intersubband relaxation in GaAs quantum wells," *Phys. Rev. Lett.,* vol. 63, pp. 1637-1640, Oct 1989.

[87] A. Fiore, P. Borri, W. Langbein, J. M. Hvam, U. Oesterle, R. Houdre, R. P. Stanley, and M. Ilegems, "Time-resolved optical characterization of InAs/InGaAs quantum dots emitting at 1.3 μm," *Appl. Phys. Lett.,* vol. 76, pp. 3430-3432, Jun 2000.

[88] T. S. Sosnowski, T. B. Norris, H. Jiang, J. Singh, K. Kamath, and P. Bhattacharya, "Rapid carrier relaxation in $In_{0.4}Ga_{0.6}As$/GaAs quantum dots characterized by differential transmission spectroscopy," *Phys. Rev. B.,* vol. 57, pp. R9423-R9426, Apr 1998.

[89] A. Markus, J. X. Chen, O. Gauthier-Lafaye, J. G. Provost, C. Paranthoen, and A. Fiore, "Impact of intraband relaxation on the performance of a quantum-dot laser," *IEEE J. Sel. Top. Quantum Electron.,* vol. 9, pp. 1308-1314, Sep 2003.

[90] L. W. Shi, Y. H. Chen, B. Xu, Z. C. Wang, and Z. G. Wang, "Effect of inter-level relaxation and cavity length on double-state lasing performance of quantum dot lasers," *Physica E: Low-dimensional Systems and Nanostructures,* vol. 39, pp. 203-208, Sep 2007.

[91] J. Lee and D. Lee, "Double-state Lasing from Semiconductor Quantum Dot Laser Diodes Caused by Slow Carrier Relaxation," *J. Korean Phys. Soc.,* vol. 58, pp. 239-242, Feb 2011.

[92] A. Markus, J. X. Chen, C. Paranthoen, A. Fiore, C. Platz, and O.

Gauthier-Lafaye, "Simultaneous two-state lasing in quantum-dot lasers," *Appl. Phys. Lett.,* vol. 82, pp. 1818-1820, Mar 2003.

[93] Y. L. Cao, T. Yang, P. F. Xu, H. M. Ji, Y. X. Gu, X. D. Wang, Q. Wang, W. Q. Ma, and L. H. Chen, "Delay of the excited state lasing of 1310 nm InAs/GaAs quantum dot lasers by facet coating," *Appl. Phys. Lett.,* vol. 96, pp. 171101-1-171101-3, Apr 2010.

[94] Z. Y. Zhang, Q. Jiang, and R. A. Hogg, "Tunable interband and intersubband transitions in modulation C-doped InGaAs/GaAs quantum dot lasers by postgrowth annealing process," *Appl. Phys. Lett.,* vol. 93, pp. 071111-1-071111-7, Aug 2008.

[95] R. R. Alexander, D. T. D. Childs, H. Agarwal, K. M. Groom, H. Y. Liu, M. Hopkinson, R. A. Hogg, M. Ishida, T. Yamarnoto, M. Sugawara, Y. Arakawa, T. J. Badcock, R. J. Royce, and D. J. Mowbray, "Systematic study of the. effects of modulation *p*-doping on 1.3-μm quantum-dot lasers," *IEEE J. Quantum Electron.,* vol. 43, pp. 1129-1139, Nov-Dec 2007.

[96] C. Y. Liu, S. F. Yoon, Q. Cao, C. Z. Tong, and H. F. Li, "Low transparency current density and high temperature operation from ten-layer *p*-doped 1.3 μm InAs/InGaAs/GaAs quantum dot lasers," *Appl. Phys. Lett.,* vol. 90, pp. 041103-1-041103-3, 2007.

[97] A. A. Dikshit and J. M. Pikal, "Carrier distribution, gain, and lasing in 1.3-μm InAs-InGaAs quantum-dot lasers," *IEEE J. Quantum Electron.,* vol. 40, pp. 105-112, Feb 2004.

[98] C. Z. Tong, D. W. Xu, and S. F. Yoon, "Carrier relaxation and modulation response of 1.3-μm InAsGaAs quantum dot lasers," *J. Lightwave Technol.,* vol. 27, pp. 5442-5450, Dec 2009.

[99] R. Wang, C. Z. Tong, S. F. Yoon, C. Y. Liu, H. X. Zhao, and Q. Cao, "Temperature characteristics of gain profiles in 1.3 μm *p*-doped and undoped InAs/GaAs quantum dot lasers," *IEEE Electron. Device Lett.,* vol. 30, pp. 1311-1313 Dec 2009.

[100] Q. Cao, S. F. Yoon, C. Z. Tong, C. Y. Ngo, C. Y. Liu, R. Wang, and H. X. Zhao, "Two-state competition in 1.3-μm multilayer InAs/InGaAs quantum dot lasers," *Appl. Phys. Lett.,* vol. 95, pp. 191101-1-191101-3, Nov 2009.

[101] H. X. Zhao, S. F. Yoon, C. Y. Ngo, R. Wang, C. Z. Tong, C. Y. Liu, and Q. Cao, "Effects of thermal annealing on the dynamic characteristics of InAs/GaAs quantum dot lasers," *Photonics Journal, IEEE,* vol. 2, pp. 630-635, Jun 2010.

[102] D. Klotzkin, K. Kamath, K. Vineberg, P. Bhattacharya, R. Murty, and J. Laskar, "Enhanced modulation bandwidth (20 GHz) of $In_{0.4}Ga_{0.6}As$–GaAs self-organized quantum-dot lasers at cryogenic temperatures: role of carrier relaxation and differential gain," *IEEE Photonics Technol. Lett.,* vol. 10, pp. 932-934, 1998.

[103] D. G. Deppe and D. L. Huffaker, "Quantum dimensionality, entropy, and the modulation response of quantum dot lasers," *Appl. Phys. Lett.,* vol. 77, pp. 3325-3327, Nov 2000.

[104] L. V. Asryan, Y. C. Wu, and R. A. Suris, "Carrier capture delay and modulation bandwidth in an edge-emitting quantum dot laser," *Appl. Phys. Lett.,* vol. 98,

pp. 131108-1-1311083, Mar 2011.

[105] S. Sanguinetti, T. Mano, A. Gerosa, C. Somaschini, S. Bietti, N. Koguchi, E. Grilli, M. Guzzi, M. Gurioli, and M. Abbarchi, "Rapid thermal annealing effects on self-assembled quantum dot and quantum ring structures," *J. Appl. Phys.,* vol. 104, pp. 113519-1-113519-5, Dec 2008.

[106] T. R. Nielsen, P. Gartner, and F. Jahnke, "Many-body theory of carrier capture and relaxation in semiconductor quantum-dot lasers," *Phys. Rev. B.,* vol. 69, pp. 235314-1-235314-13, Jun 2004.

[107] H. X. Zhao, S. Yoon, C. Z. Tong, C. Y. Liu, R. Wang, and Q. Cao, "Thermal effects and small signal modulation of 1.3-μm InAs/GaAs self-assembled Quantum-Dot lasers," *Nanoscale Res. Lett.,* vol. 6:37, Sep 2010.

[108] J. S. Kim, C. R. Lee, K. W. Seol, and D. K. Oh, "Wavelength shift of InP-based InAs quantum dot lasers above room temperature," *J. Nanosci. Nanotechnol.,* vol. 7, pp. 4443-4446, Dec 2007.

[109] S. Deubert, R. Debusmann, J. P. Reithmaier, and A. Forchel, "High-power quantum dot lasers with improved temperature stability of emission wavelength for uncooled pump sources," *Electron. Lett.,* vol. 41, pp. 1125-1127, Sep 2005.

[110] J. P. Reithmaier and A. Forchel, "Recent advances in semiconductor quantum-dot lasers," *C. R. Phys.,* vol. 4, pp. 611-619, Jul-Aug 2003.

[111] F. Klopf, J. P. Reithmaier, and A. Forchel, "Highly efficient GaInAs/(Al)GaAs quantum-dot lasers based on a single active layer versus 980 nm high-power quantum-well lasers," *Appl. Phys. Lett.,* vol. 77, pp. 1419-1421, Sep 2000.

[112] H. Tanoto, S. F. Yoon, K. L. Lew, W. K. Loke, C. Dohrman, E. A. Fitzgerald, and L. J. Tang, "Electroluminescence and structural characteristics of InAs/$In_{0.1}Ga_{0.9}As$ quantum dots grown on graded $Si_{1-x}Ge_x$/Si substrate," *Appl. Phys. Lett.,* vol. 95, pp. 141905-1-141905-3, Oct 2009.

[113] Y. D. Jang, T. J. Badcock, D. J. Mowbray, M. S. Skolnick, J. Park, D. Lee, H. Y. Liu, M. Hopkinson, R. A. Hogg, and A. D. Andreev, "Enhanced nonradiative Auger recombination in p-type modulation doped InAs/GaAs quantum dots," *Appl. Phys. Lett.,* vol. 93, pp. 101903-1-101903-3, Sep 2008.

[114] C. Chen, H. S. Djie, Y. H. Ding, B. S. Ooi, J. C. M. Hwang, and V. Aimez, "Fundamental and Dynamic Properties of Intermixed InGaAs-InGaAsP Quantum-Well Lasers," *IEEE J. Quantum Electron.,* vol. 46, pp. 1368-1374, Sep 2010.

[115] Y. Q. Wei, J. S. Gustavsson, Sadeghi. M, S. M. Wang, and A. Larsson, "Dynamics and temperature-dependence of 1.3 μm GaInNAs double quantum-well lasers," *IEEE J. Quantum Electron.,* vol. 42, pp. 1274-1280, 2006.

[116] M. Achtenhagen and A. Hardy, "Lateral current spreading in ridge waveguide laser diodes," *Appl. Phys. Lett.,* vol. 74, pp. 1364-1366, Mar 1999.

[117] C. Y. Liu, Y. Qu, S. Yuan, and S. F. Yoon, "Optimization of ridge height for the fabrication of high performance InGaAsN ridge waveguide lasers with pulsed anodic oxidation," *Appl. Phys. Lett.,* vol. 85, pp. 4594-4596, 2004.

[118] R. Wang, S. F. Yoon, H. X. Zhao, and C. Y. Ngo, "Geometrical Effects on Characteristic Temperature and Modal Gain of InAs/GaAs Quantum-Dot Lasers," *IEEE Photonics Technol. Lett.,* vol. 23, pp. 863-865, Apr 2011.